CONDENSATION OF CHROMIUM VAPOR, GENERATED IN HIGH-TEMPERATURE (>800°C) ENVIRONMENTS, AND INTERACTIONS WITH ALUMINOSILICATE SURFACES

by

Travis Kent van Leeuwen

A dissertation submitted in partial fulfillment
of the requirements for the degree

of

Doctor of Philosophy

in

Materials Science

MONTANA STATE UNIVERSITY
Bozeman, Montana

May 2024

DEDICATION

Dedicated to my wife, Jessica, the love of my life and my closest confidant who taught me patience, understanding, and empathy for myself. Dedicated to my parents, Mark and Sheila, who have always supported me and shown me love throughout my life. Dedicated to my siblings, Connor and Amy, my first and best friends who helped me become the person I am today. Dedicated to my familial in-laws, Alex, Eppie, and Ryan, who accepted me into their family as one of their own and supported my wife and me through this journey. Dedicated to my late grandfathers, Skip and Clyde, who helped foster my lifelong interest in engineering, physics, and science. I am forever grateful to have had all of them in my life.

ACKNOWLEDGEMENTS

The work detailed herein would not be possible without the guidance and mentorship of my advisor and the primary investigator on this project, Dr. Paul Gannon. The beginning of my journey towards this dissertation was neither easy nor certain, and Dr. Gannon went out of his way to make himself available as an advisor and provide a path to graduation. I consider him a mentor, a colleague, and dear friend. Cheers, Paul!

Furthermore, the work presented in this document was partially funded by industry partners from ECFIA, representing the European High Temperature Insulation Wool (HTIW) industry in matters relating to health and safety, the Montana Space Grant Consortium (MTSGC), and the Raymond E. and Erin S. Schultz Emerging Fellowship. Furthermore, the work performed herein was in part at the Montana Nanotechnology Facility, a member of the National Nanotechnology Coordinated Infrastructure (NNCI), which is supported by the National Science Foundation (Grant# ECCS-2025391).

TABLE OF CONTENTS

TABLE OF CONTENTS CONTINUED

TABLE OF CONTENTS CONTINUED

LIST OF TABLES

Table Page

LIST OF FIGURES

Figure Page

LIST OF FIGURES CONTINUED

Figure Page

LIST OF FIGURES CONTINUED

Figure Page

LIST OF FIGURES CONTINUED

Figure Page

ABSTRACT

This work represents a collection of research and reporting with the goal of improving fundamental understanding of chromium (Cr) vapor reactive condensation, relevant in many high-temperature (>800°C) process environments where Cr-containing alloys are used. While reactive evaporation of Cr from stainless steels used in high-temperature solid oxide electrochemical systems is well-documented, the dynamics of Cr condensation onto surrounding interfaces during complex and dynamic system operation is less understood. Understanding these interactions during operation is critical for improving system performance and safeguarding environmental, health and safety, as some condensed species contain hexavalent chromium (Cr(VI)), a known carcinogen. A series of studies were designed and conducted to investigate the condensation pathways of Cr vapors within representative high-temperature system environments, simulating extreme conditions for Cr evaporation and downstream aluminosilicate fibers used in high-temperature insulation. The first study focuses on the influence of water vapor concentration in the gaseous environment on reactive Cr condensation and speciation onto aluminosilicate fibers. The second study explores the effects of alkaline oxide additives in aluminosilicate fibers on Cr condensation and speciation. The third study investigates the effects of presence of alkaline oxides within the Cr vapor source on reactive evaporation and condensation of Cr vapors onto downstream aluminosilicate fibers. To accomplish the specific objectives of these studies, Cr vapors, produced by high-temperature (>800°C) air exposures of trivalent chromium (Cr(III)) oxide (Cr_2O_3) (chromia) powder with variable moisture content, were condensed onto various ceramic materials (aluminosilicate fibers) downstream at lower temperatures (100-500°C). Total condensed Cr and ratios of oxidation states were measured using inductively coupled plasma optical emission spectroscopy (ICP-OES) and diphenyl carbazide (DPC) colorimetric/direct UV-VIS spectrophotometric analyses, respectively. Results indicate presence of both Cr(III) and Cr(VI) species condensed on all samples investigated. Total Cr and ratio of Cr(VI) to total Cr detected was significantly more on those containing alkaline oxides and at higher atmospheric water vapor concentration, while the presence of alkaline oxides in the Cr vapor source (Cr_2O_3) decreased the evaporation and amount of Cr/Cr(VI) condensed on the samples downstream. Computational thermodynamic equilibrium modelling helps explain experimental results showing the relative stability of alkaline-chromate compounds.

CHAPTER ONE - INTRODUCTION

Contents of Chapter One

Chapter One serves as a brief introduction to the problem at hand and the research objectives developed to address it. First, the structure of this document is introduced. Next, an overview of the problem is presented. Finally, the accompanying research questions and proposed research to address them are presented.

Dissertation Structure Overview

This dissertation is comprised of several peer-reviewed research manuscripts written (first author) by the author of the work. The first manuscript, "*Reactive Evaporation and Condensation of Chromium: A Review*"[1], is a review article of the science and existing research into topics related to reactive evaporation and condensation of Cr vapors and is published in the **Journal of Power Sources** and is presented in Chapter Three. The second manuscript, "*Influence of Water Concentration on High-Temperature Reactive Condensation of Chromium Vapors Generated in 800°C Air*"[2], is a research article published in the **Journal of the Electrochemical Society** and is presented in Chapter Four. The third manuscript, "*Reactive Condensation of Cr Vapors on Aluminosilicate Fibers Containing Alkaline Oxides*", is a research article that is being prepared for publication in the **Journal of the Electrochemical Society** and will be submitted in April 2024. This manuscript is presented in Chapter Five. The fourth manuscript, "*Influence of Alkaline Oxides on Reactive Evaporation and Condensation of Cr*", is a research article that is also being prepared for publication in the **Journal of the Electrochemical Society** and will be submitted in May 2024.

This manuscript is presented in Chapter Six in the discussion and future work sections of the conclusion.

Problem Overview

The research presented herein began as a request from an industry group, ECFIA, representing European high-temperature insulating wool (HTIW) manufacturers. The group approached the author of this document and their research group to request an investigation into claims made by competitors that their products reduced or negated Cr(VI) formation. Specific research objectives and experiments were developed to meet the needs of ECFIA while another set of research objectives and experiments were developed by the author to meet the requirements of the PhD Materials Science program at Montana State University.

High-temperature systems such as solid oxide fuel cells/electrolysis cells (SOFC/SOECs), chemical processing plants, power plants, and exhaust systems of internal combustion engines (ICEs) employ stainless steels due to their stability over a large temperature range. For example, SOFC/SOECs use stainless steel as interconnects between cells due to their low cost, machinability, electrical and thermal properties (see Fig. 1). However, reactive evaporation of Cr from these stainless-steels when employed in high-temperature oxidizing environments with or without water vapor (in many of these applications, it is not uncommon for the gaseous environment to contain water vapor [3, 4]) is well-documented. In the case of SOFC/SOECs, the stainless-steel interconnects are the source of Cr vapors that can lead to Cr poisoning of phase-boundary points at the cathode and degrade system performance.

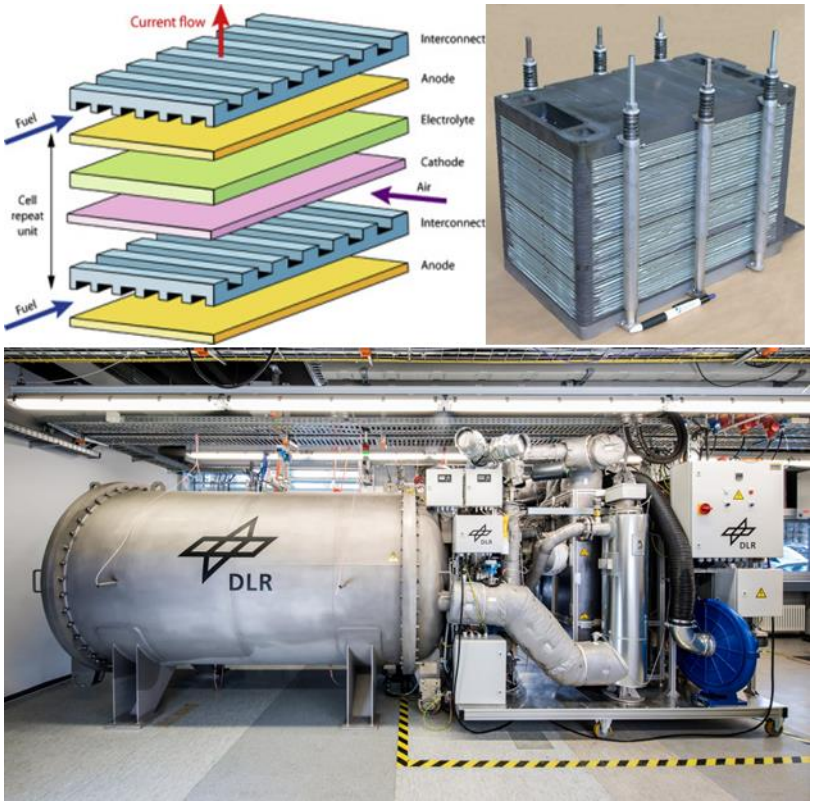

Figure 1 – A diagram of a SOFC stack (top left) [5], a SOFC stack assembly (top right)[6], and a SOFC system with stainless steel balance of plant components covered with HTIW blankets[7].

Cr deposits in the form of hexavalent Cr(VI), a known carcinogen, have also been identified as potentially problematic in multiple industries including electroplating, welding, refractories in stainless steel mills, internal combustion engine exhaust systems, and, more recently, HTIWs. However, the interactions between volatilized Cr species and surrounding interfaces during complex and dynamic system exposures is poorly understood. Applications such as chemical processing or power plants can employ large amounts of stainless steel due to the size and diversity of balance of plant components (see Fig. 2).

Figure 2 – Chemical processing plant balance of plant components are commonly built from stainless steel [8].

The components that operate at elevated temperatures are commonly covered with HTIW blankets to improve process efficiency, and the stainless steels in contact with these insulating surfaces will experience reactive evaporation of Cr (see Fig. 3). Understanding the interactions between volatilized Cr species and downstream components during operation is critical, not only for improving system performance in the case of SOFC/SOECs, but also for safeguarding environmental health, and safety as some condensed Cr forms water-soluble and toxic Cr(VI) species.

Figure 3 – HTIW blankets covering balance of plant components (left) [9] and an exhaust manifold of a large ICE (right) [10].

Proposed Research

The overall goal of this research is to improve fundamental understanding of reactive condensation pathways for chromium (Cr) vapors generated in high-temperature systems such as exhaust manifolds, steam turbines, boilers, or solid oxide fuel cell or electrolysis cell (SOFC/SOEC) stacks. Given the conditions of such high-temperature systems, several research objectives were proposed to meet the overall goal. The proposed research objectives included investigating the influence of water vapor concentration in the surrounding atmosphere, the influence of alkaline oxides in the target material on reactive condensation of Cr vapors, investigating the influence of upstream alkaline oxides on reactive evaporation and condensation of Cr. The specific research questions and respective hypotheses are as follows:

- Research Question 1: what is the influence of water vapor concentration on total condensed Cr and Cr(VI) compounds on aluminosilicate surfaces?
    - Hypothesis: Increased water vapor concentration increases total condensed Cr and Cr(VI) compounds.

- Research Question 2: what is the influence of alkaline oxides in aluminosilicate surfaces on total condensed Cr and Cr(VI) compounds?
    - Hypothesis: Alkaline oxide presence in aluminosilicate surfaces increases total condensed Cr and Cr(VI) compounds.
- Research Question 3: what is the influence of upstream alkaline oxides in the Cr source on total condensed Cr and Cr(VI) compounds formed on aluminosilicate surfaces?
    - Hypothesis: Alkaline oxide presence in Cr source increases total condensed Cr and Cr(VI) compounds formed on aluminosilicate surfaces.

All three research questions were successfully addressed through experimentation and thermodynamic equilibrium modelling. In the pursuit of answering these questions, four research articles were produced, two of which are already published while the other two are in the process of being submitted for publication. The methods behind the experimental design and thermodynamic equilibrium modelling proposed and subsequently developed to achieve these research goals are presented next in Chapter Two.

CHAPTER TWO - METHODS

Contents of Chapter Two

Chapter two provides an in-depth look into the experimental design, analytical methodologies, and thermodynamic equilibrium calculations developed to complete the research for the published manuscripts.

Experimental Design

Reactive condensation of Cr vapors occurs between volatile Cr compounds that interact with and condense on surrounding materials. To study this phenomenon, Cr vapors must be created in a controlled environment and directed towards the target material of interest. An experiment based on the "transpiration experiment" developed by Opila et. al (described in more detail in Chapter 3) was developed to study reactions between high-temperature volatile Cr compounds and a target material. This experimental design is presented in Fig. 4 as a diagram and photograph of the experimental setup operating in the lab. Gas flow starts from laboratory bench supply as regular air (21% O_2) then flows through Drierite filter or temperature-controlled water evaporator to clean air from oils or other contaminants from laboratory bench air supply and control water vapor concentration. The altered air supply then enters a quartz tube housed in a high-precision Thermo Scientific Lindberg/Blue M tube furnaces calibrated to 850°C (Fig. 4 and 5). Tube furnace internal temperature is calibrated using an Omega Engineering K type thermocouple. High-temperature gas within tube furnace interacts with Cr source in the form of 2 g of chromia powder in a quartz boat located in the center of the furnace (Fig. 4, bottom right).

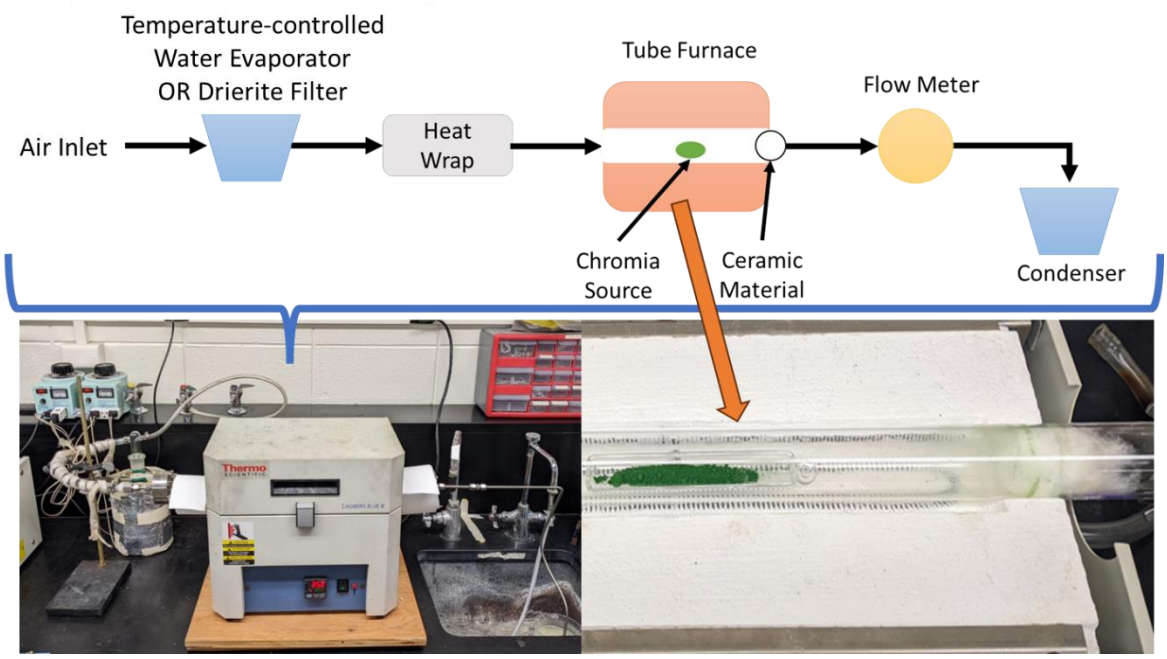

Figure 4 – Experimental design diagram (top), experimental design setup with temperature-controlled water evaporator at gas inlet (bottom left), and quartz crucible containing chromia powder placed upstream from ceramic insulating fiber plug in experimental setup (bottom right).

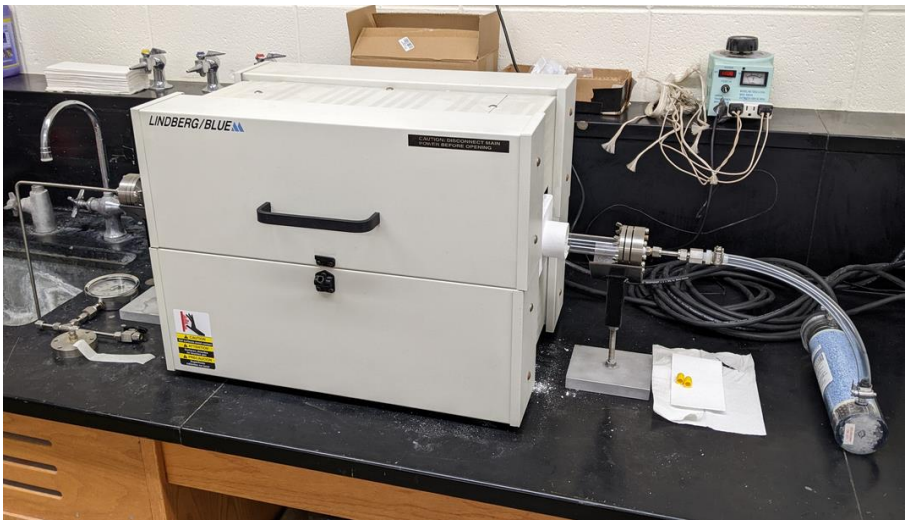

Figure 5 – Second tube furnace experimental setup with Drierite filter attached to gas inlet to reduce water vapor content.

High-temperature gases interact with chromia powder, forming gaseous Cr compounds. Formed Cr compounds depend on constituents of input gas flow (O_2 with or without H_2O). The

resulting Cr vapor species flow to the furnace exit where the target material (2 g of ceramic insulating fibers) is placed with approximately half of the sample located within the furnace and the other half located on the outside with the center of the sample placed at the furnace exit threshold. This process is presented as a flow chart in Fig. 6.

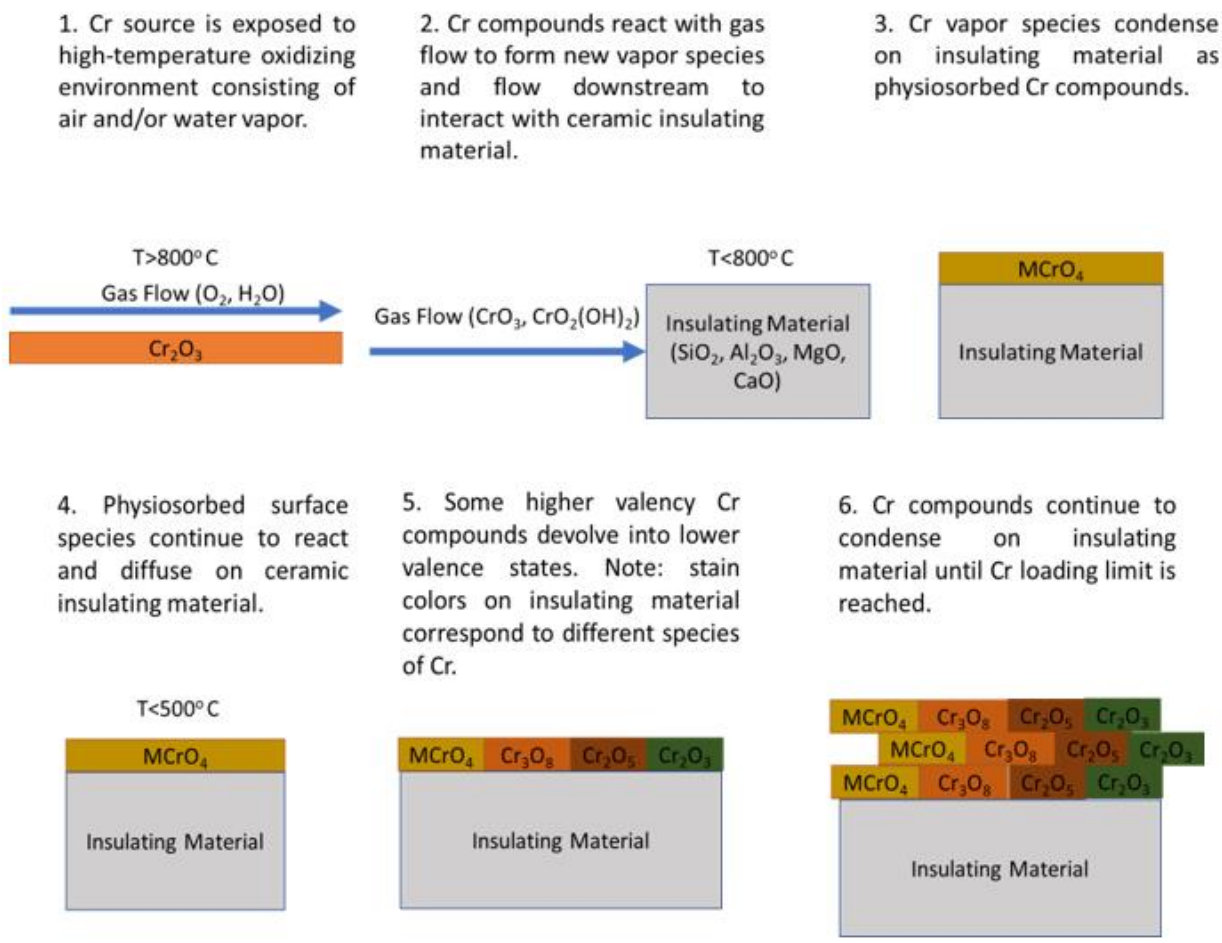

Figure 6 – Experimental design flow chart of reactions and interactions.

The temperature gradient at the exit of the furnace, where the aluminosilicate fiber samples are located, is measured using a k-type thermocouple. The resultant gradient starts at 800°C on the inside edge of the furnace, decreasing to 500°C at the furnace exit threshold, and finally decreases to 160°C on the outside edge. This temperature gradient is illustrated below in Fig. 7.

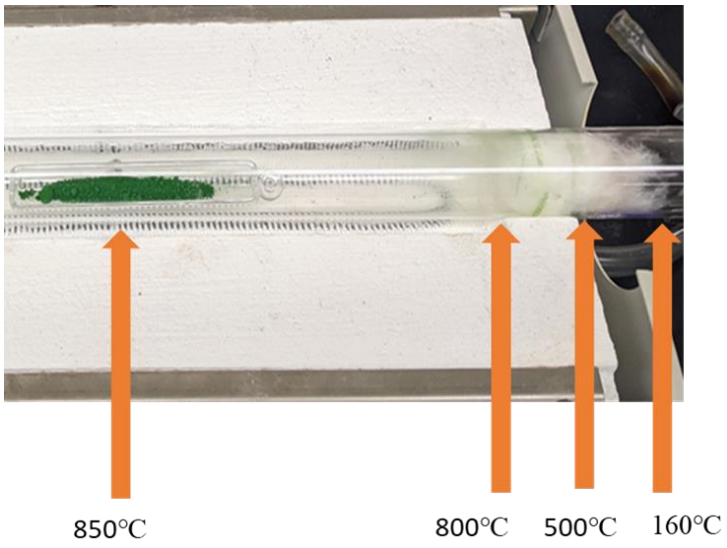

Figure 7 – Temperature gradient of tube furnace at chromia source and ceramic insulating fiber plug locations.

Analytical Methods

Analysis is completed using several instruments and techniques chosen due to their availability and practicality. Ceramic insulating fiber samples are characterized before being used in experiments to measure fiber diameters (average and standard deviation) as well as chemical composition. These measurements are completed using a Zeiss Supra 55VP Field Emission Scanning Electron Microscope (FE-SEM) with Energy Dispersive X-ray Spectroscopy (EDX) detector as seen below in Fig. 8. These measurements are cross-checked with available ceramic insulating fiber manufacturer information. EDX analysis has its limitations, however, and these include a lower limit to detectable concentrations (>0.01 wt%) and detecting lighter elements with atomic numbers below eleven. Geometry and positioning of fibers also influence EDX results. To counter this effect, each sample is prepared for analysis, positioned, and analyzed under

comparable conditions. Samples are coated in Iridium (IR) via sputtering at 20 mA for 90 s before being analyzed via FE-SEM and EDX (presented below in Fig. 9).

Figure 8 – Zeiss Supra 55VP Field Emission Scanning Electron Microscope (FE-SEM) with Energy Dispersive X-ray Spectroscopy (EDX) detector located in Imaging and Chemical Analysis Lab (ICAL) at Montana State University.

Figure 9 – Emitech K575X Peltier cooled metal coaters used for SEM sample preparation, located in Imaging and Chemical Analysis Lab (ICAL) at Montana State University.

The goals of post-exposure analysis of samples (after a transpiration experiment) are to obtain measurements of total condensed Cr compounds formed and Cr(VI) condensed compounds formed on each sample. Total Cr measurements are obtained using a SPECTROBLUE EOP TI

Inductively Couples Plasma Optical Emission Spectroscopy (ICP-OES) as seen below in Fig. 10. Post-exposure samples were analyzed for total Cr and Cr(VI). Cr(VI) measurements are made using direct UV-VIS using a ThermoSci Genesys 20 spectrophotometer with a visual colorimetric diphenyl carbazide (DPC) water test kit from Chemetrics for Cr(VI) as seen in Fig. 11 and 12 below. ICP-OES can detect metals and several non-metals in liquid samples at very low concentrations from 1-5 ppb and up to 100 ppm. Measurements above 0.01 ppm (10 ppb) obtained with the SPECTROBLUE EOP TI ICP-OES have an uncertainty of ~10%, however measurements below this threshold increase in uncertainty to ~40%. DPC is a visual or spectroscopic colorimetry technique that utilizes a reaction between DPC and Cr(VI) in acidic conditions, creating a red-violet color in direct proportion to the Cr(VI) concentration. Measurements were made against a color comparator and expressed as ppm (mg/L) CrO_4. DPC is limited to lower concentrations (0-0.8 ppm) before relative standard deviation increases to 20-50% whereas direct UV-VIS can be used for concentrations above 0.8 ppm and up to 100 ppm with relative standard deviations of 0.5%[11]. Spectrophotometer measurements are taken at λ=540 nm for DPC and λ=340 nm for direct UV-VIS.

Figure 10 – SPECTROBLUE EOP TI Inductively Couples Plasma Optical Emission Spectroscopy (ICP-OES) instrument located in Environmental Analytical Lab (EAL) at Montana State University.

Figure 11 – CHEMetrics diphenyl carbazide (DPC) reaction-based Cr(VI) detection kit (left) and color comparator (right).

Figure 12 – Thermo Spectronic Genesys 20 spectrophotometer located in Gannon Lab.

Solid samples, such as the fibers in this study, require preparation via acid digestion before analysis via ICP-OES or DPC/Direct UV-VIS. Samples are digested using an acid digestion process based on Method 3050B, a sample preparation acid digestion methodology developed by the Environmental Protection Agency (EPA) for sediments and soils[12]. The modified method used in these studies utilizes a 0.5 M nitric acid solution prepared by adding 3 mL of concentrated 68% stock HNO_3 acid and 100 mL distilled water in a laboratory glass vessel containing the fiber sample. The vessel is placed on a hot plate set to 90-95℃ in a chem hood and allowed to heat for 1 hour. After 1 hour, the vessel is removed from the hot plate and allowed to cool. Once cooled, the solution is diluted to 0.1 M HNO_3 concentration by adding an additional 62 mL distilled water before being filtered through filter paper into a secondary vessel. Filtered samples are filtered a second time using a sub-micron syringe filter before being analyzed.

Computational Thermodynamic Equilibrium Modelling

Computational thermodynamic equilibrium modelling of the system was completed by colleagues at Swinburne University of Technology and University of the Sunshine Coast using FactSage 8.2. The FactSage databases used in the calculations included FactPS and FToxid, the products selected were ideal gases, pure solids, and all solutions, and the chosen parameters used in calculations were: 1 atm total pressure, 850℃ for evaporation, 100-800℃ for condensation. The goal of the thermodynamic equilibrium calculations is to corroborate the observed trends of total condensed Cr seen in experimentation. To achieve this goal, several calculations are required. First, Cr evaporation from a pure, solid Cr source (2 g) with respect to water vapor content is calculated. This calculation is repeated for 50/50 mixed, solid alkaline oxide/Cr sources (2 g). Each resulting set of vapor species is used to calculate the condensed Cr species formed on each aluminosilicate sample. The calculations used in computational thermodynamic equilibrium modelling are presented below:

$$Cr_2O_3(s) + \langle A \rangle H_2O(g) + \langle B \rangle O_2(g) \qquad \text{Eq. 1}$$

$$\text{Gas stream of [1] + Aluminosilicate(s)} \qquad \text{Eq. 2}$$

$$Cr_2O_3(s) + CaO/MgO + \langle A \rangle H_2O(g) + \langle B \rangle O_2(g) \qquad \text{Eq. 3}$$

$$\text{Gas stream of [3] + Aluminosilicate(s)} \qquad \text{Eq. 4}$$

From the above equations, Eq. 1 was used to calculate stabilities and magnitudes of Cr vapor species with respect to water vapor content and Eq. 2 was used to calculate the stabilities and magnitudes of resulting condensed Cr species from Equation 1. Similarly, Eq. 3 was used to calculate stabilities and magnitudes of Cr vapor species with respect to alkaline oxide content in the Cr source while Eq. 4 was used to calculate the stabilities and magnitudes of resulting condensed Cr species from Eq. 3. The reactions modelled over varied water vapor concentration content as outlined below in Table 1. Tables of the thermodynamic equilibrium calculation results from FactSage are presented in Appendix A: Thermodynamic Equilibrium Modelling Data.

Table 1 – The percentage of water vapor content percentage translated into water and oxygen gas weights used in FactSage modelling.

%H_2O	**H_2O (g)**	**O_2 (g)**
0%	0	1619.9
1%	43.4	1603.7
2%	86.9	1587.6
3%	130.3	157.4
4%	173.7	1555.2
5%	217.1	1539
6%	260.6	1522.8
7%	304	1506.6
8%	347.4	1490.4
9%	390.9	1474.2
10%	434.3	1458

CHAPTER THREE - REACTIVE EVAPORATION AND CONDENSATION OF CHROMIUM: A REVIEW

Contribution of Authors and Co-Authors

Manuscript(s) in Chapter(s) 3

Author: Travis K. van Leeuwen

Contributions: Graduate research assistant

Co-Author: Ryan Dowdy

Contributions: Undergraduate research assistant

Co-Author: Amberly Guerrero

Contributions: Undergraduate research assistant

Co-Author: Paul Gannon

Contributions: Primary investigator

Manuscript Information

T. K. van Leeuwen, R. Dowdy, A. Guerrero, and P. Gannon

Journal of Power Sources

Status of Manuscript:
☐ Prepared for submission to a peer-reviewed journal
☐ Officially submitted to a peer-reviewed journal
☐Accepted by a peer-reviewed journal
[x] Published in a peer-reviewed journal

Elsevier
15 July 2023
DOI 10.1016/j.jpowsour.2023.233065

Abstract

The reactive evaporation of chromium (Cr) from stainless steels in high-temperature (>500 ◦C) service environments (e.g., air, steam) has been extensively investigated. The subsequent condensation of Cr-containing vapors and deleterious impacts on solid oxide fuel cell components has also received significant research attention. However, the condensation of Cr-containing vapors onto silica-based insulation and other common materials in high-temperature applications is poorly understood. This review briefly covers the reactive evaporation of Cr from stainless steels but focuses on reactive condensation processes and their dependencies on materials and environmental conditions. First, known Cr sources and associated health hazards are presented. Next, the corrosion behaviors of stainless steels under different exposure conditions are discussed along with the reactive evaporation of Cr species and the pathways of Cr vapor condensation on various surfaces under differing conditions. Lastly, the effects of Cr condensation on SOFC components and other industries in which Cr(VI) formation has been identified are discussed in context of ongoing research into the mobility and evolution of condensed Cr species. Current research includes expanding on the condensation mechanisms of volatile Cr species and exploring the mobility of surface Cr species. For example, the importance of substrate surface chemistry and morphology on Cr collection/surface speciation are of interest to researchers. Long-term saturation conditions via transpiration experiments for high surface area substrate materials such as glass fibers and wools are topics of investigation.

Introduction

Hexavalent Cr, Cr(VI), is an established byproduct across multiple industries including refractories, leather tanning, and dye pigment factories. Cr(VI) containing byproducts poses both a risk to the environment and a health hazard to humans. Recently, Cr(VI) species generated from stainless steels in contact with ceramic insulating materials in environments of temperatures above 500^{o} C has become a concern prompting further investigations [13, 14].

Stainless steels are a class of materials referring to iron-based metal alloys that contain varying amounts of elements such as nickel (Ni), molybdenum (Mo), and Cr to improve corrosion resistance. Ni is used in alloys to increase resistance to pitting corrosion and commonly used alongside Zinc in electroplating processes to improve overall corrosion resistance [15-17]. These iron-based alloys are often used in extreme environments and elevated temperatures (≥500°C). Stainless steels are used in applications such as internal combustion engine systems, various power/chemical plant process equipment, and interconnects for solid oxide fuel cells (SOFCs). Cr plays a key role in the oxide layer of all classes of stainless-steel alloys by forming trivalent chromia (Cr_2O_3)-based oxides on the surface that protect the underlying stainless-steel alloy. Reactive evaporation of these surface oxide layers occurs at elevated temperatures to form volatile Cr species such as $CrO_2(OH)_2$ and CrO_3. This process compromises the protection of stainless steels and can cause detrimental effects downstream from the Cr source. Such effects include SOFC performance degradation and hazardous materials generation.

High-temperature oxidizing environments with or without water vapor degrade surface passivation layers by promoting reactive evaporation of surface compounds. Eventually, this process compromises the protection of the underlying alloy by consuming the Cr reservoir required

to reform the protective surface oxide. This applies to many oxides but is especially true for chromia forming compounds such as those used in stainless steels. The protective chromia layer transforms into a mobile vapor species upon reactive evaporation and interacts with the surrounding system. These interactions form compounds that can pose risks to human health, the environment, and degrade performance in electrochemical devices like SOFCs.

Volatile Cr species generation and deposition is influenced by environmental factors such as temperature, time, and atmospheric water content [18-20]. However, the substrate material on which condensation occurs is also a critical factor. Material properties such as surface hydroxyl chemistry and available surface area of the material appear to have the most influence on deposition [21-23]. Hydroxyl groups serve as anchoring points for volatile species and Cr deposition increases with increasing surface hydroxyl populations and basicity.

Chromium Chemistry, Known Sources, and Health Hazards

Stable Cr compounds in nature form ionic solids and have a trivalent, Cr(III), or hexavalent oxidation state. Cr(III) is naturally occurring, a necessary nutrient, and is generally not hazardous to the environment [24]. Unlike Cr(III), Cr(VI) releases into the environment are largely generated from manufactured processes, is very toxic, and a known carcinogen [25, 26]. Industrial processes such as smelting, fuel combustion, leather tanning, electroplating, and textile manufacturing are responsible for most environmental releases of Cr(VI) [26].

Regulatory bodies governing environmental and industrial releases of Cr have prescribed limits for safe exposure levels. In the United States, the maximum contaminant level for total Cr (all valence states) in drinking water is 0.1 mg/L [24]. The permissible exposure limit (PEL) to which a worker may be exposed to airborne chromic acid, and/or chromates (Cr(VI)) over the

course of eight hours, is 5 μg/m^3. This limit is two orders of magnitude greater for trivalent Cr species [24]. The recommended dietary allowance (RDA) of Cr(III) is 25 - 35 μg for adults [27]. OEL (operating exposure limit) for EU countries range from 5 μg/m^3 to 0.05 mg/m^3 for Cr(VI) exposures [28]. It's also important to recognize that while Cr(III) is necessary for human health in trace amounts, it can also be toxic at high levels. Ingestion of large amounts of Cr(III) can cause nausea, vomiting, diarrhea, and ulceration of the digestive tract. Conditions exceeding prescribed limits for either Cr(III) or Cr(VI) are toxic and/or carcinogenic for plants, microbes, animals, and humans [24-26].

The toxic effects of Cr(VI) are due to its ability to generate reactive oxygen species (ROS) in the body, which can cause damage to DNA and other cellular components. In addition to its potential to cause cancer, Cr(VI) exposure can also lead to a range of other health effects, including respiratory irritation, allergic reactions, and kidney and liver damage.

Chromium in the Environment

Natural and manufactured Cr is spread to multiple environmental media including ground water, sea water, soil and sediments, rocks, and air. In ground water and soil, Cr exists primarily in two oxidation states: Cr(VI) and Cr(III). Cr(III) compounds are sparingly soluble in water whereas Cr(VI) compounds are very soluble. Cr(VI) solutions are powerful oxidizing agents in acidic conditions but are less so in basic conditions [26]. The Cr species that will form in a particular environment depends upon the pH, redox potential, and the total concentration of Cr. Cr(III) compounds are generally considered to be less toxic than Cr(VI) compounds. However, both forms of Cr can have negative impacts on the environment, depending on the specific circumstances and the levels of exposure.

Wildfires create highly oxidizing environments with the potential to affect any present chemical compounds in the soil or in residential or industrial debris. Cr species, specifically, can be converted to their more toxic form, Cr(VI). Furthermore, the combustion of wood and wood products form highly basic conditions resulting in the stabilization of any aqueous Cr(VI) compounds formed. A study was performed to measure the potential effects of fire-impacted soils and ashes on human and environmental health from samples collected after the October 2007 wildfires in Southern California [29]. Preliminary results show the Cr present from the soil and ash was in the form of Cr(VI) and the resulting high pH stabilized Cr(VI) from reducing back to Cr(III). The long-term effects of Cr(VI) on the environment can depend on the specific chemical form of the compound and the levels of exposure. It may be necessary to take remedial action to address elevated levels of Cr(VI) in fire-impacted soils and ashes to protect human and environmental health.

Cr(VI) has significantly higher solubility in water compared to Cr(III), resulting in relatively more bioavailable species and persistence in the natural environment. Cr may contaminate groundwater through leakage from chromate mines or inappropriate disposal of mining tools and supplies [30]. Water contamination is more likely to be found in surface water because Cr forms strong bonds with the soil and is generally contained within the silt layer surrounding the groundwater reservoir. Cr pollution in soil and groundwater due to various human activities has become a serious source of concern to animal and plant health over the last decade. Some studies have shown that high levels of Cr in drinking water can cause adverse health effects, such as digestive problems, skin irritation, and respiratory problems. Thus, it is important to

carefully monitor and regulate the levels of Cr in water and soil to protect human and environmental health.

Corrosion Behaviors of Stainless Steels

Stainless steels are sought after as materials for a wide range of engineering applications due to their ease of manufacturing, low costs, and stability over a large temperature range, from cryogenic conditions to temperatures exceeding 1000°C [31, 32]. Temperatures exceeding 1000°C is ambitious for many grades of stainless steel, but for some alloys, such as 310 and 330 grades, maximum operating temperatures can reach 1035 – 1150°C [33, 34]. This stability is due to the formation of a surface oxide layer on the exterior of the material, which acts as a protective barrier against corrosion of the alloy. Cr plays a key role in the surface oxide layer formed on most classes of stainless-steel alloys and ranges from ~10-27 wt% in standard alloy compositions with the exception of alumina forming austenitic alloys (AFAs) which can have as little as 2.5 wt% Cr content [35] whereas ferritic stainless steels include grades in the 400s (e.g., 430, 441, 444, 445) with a minimum of 10.5% Cr content [36].

Furthermore, reactive evaporation of Cr can compromise oxide scale integrity or oxide scale reformation. Chromia may volatilize more quickly than it can be replenished, eventually causing the formerly protective oxide to become a less protective scale such as $(Fe, Cr)_2O_3$ or iron oxides [37, 38].These iron oxides may lead to breakaway corrosion of the alloy and affect the material properties of the alloy. Spinel and perovskite phase oxides, however, are more resistant to reactive evaporation than chromia and may help reduce the breakdown in protective behavior of the oxide layer [39-42].

Reactive Evaporation

Reactive evaporation occurs when a partial pressure of a reactive gas interacts with a solid or liquid surface to form new gaseous species between the reactive gas and surface compounds. High temperature (≥500°C) oxidizing environments provide the conditions for chromia to experience reactive evaporation [43-45]. In the presence of water vapor, the dominant volatilization pathway will proceed [43-48]. Example reactions for chromia evaporation include:

$$\tfrac{1}{2}Cr_2O_3(s) + \tfrac{3}{4}O_2(g) = CrO_3(g) \qquad \text{Eq. 5}$$

$$\tfrac{1}{2}Cr_2O_3(s) + H_2O(g) + \tfrac{3}{4}O_2(g) = CrO_2(OH)_2(g) \qquad \text{Eq. 6}$$

Influence of Water Vapor

Reactive evaporation of Cr from chromia occurs more often in atmospheres of oxygen and water vapor with the respective reactions presented above in Eq. 5 and 6. For example, thermodynamic data collected from gaseous Cr compounds reveals an equilibrium partial pressure of $8x10^{-40}$ bar for $CrO_3(g)$ at 298 K [49]. An increase of 500 K increases this partial pressure by several orders of magnitude to $1x10^{-15}$ bar. The partial pressure of Cr oxyhydroxide ($CrO_2(OH)_2(g)$) is observed to be larger in the presence of water vapor by many orders of magnitude up to 1400 K, as seen below in Fig. 13.

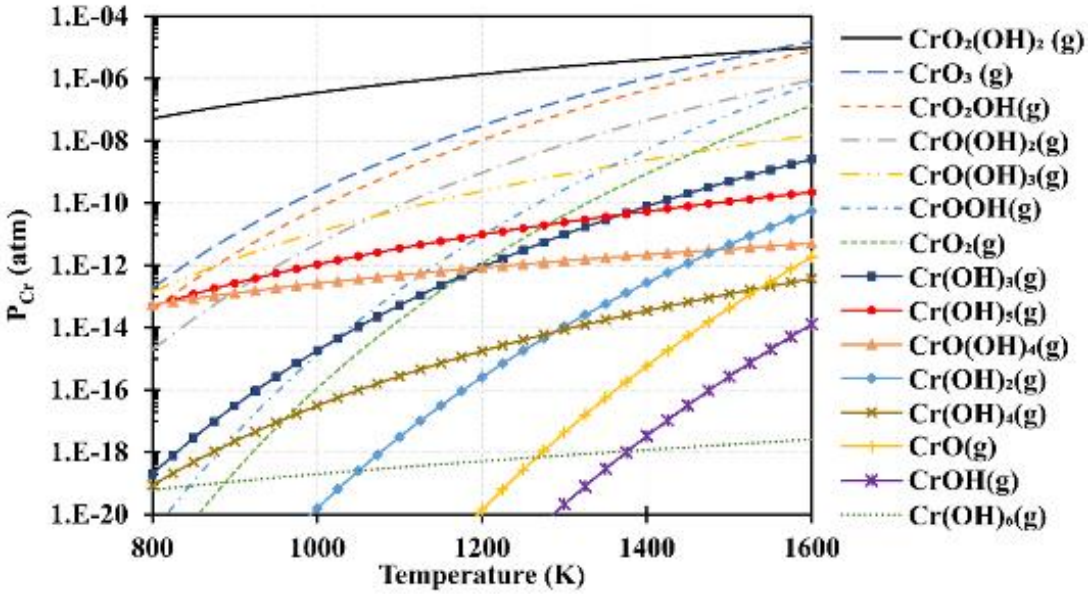

Figure 13 - Partial pressures of gaseous Cr species at 1 atm 3% P_{H2O} and 21% P_{O2} humified air [50].

Oxide scale growth of varying compositions of Fe-Cr steel alloys was investigated by researchers. [4]. In environments with 30% H_2O and low P_{O2}, water vapor led to rapid scaling kinetics and higher Cr content improved their resistance. Higher P_{O2} resulted in breakaway oxidation and volatilization of $CrO_2(OH)_2$ coupled with increased chromia growth.

The effects of fluid dynamics play a significant role in evaporation rates of Cr from oxide scales and impacts the limiting thicknesses for those scales [45, 46]. In a closed system, the equilibrium partial pressures of all created vapor species at a given temperature is eventually reached. After this point, further disturbance to the oxide scale is greatly decreased. The conditions in question, however, do not resemble a closed system and the gaseous environment will be flowing past the Cr source with some velocity. This velocity influences the thickness of the boundary layer, the region closest to a surface where viscous forces distort the surrounding flow. The Reynolds number, the ratio of inertial to viscous forces within a fluid, affects the rate of Cr

evaporation. Researchers have observed an upper limit to this rate [45, 46]. The results of the studies propose a limitation to Cr evaporation, even as the flow rate continues to increase.

The observed limits on Cr evaporation occur in laboratory settings that lack the proper environmental conditions to simulate the extreme service environments of high-pressure steam turbines or SOFCs. Evaporation rates for these conditions have been calculated in a study [48]. Calculations using conditions for an advanced steam turbine yield evaporation predictions as high as 5.18×10^{-8} kg/m^2/s of $CrO_2(OH)_2(g)$ at 760°C and 34.5 MPa. Thermodynamic modeling and transpiration experiments are used to confirm these assumptions.

Transpiration Experiments

Transpiration experiments involve generating a volatile species by flowing a reactant gas over a compound of interest in a temperature-controlled environment. With respect to the topic of this review, the compound of interest is chromia and the reactant gas is dry air or air partially saturated with water vapor. These gases react with chromia to form volatile Cr species in the forms of Cr trioxide and Cr oxyhydroxide, respectively. These gas species may diffuse through the boundary layer and part of the bulk flow. As the vapor species move downstream, the temperature decreases, and compounds begin to condense. Fig. 14 displays a diagram of the experimental setup for the transpiration experiment used [43].

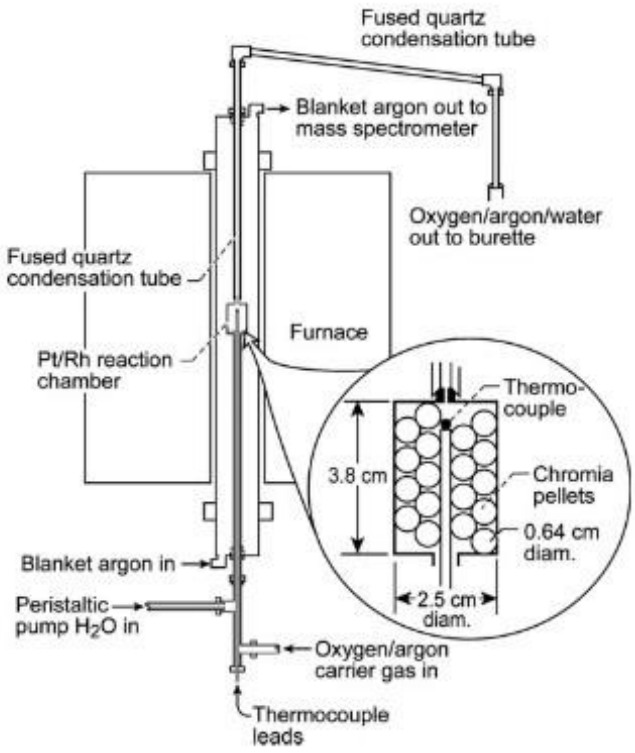

Figure 14 - Transpiration experiment setup [43]. Reprinted (adapted) with permission from "Theoretical and Experimental Investigation of the Thermochemistry of CrO2(OH)2(g)", Elizabeth J. Opila, Dwight L. Myers, Nathan S. Jacobson, Ida M. B. Nielsen, Dereck F. Johnson, Jami K. Olminsky, and Mark D. Allendorf. The Journal of Physical Chemistry A 2007 111 (10), 1971-1980 DOI: 10.1021/jp0647380. Copyright 2007 American Chemical Society.

Some of the volatile species condense on the tube walls [43, 51].Condensed species are washed from the quartz tube using solvents such as water, nitric acid, or hydrofluoric acid [43, 51, 52]. Dissolved Cr is quantified using materials characterization techniques such as inductively coupled plasma mass spectroscopy (ICP-MS). The partial pressure of volatile Cr species can then be calculated using the ideal gas law and the quantified condensate.

As for the presented study, researchers performed Cr transpiration experiments at 600°C using chromia pellets as the Cr source [43]. The goal of the experiments was to determine the effects of oxygen and water on Cr collection. The first experiment kept the oxygen partial pressure

constant while varying the partial pressure of water vapor. The other experiment held the partial pressure of water constant while varying the oxygen partial pressure. The calculated partial pressure of volatile Cr species was plotted for each run (see Fig. 15).

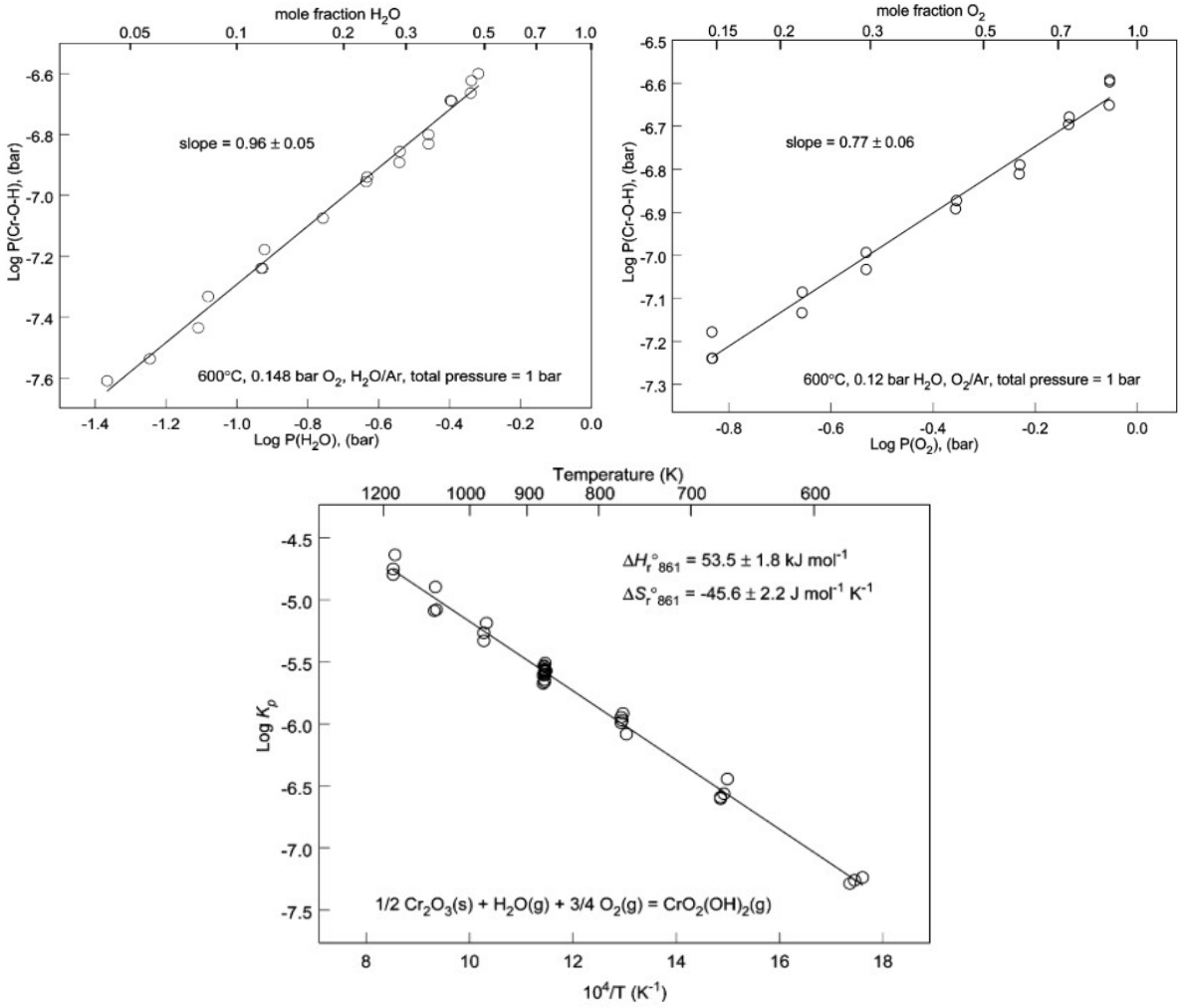

Figure 15 - Log-log plot of volatile Cr species partial pressure against varied water partial pressure (left), oxygen partial pressure (right), and natural log of equilibrium constants plotted against inverse temperature [43]. Reprinted (adapted) with permission from “Theoretical and Experimental Investigation of the Thermochemistry of CrO2(OH)2(g)”, Elizabeth J. Opila, Dwight L. Myers, Nathan S. Jacobson, Ida M. B. Nielsen, Dereck F. Johnson, Jami K. Olminsky, and Mark D. Allendorf. The Journal of Physical Chemistry A 2007 111 (10), 1971-1980 DOI: 10.1021/jp0647380. Copyright 2007 American Chemical Society.

The best fit lines with slopes of 0.96 ± 0.05 and 0.77 ± 0.06 are indicative of monomial relationships. The transpiration experiments were performed at temperatures between 300-900°C and an equilibrium constant for each set was then calculated. The natural log of these equilibrium constants is plotted against inverse temperature (see Fig. 15, bottom). The slope relates to the enthalpy and y-intercept relates to entropy through a form of the van't Hoff expression.

Reactive evaporation of Cr in the field often occurs in complex dynamic environments containing a variety of chemical components. These environments and their constituent chemical components can affect the Cr evaporation rate. A study evaluated Cr evaporation rates from various stainless steel alloys containing varying amounts of Ni, Al, and Mn [53]. The study found that the presence of these elements lowers the evaporation rate of Cr, indicating that the volatility of Cr can be influenced by the presence of other elements. Another study investigated the influence of manganese (Mn) from Ni-Cr alloys. It was found that Mn additions lead to the formation of Mn–Cr spinels and can reduce Cr evaporation by as much as a factor of 35 at 800 °C and 55 at 700 °C [40].

Thermodynamic Modeling

Thermodynamic modeling is used to calculate the most stable condition using Gibbs free energy according to the second law of thermodynamics. This process involves modeling a condensed phase with a gas phase. The sum of chemical potential multiplied by their molar quantities yields the total Gibbs free energy of the system. In the gas phase, each component chemical potential is determined by its partial pressure and, assuming the ideal gas condition, substituting the partial pressure for fugacity. Pure chromia in the condensed phase has an activity equal to one and therefore requires no chemical potential adjustment.

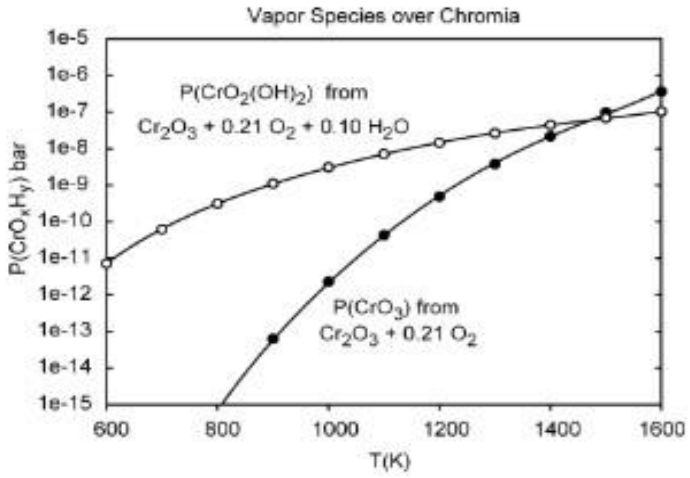

Figure 16 - Thermodynamic modeling [44].

Thermodynamic modeling of $CrO_2(OH)_2$ and CrO_3 over temperatures ranging from 600-1600 K is displayed in Fig. 16. The vapor pressure of $CrO_2(OH)_2(g)$ is greater than that of $CrO_3(g)$ over chromia until ~1400 K. The disparate vapor pressure of $CrO_2(OH)_2(g)$ and $CrO_3(g)$ is unexpected as $CrO_2(OH)_2(g)$ is larger than $CrO_3(g)$. It is important to note here that there is a discrepancy between Fig. 13 and Fig. 14 despite representing the same data. There is a lack of sufficient empirical data to obtain accurate approximations with appropriate margins for error as currently there are orders of magnitude difference [54]. Further experimentation and modeling are needed to confirm the relationship between the partial pressures of $CrO_2(OH)_2/CrO_3$ and temperature.

Volatility is dependent on two attributes: the stability of the resulting vapor phase compound and the strength of intermolecular forces in the condensed phase. There is an inverse relationship between the vapor pressure of a compound and its size due to London dispersion forces as these forces typically increase with larger molecule with more electrons [55]. However, this relationship does not hold for all cases such as polar molecules. For example, CF_4 is larger

than CHF_3, but has a lower vapor pressure than the latter [56, 57] due to Gibbs energy of vaporization becoming less favorable with increasing molecule size. This observation applies when comparing alkanes, alkenes, alkynes, and alcohols with other molecules within the same family [55]. Unfavorable energy of vaporization corresponds with lower vapor pressures and results in unstable products in the gas phase relative to the liquid phase. This agrees with the stated inverse relationship between vapor pressure and molecule size. Differences in vapor pressure between CrO_3 and $CrO_2(OH)_2$ are attributable to both stability and intermolecular forces.

Researchers have proposed a mechanism for the formation of surface CrO_3 species in wet and dry conditions [58, 59]. First, oxygen reacts with chromia to form [-O-(CrO_2)-O-(CrO_2)-] repeating units with a given vapor pressure at a given temperature (see Fig. 16). Conversion of CrO_3 to $CrO_2(OH)_2$ occurs through hydrolysis reactions with repeat surface units that results in the severing of Cr-O-Cr bonds to form $CrO_2(OH)_2$. If CrO_3 volatilizes first, then gas phase hydrolysis occurs to form $CrO_2(OH)_2$. These reactions are exothermic in nature, which coincides with the gap between the equilibrium partial pressures of the two volatile species in Fig. 16. The gap decreases with increasing temperature. Fig. 16 does not account for interactions between the two volatile species and is strictly derived from thermodynamic information on stability of the two molecules. The previously mentioned decreasing partial pressure difference is due to the already unfavorable entropy of $CrO_2(OH)_2$ formation becoming less favorable with increasing temperature. The difference in vapor pressure of CrO_3 and $CrO_2(OH)_2$ is attributed to two factors: dissociation reactions of $CrO_2(OH)_2$ facilitated by hydrolysis and the thermodynamic stability of $CrO_2(OH)_2$ up to 1400 K.

Reactive Condensation

Reactive condensation is defined as a condensation reaction in which the condensate interacts with the surface to form new compounds between the condensate and surface material. Cr reactive condensation mechanisms have been studied regarding preparing Cr catalysts on ceramic supports such as silica, alumina, and aluminosilicate fibers. Cr vapor condensation has also been investigated within SOFC systems as the condensed Cr compounds formed within these systems can degrade performance and affect the overall lifetime of the system. Studying the reaction mechanisms between Cr and ceramic surfaces has direct application to SOFCs as these materials are widely used in the field. For example, alumina-silica glass-ceramics are used as sealants in SOFCs [60, 61]. These materials belong to the SiO_2–Al_2O_3 system and contain different compositions of oxides including CaO, Na_2O, MgO, K_2O, B_2O_3, Y_2O_3, and BaO. Another commonly used sealant material is compressed mica paper [62, 63]. Another sealing material used in SOFCs is mica, a class of silicate minerals that forms into distinct layers. Two types of mica commonly used in SOFC applications are muscovite (potassium aluminum silicate hydroxide fluoride, $KAl_2(AlSi_3O_{10})(F,OH)_2$), and phlogopite (potassium magnesium aluminum silicate hydroxide, $KMg_3(AlSi_3O_{10})(OH)_2$).

Ceramic Catalyst Supports

Industrial Cr catalysts are manufactured upon support materials such as silica, alumina, and aluminosilicates [64]. Techniques such as wetness impregnation or incipient wetness impregnation are used to produce these catalysts. Wetness impregnation involves immersing the support in a solvent then diffusing the impregnating solution from a bulk source into the solution. The pores of the support material are then able to receive the catalyst compounds. Incipient wetness

impregnation drives the introduction of the impregnating solution to the pores of the support material via capillary action. The prepared catalyst and support are dried at 120°C and calcined at temperatures between 500-1000°C.

Deposition of Cr on catalyst supports depends on the support material, temperature, and Cr loading. The behavior of Cr compound formation depends on temperature and whether the surface is aqueous or nonaqueous. Cr present on a hydrated surface form ionic compounds and the most common will be in the forms of Cr^{6+} or Cr^{3+}. Hydrated Cr(III) forms a complex ion that is stable at low pH but may hydrolyze to form hydroxide ligands. At higher pH, in the range of 6-7, Cr(III) exists as a solid Cr hydroxide precipitate [65]. Cr(VI) is stable over most of the pH range and is governed by pH dependent reactions [21, 66]. Similarly, the hydroxyl populations of catalyst support materials are also influenced by pH. Each support material has an isoelectric point (IEP) which is the pH at which the surface of the oxide has a net zero charge. When the solution pH is above the IEP of the catalyst support the surface has a net negative charge. Inversely, when the solution pH is below the IEP of the catalyst support the surface has a net negative charge (see Fig. 17).

Calcined Cr species interact with catalyst supports such as alumina, silica, zirconia, titania, and niobia [67-73] [74-76]. Cr particles undergo esterification reactions with surface hydroxyl groups as alumina and silica supports loaded with Cr are calcined. An esterification reaction produces an ester by replacing a hydroxyl group with an –OR group, where “R” is an unspecified compound. Infrared spectroscopy performed on silica supports reveals that hydroxyl groups are consumed with increasing Cr loading [74, 76, 77]. The transition between hydrated and calcined conditions is shown in Fig. 17 as well.

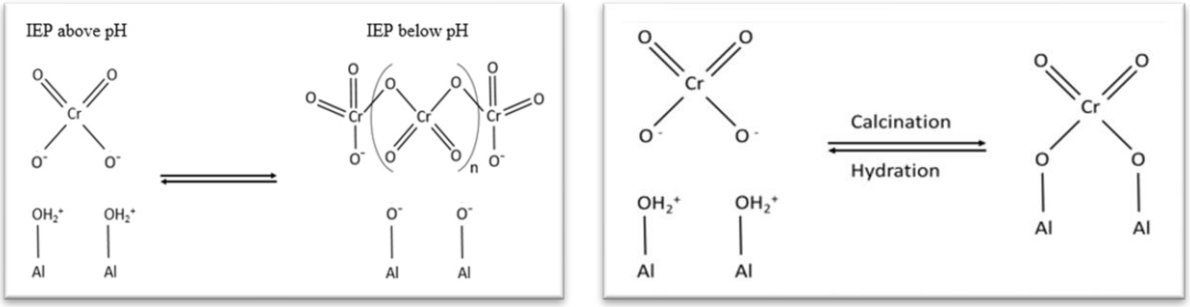

Figure 17 - Hydroxyl groups on catalyst support influenced by IEP and pH (left). Chromate under hydrated/calcined conditions on alumina catalyst support (right) [78].

Researchers measured silanol (Si-OH) using a reaction between methyl magnesium iodide and hydroxyl groups [79]. The results show that collected methane gas relates to hydroxyl group concentration. Increased Cr loading decreases surface hydroxyl populations for temperatures ranging from 200-800°C. In another study, silica exposed to CrO_2Cl_2 was observed to release HCl and was attributed to gas interaction with hydroxyl groups [80]. CrO_2Cl_2 vapor was reproduced following dry HCl exposure. Differential thermal analysis reveals an exothermal peak around 250°C attributed to the esterification reaction [64, 70, 81]. Esterification reactions may occur at temperatures between 150-300°C [22, 82, 83].

Stability of anchored Cr depends on multiple factors including surface material, temperature, and total Cr loading. Varying the Cr loading on the same material at the same temperature has been observed to influence speciation. Researchers investigated Cr supported on silica in different gas atmospheres (1-5 wt% oxygen) for two-hour exposures at 425, 650, and 870°C [84]. Resultant Cr loading was quantified using reflectance infrared spectroscopy. Total Cr(III) was observed to increase by an order of magnitude for all spectra as loading increased. Atmospheric conditions were also observed to have an effect. Dry oxygen resulted in more stable

Cr surface species than wet oxygen, meaning the tendency for anchored Cr to volatilize is greater for the latter.

Researchers have studied alumina and silica supports with Cr loading between 1-9 wt% for alumina and 1-3 wt% for silica [74]. Chromia did not form on alumina until loading at 12 wt% and formed at 3 wt% on silica. In a separate study, alumina loaded with 1-30 wt% Cr was exposed to air at 550°C for four hours. Increasing the loading resulted in polymerization of surface chromate [85].

Chromate on silica has also been shown to polymerize with increased loading, though at lower loading weight percent. Researchers have also investigated the ability of alumina and silica supports to stabilize the monochromate species [86]. The stability of chromate species on alumina is due to its large monolayer coverage [84, 87]. Silica has more surface area, but a hydroxyl population up to four times lower than alumina, resulting in alumina having double the surface coverage [80, 88-90].

Cr species have been observed to be highly mobile on silica surfaces [91]. Chromia was observed to spread on a silica fixed bed in an environment of flowing oxygen at 800°C and resulted in Cr oxidation. This effect was also observed with a mix of chromia and silica powder at 900°C. When mixed the surface Cr species re-oxidized, displaying a color change of green to yellow.

Re-oxidation behavior is related to Cr loading and mobility. A silica surface can unload Cr through migration of surface Cr species resulting in a decrease of Cr loading on the original surface and enabling reoxidation. Several studies have varied the temperature at a given Cr weight percent for the same material as an alternative to varying the Cr loading. For example, researchers exposed silica and alumina supports loaded with 10 mole% Cr to air at 300 and 600°C for five hours [92].

UV-VIS diffuse reflectance spectroscopy and XRD were used to characterize the structure. Temperature programmed reduction (TPR) was used to determine Cr content. Samples did not yield a defined diffraction pattern at 300°C, but at 600°C crystalline Cr_2O_3 was observed. Furthermore, the observed diffraction pattern was far weaker for alumina.

Similar behavior for alumina has been observed when loaded with 5 wt% Cr and exposed to air from 250-1050°C for 16 hours [66]. Researchers reported similar findings for silica loaded with 8 wt% Cr exposed to temperatures ranging from 300-600°C [67]. Analysis using x-ray photoelectron spectroscopy revealed a predominance of Cr^{6+} from 300°C exposure and negligible Cr^{6+} from 500 and 600°C. The difference in behaviors between alumina and silica are attributed to differences in the hydroxyl group population densities of each material. Hydroxyl populations are up to four times as numerous on certain phases of alumina, such as γ-Al_2O_3, when compared to amorphous silica.

Trivalent aluminum, Al(III), is a harder Lewis acid than tetravalent silicon Si(IV) where “hard” is in reference to the Hard Soft Acid Base (HSAB) theory. This theory classifies hard acids as small molecules with high oxidation states and low polarizability. Whereas hard bases are classified as small molecules with high polarizability and electronegativity. Interactions between hard acids and bases result in bonding with strong ionic properties. For example, aluminum is a harder acid than silicon and oxygen is a hard base. Bonding between aluminum and oxygen is predicted to be more stable than that of silicon and oxygen.

Ceramic surfaces undergo de-hydroxylation as the temperature increases. The stronger bonding between oxygen and alumina is influenced by the greater retention of hydroxyl groups by alumina as the temperature increases. At 400°C amorphous silica has been observed with hydroxyl

group density of 2.35 OH/nm^2 whereas γ-Al_2O_3 has been observed with 4-6 OH/nm^2 [80, 88]. This is important to note for alumina as it has a denser hydroxyl group population and is expected to collect more Cr than silica.

Interactions Between Volatile Chromium Species and Ceramic Surfaces

Reactive condensation of Cr on catalysts supports, such as alumina and silica, and on SOFC components, such as those made from manganese or strontium, are well documented. However, there is a distinct lack of publications that focus purely on the chemical and physical processes that occur during condensation reactions of Cr on a variety of materials and surface conditions, e.g., [78, 93, 94]. In this work, aluminosilicate fibers were exposed to volatile Cr species for 150 hours at temperatures between 100-230°C. X-ray photoelectron spectroscopic (XPS) analysis was used to characterize the condensed species, revealing that Cr(VI) and Cr(III) content varied by location on the sample. The resultant condensed species were correlated with different regions and discoloration on the exposed fibers. The experimental setup used was like the transpiration experiment previously presented (see Fig. 14) [43]. T409 stainless steel was used to generate volatile Cr species to contaminate aluminosilicate fibers placed downstream at the exit of the furnace. The inlet gas enters the temperature-controlled furnace, interacts with the T409SS strips at 700°C, and interacts with the aluminosilicate fibers outside of the furnace. Temperature zones of 100–230°C were recorded at the location of the fibers.

XPS was used to characterize color-stained regions on the exposed aluminosilicate fibers. Stains of varying color were observed to collect on the aluminosilicate fibers upon exposure to volatile Cr species for 150 hours at 100-230°C. Fig. 18 shows the observed color gradient of dark

brown to light brown (right to left) and these colors correspond with high to low temperature. Dissecting the sample reveals three colors: brown, green, and yellow.

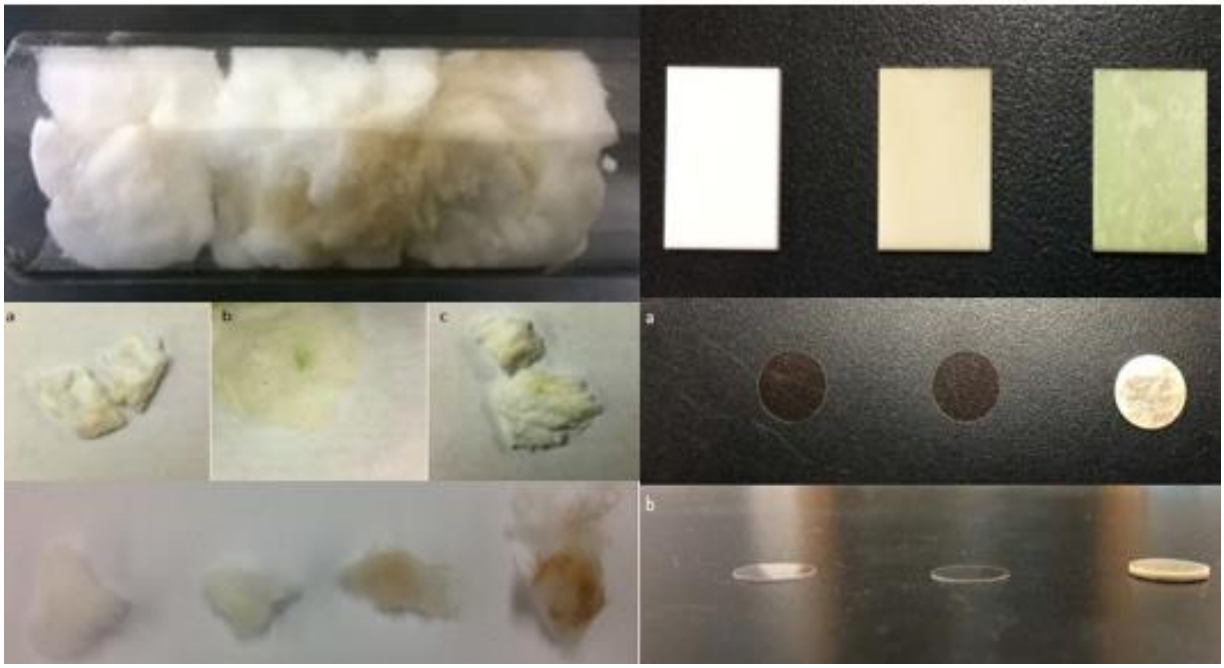

Figure 18 – Staining on aluminosilicate fibers post exposure (top left) and separated (middle left). From left to right: brown (a), green (b), and yellow (c). Discoloration on quartz wool after exposures (bottom left). From left to right: non-exposed quartz wool, yellow, light brown, and dark brown. Discoloration on alumina after exposures (top right). From left to right: non-exposed alumina, brown, and green. Mica samples and thicknesses post exposure (middle right and bottom right). From left to right: non-exposed mica, 150-500°C mica, and 700-900°C mica with top view (a) and side view (b) [78].

Some colors have been linked to different Cr oxidation states and compounds. Brown and yellow are attributed to hexavalent Cr species and green to trivalent Cr species [18, 21, 95]. Visual inspection provides some information into Cr oxidation states and speciation, but this method is inadequate for distinguishing all present compounds in subtle mixtures of color. As a result, it is expected to see a mixture of compounds in the XPS spectra generated from individual samples.

Fig. 19 displays the Cr $2p_{3/2}$ energy windows ranging from about 572-582 eV for brown, green, and yellow staining.

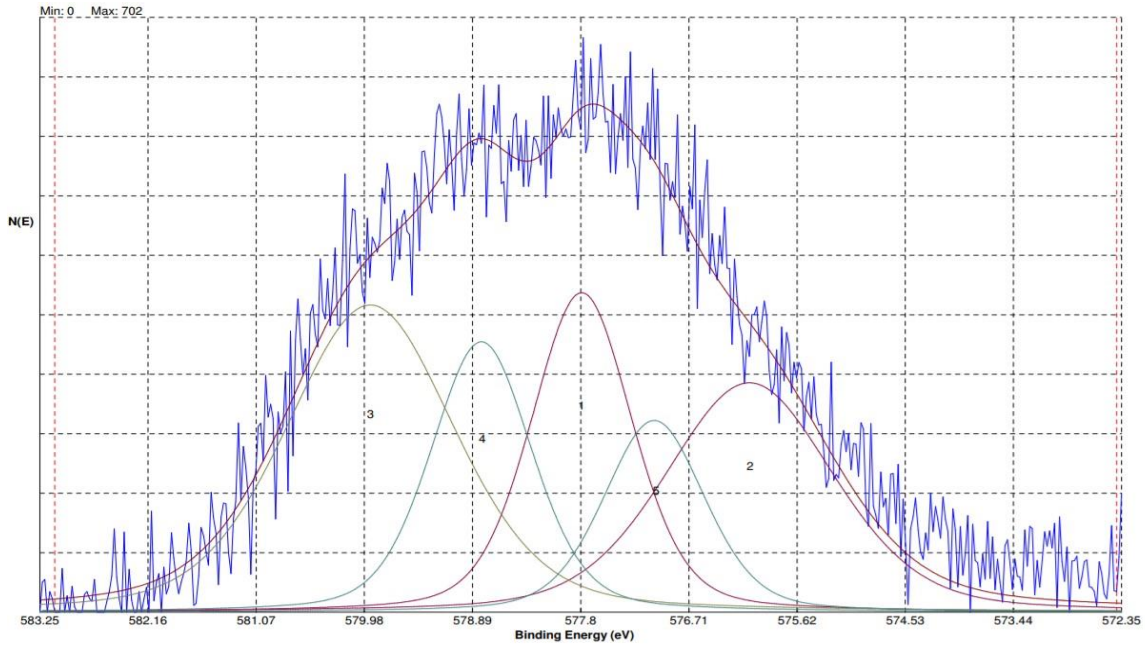

Figure 19 - Cr $2p_{3/2}$ energy window for brown staining on aluminosilicate fibers. Peaks 1, 2, 4, and 5 are trivalent multiplet-split components. Peak 3 is the hexavalent component [78].

A range of binding energies for chromate and Cr trioxide from 578.3-581.1 eV with some conflicting reports of higher chromate or Cr trioxide binding energy has been observed [83, 96-101]. Overlapping binding energies make it difficult to differentiate individual peaks with which compound is present based on binding energy alone. Based on color, yellow staining is associated more with hexavalent monochromate and brown staining with hexavalent Cr trioxide.

The peak associated with the lowest binding energy is assigned to Cr^{3+} and represents a contribution from chromia. The binding energy range of 576-576.3 eV agrees with literature reports on Cr_2O_3 [66, 99, 101]. Peak contribution from Cr^{4+} is likely in the form of CrO_2 and the Cr $2p_{3/2}$ peak for CrO_2 has been observed to occur around 575.2 eV [100, 102]. CrO_2 has been

observed to have a lower binding energy than Cr^{3+} species repeatedly [96, 100, 102, 103]. The peak is not easily discernible for spectra taken from any of the stains. The binding energy of CrO_2 may appear larger than actuality due to de-hydroxylation of silica/alumina surfaces as the temperature increases. Electron density at the surface decreases as more hydroxyl sites are lost and decreased electron density results in decreased electron density of surface Cr species. This phenomenon results in an increase of binding energy.

Researchers have studied the influence of temperature for hexavalent species from 100–800°C. The binding energy was observed to increase by approximately 3 eV over the given temperature range [83]. The effect of this phenomenon can be quantified using the binding energy of Cr^{6+}. The binding energy of Cr^{6+} presented in the aluminosilicate fiber study ranges from 579–579.92 eV [94]. These values are within known values for the binding energy of Cr^{6+} species [86, 97-99]. The observed peaks from 576– 576.3 eV (lowest binding energy peak the spectra) are from Cr^{3+}.

A sequence of events was proposed to explain why regions display multiple colors [94]: Aluminosilicate fiber surfaces are exposed to Cr oxyhydroxide, the dominant volatile Cr product formed in the presence of water vapor, in an environment of 100–230°C. The volatile Cr species is physiosorbed to the aluminosilicate fiber surface. The upper range of this temperature is near the condensation point for Cr vapor, the boiling point of chromic acid being 250°C. Deposition in literature at temperatures above the upper temperature range has not been observed [43].
Once physiosorbed, $CrO_2(OH)_2$ may dehydrate and form CrO_3 allowing chromate species to then form from reactions with the surface [76, 77, 79, 80, 82, 83, 104]. Hydroxyl groups function as anchoring points, allowing for stabilization and diffusion of hexavalent chromate [19, 21, 74, 76,

84, 105]. The color of the substrate material loaded with these chromate species appears to be yellow color [19]. As Cr loading increases, available hydroxyl groups diminish and chromate species begin to form O-Cr-O bonds that result in polychromate species formation, and eventually CrO_3 [104, 106].

The resultant polychromate species are not as attached to the surface and are therefore less stable than chromate species. At this stage, the color shifts to brown [85]. Thermal decomposition of CrO_3 ensues and oxygen is lost over time. Formation of Cr_3O_8, then Cr_2O_5, followed by CrO_2, and lastly Cr_2O_3 follow. At this stage, the color appears to be green [107]. Decomposition of CrO_3 to Cr_2O_3 leaves the remaining surface chromate species as the primary hexavalent species.

Interactions with Alumina, Quartz Wool, and Mica

Alumina, quartz wool, and mica are exposed to humidified air in an environment of temperatures ranging from 150-900°C for 24- and 100-hour exposures. The samples are then analyzed using XPS. Temperature, material, and exposure time were observed to influence surface Cr speciation and total Cr deposition [93].

Similar colors noted in the previously presented study appear on the quartz wool and alumina wafers. Fig. 18 above displays the yellow, brown, and green discoloration on quartz wool and alumina wafers. These colors were not observed on mica as the sample remained transparent below 700°C. Above this temperature, the mica samples became opaque, grew in thickness, and developed a silver sheen due to a de-hydroxylation effect [108]. De-hydroxylation occurs at elevated temperatures and is the process by which a surface hydroxyl group is effectively removed by bonding with hydrogen to form water.

Green is indicative of trivalent species whereas brown and yellow are indicative of hexavalent species. The previously presented study linked the following compounds to specific colors: CrO_3 (brown staining), chromate (yellow staining), and Cr_2O_3 (green staining).

Alumina collects more Cr than mica which collects more than quartz wool. The bottom side of the wafers collect less Cr than the top side. Both 100- and 24-hour 250-300°C alumina exposures created green staining on the bottom side and brown/yellow staining on the top side. Alumina collects enough Cr at all temperatures and exposure times to meet the detection limit whereas mica and quartz wool did not collect enough Cr to meet the detection limit for 500°C. Quartz wool collects a negligible amount at 500°C for both exposure times. Mica collects a detectable amount of Cr at 150-200°C for 100-hour exposure.

In the previously proposed mechanism, volatile Cr species are physiosorbed first and then chemisorbed to the surface via esterification reactions with hydroxyl groups. Species are chemisorbed as chromate and decompose with increased Cr loading to form several Cr compounds including Cr2O3. This proposed mechanism is adjusted for high (≥500°C) temperatures, as the equilibrium of the adsorption step shifts to favor desorption. Volatile Cr must collide with hydroxyl groups with sufficient energy and at the correct orientation for Cr species to form on surfaces at elevated temperature. Hydroxyl groups function as Cr anchors and their properties impact Cr collection.

Alumina, mica, and quartz wool have different hydroxyl group properties. As evident from the experimental results in the previously presented studies, some of these properties are beneficial for Cr uptake and some are detrimental. Alumina has more hydroxyl groups and are of greater basicity. Furthermore, alumina is more resistant to de-hydroxylation than silica [19] [20-23, 109]

as silica surfaces dehydrate more easily, and Cr uptake is diminished. The volatility of silica is greater than alumina given these conditions [54, 110].

These observations agree with HSAB theory that states hard acid-hard base interactions have a significant difference in electronegativity and result in a bonding with strong ionic properties. Aluminum is a harder acid than silicon and is predicted to form a more stable bond with a hard base such as oxygen. This results in a higher electron density for hydroxyl groups on alumina which translates to enhanced Lewis basicity. Hydroxyl groups present interaction area on the surface for volatile Cr to anchor. The basic nature of these hydroxyls allows for a stronger bond to form with a volatile Lewis acid such as Cr.

Chromate species condensed on alumina surfaces remain stable at higher Cr loadings than chromate species condensed on silica. This possibly explains the trend observed for alumina between 250-300° C, but not for the other temperature ranges. CrO_3 melts at approximately 200° C and decomposes around 250° C [111]. CrO_3 exists as liquid in the 250-300^o C temperature range, and this increases the contact area CrO_3 makes with the alumina surface.

Cr is soluble in α-Al_2O_3 as both have similar atom size, crystal structure, valence state, and electronegativity [112]. Surface hydroxyl groups act as anchoring points for volatile Cr species. Hydroxyl populations and their basicity are determined by the material and surface conditions. Infrared spectroscopy reveals at least five -OH stretching bands with stretching frequency increasing with. This claim is supported by increasing preferential consumption of OH groups upon Cr loading and noted stability at elevated temperatures [19, 105, 113, 114].

Infrared spectroscopy has also been used to identify three -OH stretching bands on silica [115]. Observations of differences in hydroxyl group populations of alumina and silica surfaces

are supported by pKa measurements. Silica has been observed to display bimodal behavior with pKa values of 4.5 and 8.5. More complex behavior has been observed on alumina with pKa values < 3, 4.5, 6.7, and 9.5-9.8 [114, 116]. These observations lead to the conclusion that hydroxyl group populations on material surfaces are nonhomogeneous and are not interchangeable. As a result, Cr deposition has a preferential attachment for more basic hydroxyl groups followed by less basic hydroxyl groups. This observation is in agreement with observations seen in literature [105].

Solid Oxide Fuel Cell Degradation

Solid oxide fuel cell (SOFC) technology provides a flexible energy source by converting fuels into heat and electricity. These systems operate at elevated temperature (>650°C) and oxidize carbon monoxide, hydrocarbons, or hydrogen to produce electricity and heat. Carbon dioxide or water are produced as byproduct depending on the fuel [117].

The general structure of a SOFC consists of two electrodes separated by an ion-conducting electrolyte, commonly yttria-stabilized zirconia (YSZ) [117]. Hydrogen is oxidized at the anode/electrolyte interface whereas oxygen is reduced at the cathode/electrolyte interface. The exchange of ions across the electrolyte forces electrons through an external circuit to create a current. The cathode/electrolyte interface is referred to as the triple-phase boundary (TPB). The TPB is the point at which the gas phase, electrolyte, and cathode meet. Individual cells, consisting of an anode, cathode, and electrolyte, produce less than 1 Volt [118]. To achieve useful voltage and power, cells are stacked and connected via interface materials called interconnects. SOFCs that operate at lower temperatures (≤ 800°C) may use metallic interconnects, such as ferritic stainless steel (FSS) [119]. At these temperatures, interconnects exposed to air and adjacent to the cathode may release volatile Cr trioxide and/or Cr oxyhydroxide. These volatile species proceed

downstream and deposit on the cathode through chemical and electrochemical deposition, an occurrence known as “chromium poisoning” [120-123].

Cr deposition occurs at phase boundary points including the TPB as well as two-phase boundary points (cathode/gas, electrolyte/gas). These deposits degrade SOFC performance over time by decreasing the efficiency of ion exchange. The US Department of Energy defines acceptable performance degradation as less than 0.2% per 1000 hours over 40,000 hours of operation [124]. Modern SOFC designs from the Jülich Research Centre have achieved less than 0.1% performance degradation per 1000 hours for stacks operated for 17,000 and 19,000 hours [125, 126]. There is promise for SOFC technologies, but improvements in performance leading to longer operation times with conventional fuels are needed. Studying and understanding degradation, such as Cr poisoning, are critical to achieving these goals.

At a stack level, degradation mechanisms include poisoning of the cathode by gaseous Cr species from metallic interconnects and chemical interactions between glass–ceramic sealants and ferritic steel interconnects [127]. Cr poisoning can cause electrochemical and microstructural changes in the cathode. Some studies suggest that the driving force for the Cr poisoning is the oxygen potential gradient caused by the cathode overpotential. Other elements present in the environment may affect Cr poisoning mechanisms. One study examined the influence of sulfur on (La, Sr)MnO_3-(Zr, Y)O_2 cathodes [128]. The authors found that formation of $SrCrO_4$ is promoted under combined Cr and S contaminating conditions. Furthermore, Cr accumulations act as anchoring points for sulfur and form Sr(Cr, S)O_4 compounds.

Interactions between Volatile Chromium Species and Cathode/Electrolyte

As noted, volatile Cr species interact at the TPB and two-phase boundary points. Volatile Cr species reduce and deposit as chromia via electrochemical deposition at the TPB. Two phase boundary interactions include both gas/cathode and gas/electrolyte. Some SOFC materials show deposition predominantly at the TPB, however others show deposition along the cathode away from the TPB. For example, results from a study revealed Cr_2O_3 deposits over extended distances (40–50 to 500 um) that are much larger than estimates of the TPB (< 1 um) [120]. Researchers have proposed that this phenomenon extended the TPB, as the conductivity of chromia (0.2 to 0.02 S/cm at 800°C) may be comparable to the hole conducting cathode [129].

Electrochemical reduction of Cr oxyhydroxide and open circuit chemical reactions have been observed with cathodes containing Mn or Sr [120, 130-133]. According to one study, Mn^{3+} at the LSM surface reduces to Mn^{2+} during polarization and reacts with Cr oxyhydroxide to form Cr-Mn-O nuclei with oxygen vacancies supplied by the electrolyte [133]. The nuclei continue to react with Cr oxyhydroxide to form chromia and $(Cr, Mn)_3O_4$.

As for LSCF or SrO coated LSM, chemical deposition has been observed at the cathode/gas interface. Strontium oxide reacts with Cr oxyhydroxide to form Cr-Sr-O nuclei leading to the formation of chromia and strontium chromate. Researchers have also observed significant vapor and solid-state transport of Cr through SrO and LSCF at temperatures of 700-1000°C for 150-hour exposures [134]. Manganese oxide and LSM allowed for significant solid-state diffusion of Cr with contacting steel, but only trace vapor deposition resulting in an undetectable amount of Cr on LSM has been observed through vapor transport for MnO.

Another study placed chromia-containing interconnect alloys in contact with LSM in SOFC operating conditions. The authors observed evidence that the reaction between Cr containing species and porous LSM at the electrode/electrolyte interface occurs due to vapor transport of volatile Cr species [131]. Furthermore, the amount of the spinel phase and Cr_2O_3 detected at the cathode/electrolyte interface was much greater than that within the porous layer of LSM.

Other studies have exposed LSM, LSCF, and LNF material to SOFC operating conditions containing volatile Cr sources. One study exposed these materials to 700°C environments containing volatile Cr species for 300 hours [130]. A portion of the surfaces were placed in contact with stainless steel interconnects and a chromia source. Reaction couples were also used for experimentation and were prepared by mixing chromia and one of the cathode materials. LSM and LSCF reaction couples were observed reacting with chromia to produce compounds such as $(Cr, Mn)_3O_4$ and $SrCrO_4$, respectively. The most vigorous reactions were observed for LSCF as no pure chromia or LSCF was observed in the XRD pattern. On the other end of extremes, no reaction was detected for LNF-chromia reaction couples. Similar observations were made to those made in the previous study with respect to solid state and vapor transport: surface diffusion of Cr was observed for LSM and LSCF whereas vapor transport was not observed for LSM but was significant for LSCF [131, 134]. Cr was observed to collect on LNF through both solid-state diffusion and vapor transport.

Interactions between Volatile Chromium and Sealing Glass

As mentioned previously, sealing materials in SOFCs are ceramic glasses or compressed papers. These materials are used in SOFC stacks to protect against air and gas leaks between

interconnects. Two such materials are classified as G18 and G#36. G18 is a barium alumino-silicate (BCAS)-based glass–ceramic [135] and G#36 is a mixture of $SrCO_3$, $CaCO_3$, boric acid, and various oxides [136].

Strontium chromate was observed to form from interactions between volatile Cr species and LSCF and on sealing glasses containing SrO. Researchers placed G#36 pastes on 430SS substrate surfaces and held them at 800°C for one to two weeks [136]. Yellow staining on the glass was observed first forming around the edges before progressing inward over time. Auger electron depth profiling revealed diffusion of Cr into the glass with a greater Cr content observed at the edge than the content observed at the center.

Thermodynamic modeling was performed for strontium chromate formation from interactions between chromia and SrO. The reaction is energetically favorable beyond 1000°C at 0.2 atm pO_2. A pO_2 of ~10^{-7} atm or greater was found to be necessary for energetic favorability at 900°C. Modeling was also carried out for strontium chromate formation from CrO_3(g) and SrO and was reported to be energetically favorable over 1000°C at 0.2 atm pO_2 [136].

In another study, chromia and G18 powder were mixed and heated to 950°C in dry air for 24 hours. The resultant product was stained yellow and was analyzed via XRD which confirmed the formation of $SrCrO_4$ [137]. The study's authors propose that strontium chromate forms near the edge where the pO_2 is higher because of interactions between chromia and/or CrO_3. pO_2 increases inwards as the ingress of oxygen increases due to the formation of a more porous $SrCrO_4$ phase. The reaction follows inward and allows reactions with chromia and/or CrO_3.

Researchers have reported similar findings from barium-calcium aluminosilicate-based glass-ceramic G18 and FSS. Reaction couples between G18 and FSS 446 coupons were heated to

850°C for one hour then lowered to 750°C for an additional four hours. Barium oxide was observed reacting with chromia and/or volatile Cr species to form $BaCrO_4$ ultimately resulting in the G18 detaching from the FSS 446 coupon. Separation of the two materials was due to differences in the respective coefficients of thermal expansion between $BaCrO_4$ and G18/FSS 446. G18 displayed yellow staining after experimentation and was attributed to $BaCrO_4$ formation. While $BaCrO_4$ was not identified using a phase identification technique in this study, a separate study identified the phase using XRD [138].

The presented studies show the potential for reactive condensation of volatile Cr species onto ceramic surfaces such as chromia, Cr(III), and chromate, Cr(VI). Chromate formation was observed to increase in the presence of Sr and Ba. With these observations in mind, it is worth noting that chromate formation has occurred without the influence of alkaline earth metals. For example, Cr oxide catalysts on ceramic supports often lack alkaline earth metals, but still support chromate formation.

To combat Cr poisoning of SOFC systems, materials that readily absorb and trap volatile Cr species have been developed and have been dubbed “chromium getters”. These materials are those that readily react with gaseous Cr to form stationary surface species.

Chromium “Getters”

Cr getters are of interest to SOFC researchers as a means of controlling Cr poisoning of electrodes and/or sealing glasses. Cr getters are inserted within SOFC stacks to attract gaseous Cr and decrease the total amount of free-floating species within the system. A commonly used design involves coating fibers, wools, or honeycomb substrates with a $Sr_xNi_yO_z$ solution [139-142].

Researchers have demonstrated novel methods to mitigate cathode degradation using Cr getters manufactured from low-cost materials [140, 142]. The getters use a cordierite honeycomb substrate coated with alkaline earth and transition metal oxides. The first getter design was tested for 500 h under SOFC cathode exposure conditions [142]. Chemical and structural analyses show gaseous Cr predominantly concentrated at the getter with only the end of the getter free of Cr. The second study measured the electrochemical performance of the SOFC system for 100 h at 850°C with and without the Cr getter [140]. Stable electrochemical performance was maintained for the cell tests with getters, whereas the cell performance in the test without Cr getters rapidly decreased after 10 h. Results from tests with SOFCs and getters demonstrated the high efficiency of Cr capture technology for the preservation of cell performance.

Another SOFC-focused Cr getter design was demonstrated as a cost-effective approach for the capture of gaseous Cr species [141]. The design incorporates a porous and electrically conducting layer, comprising of a mixture of complex metal oxide getter, and electrically conducting perovskite phase, into the SOFC stack. The getter layer is deposited on the cathode surface or placed away from the cathode. Effectiveness of the design was electrically tested in a half cell configuration at 850ºC for 100 hours. After testing, cells were analyzed for composition and changes in the morphology. Results from these tests reveal that getters both placed away from the cathode and getter paste deposited on cathode surface successfully capture all Cr from the incoming gas flow.

Lastly, researchers performed experiments in the presence of a Cr getter and showed stable polarization resistance [139]. The electrochemical performance of half-cells in humid air and in the presence of Cr getter also remained stable during 100-h tests for 550 and 650°C conditions.

The structural and chemical qualities of the electrode, electrode-electrolyte interface and getter are analyzed post-test by scanning- transmission electron microscopy, energy dispersive X-ray and Raman spectroscopy. These analyses showed that the cathode bulk and cathode-electrolyte interface remained free of Cr whereas Cr was deposited near the gas inlet region of the getter.

Cathode Restoration

Cathode poisoning can sometimes be reversed, as is the case for cathode degradation due to acidic Cr-species poisoning. One study demonstrates the feasibility of reviving degraded SOFC cathodes using relative acidity [143]. Experiments involved poisoning a cathode using Cr species infiltration and subsequent revival using calcium species infiltration. Results showed no further degradation during operation for 100 h after restoration.

Another study restored performance to Cr-poisoned SOFC cathodes by electrochemically cleaning them [144]. The authors fabricated two cells and poisoned them under identical conditions at 800°C in the presence of a Cr source. The electrochemical cleaning process involved running the cell in SOEC mode for 2 h at a current of 0.15 A/cm2. 10% humidified air was supplied to the air side and 10% humidified H2 to the fuel side to reduce cell polarization while using a higher supplied current. Cell degradation from void formation in YSZ grain boundaries and delamination of the air electrode can occur in higher electrolytic cell polarization conditions. Analysis of the unrestored cell showed significant contamination of the cathode by Cr oxide and (Cr, Mn) spinel deposits. Analysis of the restored cell showed a reduction of Cr concentration in the cathode and at the cathode/electrolyte interface. This reduction also resulted in a substantial reversal of the cell's degradation in performance. Fig. 20 below depicts the mechanisms of Cr-

poisoning at the TPB and subsequent electrochemical restoration. Voltage current curves for each scenario are also presented for comparison.

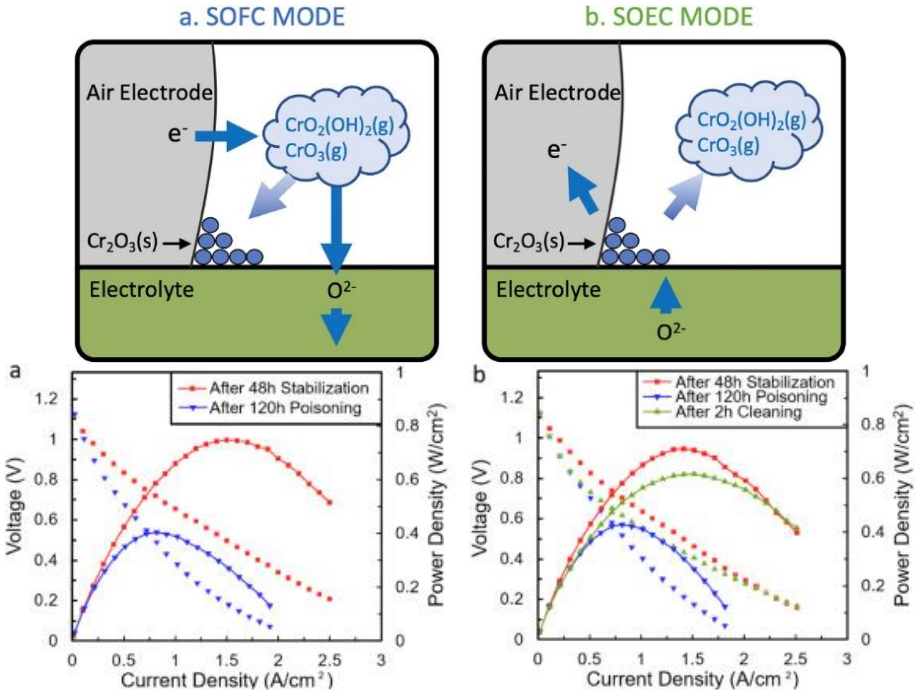

Figure 20 - Diagram of Cr poisoning (top left) and electrochemical cleaning (top right) at TPB. Voltage current curves for the Cr-poisoned cell (bottom left) and electrochemically cleaned cell (bottom right) [144].

Hexavalent Chromium Formation in Industry

Besides SOFCs, volatile Cr has been identified as a possible issue in other industries involving high-temperature applications of stainless steel such as power processing equipment and large combustion engines. Many of these applications involve wrapping the high-temperature stainless steel with insulating blankets, leading to complicated interactions between the volatile Cr and insulating materials.

Concern with Cr(VI) formation from industrial applications is well established in areas such as leather tanning, electroplating, anodizing, and dye production [26]. However, other

industries have more recently recognized a potential emerging issue with hexavalent Cr formation. Industries involved with elevated temperature environments requiring insulation such as chemical processing plants, power processing plants, and large internal combustion engines have identified hexavalent Cr formation.

"Hot Work" of Stainless Steels

"Hot work" of stainless steels includes all processing techniques that elevate the temperature of stainless steel above the recrystallization temperature, which ranges from 500 – 1300°C (e.g., welding, forging, and drawing). At these temperatures, reactive evaporation of Cr from the stainless steel occurs and may cause the same deleterious downstream effects as previously mentioned. It is important to accurately determine the levels of different forms of Cr in welding fumes to understand the potential risks and to implement appropriate control measures to protect workers and the environment from exposure.

A study for determining the quantities of the different chemical compounds of Cr in welding fumes is presented [145]. Cr(VI) content was analyzed via spectrophotometric measurements by the diphenyl carbazide (DPC) method. Spectrophotometric methods used for determination of different Cr species using reagents that form absorbing species. A common method used to determine Cr(VI) content in aqueous solutions is based on the reaction of DPC with Cr(VI) in acidic conditions (pH of 1.0). Spectrophotometric analysis of the magenta chromogen (λ max~540 nm) which is formed by the reaction of Cr(VI) with 1,5-diphenylcarbazide (DPC) in strongly acidic solution [146]. Cr(III) and Cr(0) were determined by atomic absorption spectrometry (AAS). Cr in all the three oxidation states (hexavalent, trivalent, and metallic) was present in the examined welding fumes with Cr(VI) being the most prevalent in all samples.

In another study, the metal fumes emitted from stainless steel plasma cutting are characterized for Cr content. It is not uncommon for stainless steel plasma cutting to produce higher levels of Cr fumes compared to other hot work processes. Plasma cutting involves the use of a high-temperature plasma arc to cut through conductive materials, and this process can generate significant levels of fumes. The levels of Cr in the fumes can vary depending on the specific type of stainless steel being cut and the operating conditions of the plasma cutting process. The fumes produced from plasma cutting ER308L stainless steel plates with arc currents varying between 20 and 50 A are collected in a fume chamber using a high-volume pump. Cr(VI) and other oxides in the collected fume were analyzed using ion chromatography. It was found that Cr(VI) emissions (219.8 –480 μg/min) from the plasma cutting were higher than those found in welding fumes from a previous study and higher arc currents result in higher emissions [147].

Even in less extreme environments, such as those found in one's home kitchen, stainless steel has been observed to leach Cr. A study examined the effects on Ni and Cr leaching from different stainless-steel grades, cooking time, cooking cycles, and types of tomato sauces [148]. After simulating the cooking process, samples were analyzed by ICP-MS for Ni and Cr. The tenth cooking cycle resulted in an average leaching of 88 μg of Ni and 86 μg of Cr per 126 g serving of tomato sauce.

High-Temperature Insulating Materials

EnergyUK released a series of safety bulletins related to Cr(VI) formation and its hazards. The bulletins identify potential for Cr(VI) to form in steam pipework, gas turbine combustion components, combustion engine exhausts systems in contact with insulation materials [13]. The bulletins also outline three parameters for these environments that, when met, could encourage

Cr(VI) formation: calcium-based products present, temperature environment greater than 300^{o} C, and stainless-steel containing Cr present. Calcium can be present in insulation materials and anti-seize lubricants, for example.

Kavarmat and Aletek, two producers of industrial insulation materials for elevated temperature applications, such as steam pipes and exhaust manifolds, have acknowledged the formation of Cr(VI) with traditional insulating materials. In response to these revelations, they have each released products with low/no calcium and claims of reducing or eliminating hexavalent Cr formation [149, 150]. However, Cr(VI) is also found on calcium-free insulation materials, including silica and alumina, and thus these claims may be challenged. Eneria, a dealer of Caterpillar engines and power systems, has also identified solid and non-volatile hexavalent Cr deposits that can be observed on some exhaust manifolds and exhaust thermal insulations, identifying the source of the Cr as volatilized from stainless steel components [14]. Eneria recognizes several risks for technicians replacing, cleaning, and maintaining exhaust system components related to Cr(VI) deposits. These include exposure to airborne Cr(VI) dust and Cr(VI) deposits on exhaust manifold components.

Although in relatively small quantities compared with direct sources, it is important to recognize the potential for Cr(VI) formation in industries that use high-temperature environments as described. The presence of certain parameters, such as calcium-based products, high temperatures, and stainless-steel containing Cr, can increase the likelihood of Cr(VI) compound formation, although other Cr(VI) species can form without the presence of alkaline materials. This highlights the importance of identifying and managing potential sources of Cr(VI) in these industries and taking appropriate precautions to protect workers and the environment from the

hazards of Cr(VI) exposure. It's also important for industries to be aware of the potential for Cr(VI) formation and to take steps to prevent or mitigate its formation from the stainless-steel sources.

Current Developments and Summary

The general mechanism, as it is currently understood, in which Cr compounds condense is as follows: monochromate formation from esterification reactions with surface hydroxyl groups, Cr loading increases leading to polychromate formation up to CrO_3, and finally decomposition into Cr_2O_5, Cr_3O_8, CrO_2, and Cr_2O_3. Further experimentation and thermodynamic modeling are required to verify these proposed mechanisms of condensation and speciation of Cr on ceramic surfaces. Contemporary research includes expanding on the condensation mechanisms of volatile Cr species and exploring the mobility of surface Cr species.

Current Developments

The effects of water vapor reactive evaporation of Cr have been well documented, but the effects on reactive condensation of Cr have not. Reactive Cr from chromia occurs in atmospheres of oxygen, forming $CrO_3(g)$, and increases in the presence of water vapor, forming $CrO_2(OH)_2(g)$. Partial pressure of $CrO_2(OH)_2(g)$ is larger in the presence of water vapor by many orders of magnitude up to 1400 K. Vapor pressure of Cr oxyhydroxide varies with temperature. For example, at 500°C the partial pressure is three orders of magnitude less than 900°C according to thermodynamic modeling [41, 44]. The effects of water vapor on reactive condensation of Cr can be explored by altering the water vapor content of the gas atmosphere in a transpiration experiment between a Cr source and a substrate material.

The importance of Lewis acidity could be explored by studying alumina as some phases of alumina have similar hydroxyl populations but vary in acidity [88, 113, 151] [88, 113, 152]. More acidic alumina phases, such as γ-alumina, are expected to collect more Cr than less acidic phases, such as θ-alumina [113, 152, 153]. Volatile Cr condensation experiments could be performed on different alumina phases at the same temperature and exposure time. A variation on this experiment could evaluate the same alumina phase at different temperatures as higher temperatures increase Lewis acidity and should result in increased Cr collection. Other materials with denser hydroxyl populations than silica, such as ceria and titania, may be evaluated for intermediate behavior similar to mica in the presented studies [154]. Observing aluminosilicates with different compositions like previous presented studies would also be useful [18, 22, 155].

Surface sensitive reactive condensation on materials of interest to SOFCs, such as LSCF and its constituent element oxides, may be of value. These experiments can be modeled after the work performed on Cr interaction with strontium and LSCF at 700-1000°C for 150-hour exposures, but with greater attention to surface chemistry [134]. Cr has not been observed to react with quartz wool, mica, or alumina to form new phases. However, elemental oxides from LSCF (SrO, La_2O_3, etc.) have been observed to form $FeCr_2O_4$ above 600°C [156], $SrCrO_4$ above 700°C [130], $CoCr_2O_4$ [123], and $LaCrO_3$ 800°C [119]. An experiment could include exposure of SrO and varying compositions of $SrO{\cdot}SiO_2{\cdot}Al_2O_3$ glass to different elevated temperatures and Cr loading. Varying the degree of crystallinity of $SrO{\cdot}SiO_2{\cdot}Al_2O_3$ compounds to observe the effects crystalline character of a ceramic has on Cr collection and subsequent surface Cr speciation.

Experiments with longer exposure times (e.g., >1000 hours) to adequately saturate materials such as fibers and wool with high surface areas could provide an ability to verify the

proposed condensation mechanisms. These experiments could also be used to assess long-term saturation conditions, after which materials will no longer collect Cr. ICP-MS could be used to quantify Cr content and characterization techniques capable of speciation identification, such as XRD or EBSD, could support or question reaction mechanisms listed in this review. Other techniques, such as commercial water testing kits, could be used to quantify Cr compounds with a specific oxidation state.

The effects of alkaline additives in the insulation material Experimental series will explore. A class of materials exist known as “chromium getters” that are designed to control Cr poisoning of electrodes and/or sealing glasses within SOFCs. Cr getters attract gaseous Cr decrease the total amount of free-floating species within the system and some getters use a cordierite honeycomb substrate coated with alkaline earth and transition metal oxides. Standard temperature humidity conditions will be used for all experiments in this category. Varying the alkaline composition of insulating materials with similar silica or alumina content will allow the testing of the hypotheses: Cr collection and speciation changes between pure silica/alumina and silica/alumina with alkaline additives in addition to the hypothesis of alkaline additives increase Cr collection and hexavalent Cr formation. It is expected that differences in total amounts of Cr and Cr speciation condensed on the insulating material will correspond with the types and amounts of alkaline additives present in the insulating material. Materials for this experiment include Cr_2O_3 powder, stainless steel, and ceramic insulating materials with varying levels of alkaline additives (e.g., calcium silicate, Perlite, mica, etc.). The evaporator used in these experiments was kept at room temperature, creating a water vapor content of approximately 3% within the experimental control volume. The desired information from analyses for this experiment is also total Cr collection quantification and specific

Cr species quantification. The same techniques such as ICP-MS, XPS, or water test kits can be used and some of the results can be obtained immediately after experimentation by observing the color of staining on the insulating material.

Summary

This review comprises a non-exhaustive collection of 70 years of literature relevant to Cr speciation on ceramic surfaces. Cr, a naturally occurring element found in rocks and soil, can be a necessary nutrient or an environmental/health hazard depending on its oxidation state. Cr has found uses in a variety of industries including textile manufacturing, leather tanning, and stainless-steel production. Environmental release of Cr due to these industries is a concern as conditions exceeding prescribed limits are toxic and/or carcinogenic for plants, microbes, animals, and humans. In stainless steel, Cr is used to improve resistance to corrosion and can contribute up to 27 wt% of the total alloy. Reactive evaporation, a process by which a reactive gas interacts with a solid or liquid surface to form a new gaseous compound, can cause Cr to volatilize from stainless steels in high-temperature oxidizing environments. The rate of evaporation is influenced by water vapor and fluid dynamics, generally increasing the rate for increased water vapor/fluid flow. An experiment referred to as a transpiration experiment is used to conduct reactive evaporation and condensation experiments. Transpiration experiments have been modified to accommodate a variety of research interests including those associated with volatile Cr species. Reactive condensation, the process by which a volatilized species interacts with a solid or liquid surface to form new condensed species, can occur between volatile Cr species and the surrounding environment. Ceramic materials, such as those that belong to the SiO_2–Al_2O_3 system, are commonplace in SOFC systems as sealant materials and insulation. Volatile Cr experiencing

reactive condensation with ceramic surfaces can create Cr(VI) compounds, leading to deleterious downstream effects. These effects include system performance degradation or generation of hazardous materials. Volatile Cr species in SOFCs can poison the electrodes and electrolyte, causing irreversible damage to the system and degrading system performance. A novel method of controlling Cr poisoning in SOFC systems is to introduce a "chromium getter" into the system. These materials are used to attract and trap volatile Cr species to reduce degradation of the system's performance. It is also possible to restore Cr-poisoned cathodes by removing deposited Cr via electrochemical "cleaning". Besides SOFCs and well-established industry sources of Cr (refractories, leather tanning, dye pigment, etc.), relatively new sources of hexavalent Cr have been identified in industries involving high-temperature applications of stainless steel and insulating materials. Reactive evaporation and subsequent condensation of volatile Cr species are influenced by environmental factors such as temperature, time, atmospheric water content, and the material on which condensation occurs. Material properties such as surface hydroxyl chemistry and available surface area of the material have the most influence on deposition.

CHAPTER FOUR - INFLUENCE OF WATER CONCENTRATION ON HIGH-TEMPERATURE REACTIVE CONDENSATION OF CHROMIUM VAPORS GENERATED IN 800°C AIR

Contribution of Authors and Co-Authors

Manuscript(s) in Chapter(s) 4

Author: Travis K. van Leeuwen

Contributions: Graduate research assistant

Co-Author: Ryan Dowdy

Contributions: Undergraduate research assistant

Co-Author: Amberly Guerrero

Contributions: Undergraduate research assistant

Co-Author: Paul Gannon

Contributions: Primary investigator

Manuscript Information

T. K. van Leeuwen, R. Dowdy, A. Guerrero, and P. Gannon

Journal of the Electrochemical Society

Status of Manuscript:
☐ Prepared for submission to a peer-reviewed journal
☐ Officially submitted to a peer-reviewed journal
☐ Accepted by a peer-reviewed journal
[x] Published in a peer-reviewed journal

IOP Publishing Limited
17 January 2024
DOI 10.1149/1945-7111/ad1acd

Abstract

Reactive evaporation of chromium (Cr) from stainless steels used in solid oxide electrochemical systems, such as solid oxide fuel cell (SOFC) and solid oxide electrolysis cell (SOEC) systems, is well-documented. However, the condensation and interactions of volatilized Cr species onto and with surrounding interfaces during complex and dynamic system exposures is less understood. Understanding these interactions during operation is critical for improving system performance and safeguarding environmental, health and safety, as some condensed species contain toxic hexavalent Cr (Cr(VI)). The objective of this study is to investigate the condensation pathways of Cr vapors within representative high-temperature system environments. To accomplish this objective, Cr vapors, produced by high-temperature (800 °C) air exposures of trivalent chromium (Cr(III)) oxide (Cr_2O_3) powder with variable moisture content, were condensed onto various ceramic materials at lower temperatures (<400 °C). The total amount of Cr and ratios of oxidation states were measured using inductively coupled plasma optical emission spectroscopy (ICP-OES) and diphenyl carbazide (DPC) colorimetric/direct UV−vis spectrophotometer analyses. Increased Cr condensation was observed with increased water content, with similar Cr(VI) to total Cr ratios. Results and interpretations are discussed in context of improving understanding of Cr reactive condensation in SOFC/SOEC and related high-temperature materials and systems.

Introduction

The goal of this research is to improve fundamental understanding of reactive condensation pathways for chromium (Cr) vapors generated in high-temperature systems such as exhaust manifolds, steam turbines, boilers, or solid oxide fuel cell or electrolysis cell (SOFC/SOEC) stacks. Understanding the interactions between volatilized Cr species and downstream components during operation is critical for improving system performance, environmental health, and safety as some condensed Cr forms toxic hexavalent Cr(VI) species, which is a known carcinogen. Reactive evaporation of Cr from stainless steels commonly used in these systems is well-documented as the primary Cr vapor source implicated in Cr poisoning of SOFCs; however, the interactions between volatilized Cr species and surrounding interfaces during complex and dynamic system exposures is poorly understood[1]. The objective of this study is to explore the effects of water vapor in the atmosphere on Cr collection and speciation on various ceramic fiber surfaces. First, an overview of high-temperature corrosion of stainless steels, reactive evaporation / reactive condensation of Cr vapors, and deleterious downstream effects these processes have on systems such as SOFCs/SOECs is presented. Next, the experimental methods and analytical techniques chosen for studying the nature of reactive condensation of Cr vapors are introduced. Finally, the results of this study are presented in relation to improving performance and safeguarding human and environmental health associated with the forementioned representative high-temperature systems.

Corrosion of Stainless Steels

Stainless steels are sought after as materials for a wide range of engineering applications due to their ease of manufacturing, low costs, and stability over a large temperature range, from cryogenic conditions to temperatures exceeding 1,000°C [31, 32].This stability is due to the

formation of a surface oxide layer on the exterior of the material, which acts as a protective barrier against corrosion of the alloy. Cr plays a key role in the oxide layer of all classes of stainless-steel alloys and ranges from ~10-27 wt% in standard alloy compositions.

High-temperature (>500°C) oxidizing environments (e.g., air) with or without water vapor degrade protective passivation layers by encouraging reactive evaporation of surface compounds. This phenomenon is true for many oxides including chromia compounds such as those used in stainless steels. The oxide layer grows until a limiting oxide thickness is reached and the limiting thickness increases while the time required to reach it decreases with increasing temperature. Once this limiting thickness is reached, the rate of Cr evaporation is balanced with the rate of oxide scale growth [157]. Chromia may volatilize at a greater rate than it is reformed, eventually causing the oxide layer to become less protective, forming compounds such as $(Fe, Cr)_2O_3$ or iron oxides [37, 38]. Chromia in the oxide layer transforms into mobile vapor species upon reactive evaporation, which interact with the surrounding system components. These interactions can form compounds that pose risks to human health, the environment, and degrade performance in electrochemical devices like SOFCs.

Reactive Evaporation

The reactive evaporation of Cr from chromia occurs in atmospheres of oxygen, forming $CrO_3(g)$, and increases significantly in the presence of water vapor, forming $CrO_2(OH)_2(g)$ [43-45]. Partial pressure of $CrO_2(OH)_2(g)$ is larger in the presence of water vapor by several orders of magnitude up to ~1400 K [43-48]. At ~298 K, published thermodynamic data reveals an equilibrium partial pressure of $\sim 8 \times 10^{-40}$ bar for $CrO_3(g)$ [49]. At ~800 K, this partial pressure increases by several orders of magnitude to $\sim 1 \times 10^{-15}$ bar. The partial pressure of Cr oxyhydroxide

($CrO_2(OH)_2(g)$) at ~800K is ~$1x10^{-7}$ bar and increases to $1x10^{-8}$ at ~1400 K [49]. Example reactions for chromia evaporation include:

$$½Cr_2O_3(s) + ¾O_2(g) = CrO_3(g) \quad \text{Eq. 1}$$

$$½Cr_2O_3(s) + H_2O(g) + ¾O_2(g) = CrO_2(OH)_2(g) \quad \text{Eq. 2}$$

Reactive Condensation

Reactive condensation of Cr on catalyst supports, such as alumina and silica, and on SOFC components, such as those made from manganese or strontium, is well-documented. For example, industrial Cr catalysts are manufactured upon support materials such as silicas, aluminas, and aluminosilicates via aqueous impregnation. Deposition of Cr on the catalyst support depends on the support material, processing temperature, and Cr loading. SOFCs operate at elevated temperatures (800℃) and may use metallic interconnects, such as ferritic stainless steel. At these temperatures, interconnects are exposed to ambient (moist) air and release volatile CrO_3 and/or $CrO_2(OH)_2$. These volatile species proceed downstream and deposit on the cathode through chemical and electrochemical deposition and impede SOFC operation, an occurrence known as "Cr poisoning". However, there are far fewer publications that focus on the chemical and physical processes that occur during condensation reactions of Cr on other materials and surface conditions, e.g., [78, 93, 94]. Condensed species can be initially identified by the color of stains appearing on light colored ceramic substrate materials (e.g., alumina). Green is indicative of trivalent Cr species whereas brown and yellow are indicative of hexavalent Cr species, or mixtures thereof. In one study, the following compounds were linked to specific staining colors: CrO_3 (brown staining),

chromate (yellow staining), and Cr_2O_3 (green staining) [95]. However, stain colors alone are insufficient for detection and quantification of the wide variety of Cr-containing compounds often found within the stains.

Solid Oxide Fuel Cell Degradation

SOFCs consists of two electrodes separated by an ion-conducting electrolyte [117]. In operation, fuel (e.g., hydrogen) is oxidized at the anode/electrolyte interface and oxygen is reduced at the cathode/electrolyte interface. Oxygen ions transport across the electrolyte and electrons through an external circuit to create a current. SOFC systems consist of many cells each with their own anode, cathode, and electrolyte. Individual cells typically produce less than 1 volt and to achieve useful voltage and power, cells are stacked and connected via interface materials called interconnects [118]. SOFCs that operate at lower temperatures (600-850 °C) may use metallic interconnects, such as ferritic stainless steel [119]. As discussed, stainless steel interconnects exposed to air and/or H_2O may release volatile Cr trioxide (CrO_3) and/or Cr oxyhydroxide ($CrO_2(OH)_2$), also known as chromic acid. These volatile species proceed downstream and deposit on the cathode through chemical and electrochemical deposition, adversely impacting fuel cell performance, an occurrence known as “Cr poisoning” [120-123].

The cathode/electrolyte interface is referred to as the triple-phase boundary (TPB), the region at which the gas phase, electrolyte, and cathode meet. Cr deposition occurs at phase boundary points including the TPB as well as two-phase boundary points (cathode/gas, electrolyte/gas). These deposits degrade SOFC performance over time by decreasing the efficiency of ion exchange. Acceptable performance degradation is defined by the US Department of Energy as less than 0.2% per 1000 hours over 40,000 hours of operation [124]. Modern SOFC designs

have achieved less than 0.1% performance degradation per 1,000 hours when operated for 17,000 and 19,000 hours [125, 126]. Studying Cr reactive condensation / interaction with components present in SOFC/SOEC systems is an important part of achieving this goal of <0.2% performance degradation over 40,000+ hours operation time.

Cr poisoning at the TPB can be exacerbated by chemical interactions between glass–ceramic sealants and ferritic steel interconnects, contributing to degradation of the system. Cr poisoning at the TBP may lead to a breakdown of the ceramic sealing glass, changes in anode porosity, separation of phases, horizontal and vertical cracking, or delamination[127]. SOFC technology has great potential, but improvements in performance and longer operation times are needed and investigating degradation, such as Cr poisoning, is critical to achieving these goals. A path towards this goal includes exploring the interactions between volatile Cr and ceramic surfaces such as aluminosilicates. These materials, used as sealants in SOFCs, belong to the SiO_2–Al_2O_3 system and contain different compositions of oxides including CaO, Na_2O, MgO, K_2O, B_2O_3, Y_2O_3, and BaO [60, 61]. Another commonly used sealant material is compressed mica paper [62, 63]. Two types of mica commonly used in SOFC applications are muscovite (potassium aluminum silicate hydroxide fluoride, $KAl_2(AlSi_3O_{10})(F,OH)_2$), and phlogopite (potassium magnesium aluminum silicate hydroxide, $KMg_3(AlSi_3O_{10})(OH)_2$). Studying the interactions between these materials and Cr vapors has a direct effect on the development of improved SOFC systems.

Experimental

Transpiration in biological sciences normally refers to gas exchange through plants. However, in high-temperature oxidation studies, transpiration refers to experiments that involve flowing a reactant gas over a compound of interest in a temperature-controlled environment[158].

Pertaining to this investigation, the compound of interest is chromia and the reactant gas is dry air or air saturated with water vapor at varied levels. The gases then react with chromia to form volatile Cr species (see Eqs. 1&2). As the vapor species move downstream toward the furnace exit, the temperature decreases, and compounds begin to condense. This is where the experimental samples were positioned, with temperatures ranging from ~100-400°C. Fig. 21 displays a schematic of experimental design, based on experimental designs used in similar studies[43, 159]. Precision-controlled furnace systems were used to simulate common service environments. Temperature-controlled evaporators or a desiccant (Drierite) filter is attached to the inlet air line from a laboratory bench to effectively dehydrate and filter incoming air, which is then controlled for water vapor content varying from dry (~0%) to humid (>10%) conditions, before reaching the furnace. Heat wrap is used to avoid condensation before delivery to the tube furnace system. A flow meter is positioned near the exit of the furnace and a water-cooled condenser is used to further filter exhaust material.

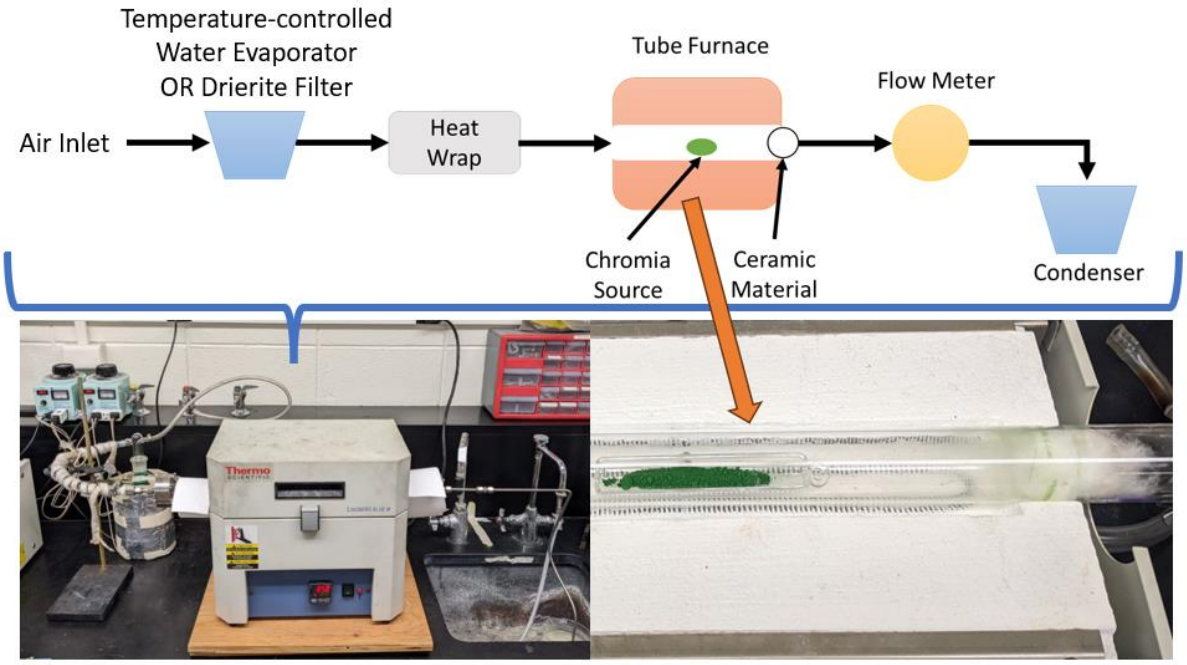

Figure 21: Experimental design diagram (top), experimental setup (bottom left), and chromia powder with ceramic insulation in furnace (bottom right).

A series of experiments were conducted to assess the influence of water vapor concentration on Cr reactive evaporation and condensation onto various materials. Adjusting the water vapor content using a Drierite filter or temperature-controlled water evaporator between dry (0 vol% H_2O), room temperature saturated air (~3 vol% H_2O), and elevated temperature (T=45°C) saturated air (≥10 vol% H_2O) conditions with different ceramic fiber insulation materials were the variables explored in this study. The location of the laboratory in which these experiments were conducted is at an elevation of 1,470 meters (4,820 feet) above sea level where the ambient pressure is approximately 84.87 kPa (636.58 mmHg). The ≥10 vol% H_2O saturation temperature of 45°C is calculated based on ambient pressure.

Materials for the experimental series include Cr_2O_3 powder as a Cr vapor source and ceramic fiber materials (e.g., silica, alumina, aluminosilicates, etc.) as substrates for Cr collection.

Prototypical ceramic fiber materials in this study include laboratory standard quartz and alumina wools, and quartz-based aluminosilicate fiber samples from two manufacturers of industrial thermal insulation materials. Approximately 2 grams of chromia powder and 2 grams of insulating material were used in each experiment. Fiber samples are placed in the tube with little resistance, but in a way to completely encompass the quartz tube at the threshold of the furnace exit. This manner of packing technique is repeated as closely as possible from experiment to experiment. Multiple experiments with each sample following these protocols yielded similar results. The temperature of the furnace is calibrated to 850^{o} C and is also recorded at the exit in three different locations where the ceramic material is placed using a thermocouple probe. These locations are marked on the 2.54 cm (1 inch) diameter quartz tube to ensure repeatability and are located inside the furnace at the exit, at the threshold of the furnace exit, and outside the furnace exit. The temperatures at each location are ~800^{o} C, ~500^{o} C, and ~160^{o} C respectively. Flow is calibrated to ~2 cm/s at temperature for each experiment and the experiment is run for 150 hrs. The resulting volumetric flow rate is ~10 cc/s or ~600 cc/min which places the Cr evaporation rate within the non-equilibrium regime according to Stanislowksi et al [160] or, according to Froitzheim et al [161], the linear evaporation rate regime. However, these Cr evaporation studies were conducted using alloys as the Cr source and not pure chromia.

Ceramic fiber diameters as well as chemical composition were analyzed using a Zeiss SUPRA 55VP field emission scanning electron microscope (FE-SEM) with an energy-dispersive x-ray spectroscopy (EDX) detector. Pre-exposure analysis of the fiber samples was conducted to verify manufacturer claims of chemical composition. EDX analysis has its limitations , however, and these include a lower limit to detectable concentrations (>0.01 wt%) and detecting lighter

elements with atomic numbers below eleven. Geometry and positioning of fibers also influence EDX results. To counter this effect, each sample is prepared for analysis, positioned, and analyzed under comparable conditions. Post-exposure samples were analyzed for total Cr and Cr(VI). These measures were separately quantified using: 1) a SPECTROBLUE EOP TI inductively coupled plasma optical emission spectrometry (ICP-OES) instrument for total Cr; and 2) direct UV-VIS using a ThermoSci Genesys 20 spectrophotometer with a visual colorimetric diphenyl carbazide (DPC) water test kit from Chemetrics for Cr(VI). ICP-OES can detect metals and several non-metals in liquid samples at very low concentrations from 1-5 ppb and up to 100 ppm. DPC is a visual or spectroscopic colorimetry technique that utilizes a reaction between DPC and Cr(VI) in acidic conditions, creating a red-violet color in direct proportion to the Cr(VI) concentration. Measurements were made against a color comparator and expressed as ppm (mg/L) CrO_4. DPC is limited to lower concentrations (0-0.8 ppm) before relative standard deviation increases to 20-50% whereas direct UV-VIS can be used for concentrations above 0.8 ppm and up to 100 ppm with relative standard deviations of 0.5%[11]. ICP-OES, DPC, and direct UV-VIS under these conditions produce uncertainties no greater than 10%. Solid samples, such as the fibers in this study, need to be prepared via acid digestion before being analyzed. 0.5 M nitric acid is used to digest samples on a hot-plate at 90-95℃ for one hour. Resulting solutions were dilute to 0.3 M before being analyzed via ICP-OES or DPC/direct UV-VIS at λ=540 nm for DPC and λ=340 nm for direct UV-VIS. Fig. 22 below displays the three fiber samples used in this study pre-exposure. Table 2 below presents the physical and chemical characteristics of each sample.

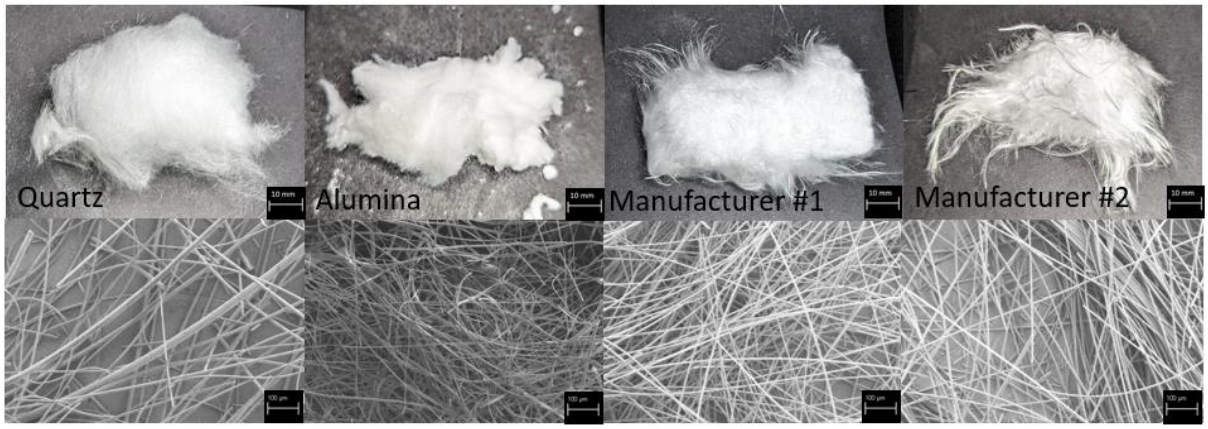

Figure 22: Fibers pre-exposure photographs (top) and SEM images (bottom).

Table 2 – Information on the ceramic fibers.

	Quartz	**Alumina**	**Insulation#1**	**Insulation#2**
Fiber Diameter, µm (Avg, Std Dev)	21.5, 14.3	9.7, 3.6	9.4, 2.1	10.7, 1.3
EDX Chemical Analysis (wt%) (Oxygen Balance)	Si (46.3%), S (0.5%), Na (0.3%)	Al (54.2%), Si (1.83%)	Si (46%), Al (1.6%), Na (0.5%)	Si (44.9%), Al (1.3%), Na (0.7%)

Results

Results below are presented as photos of samples as well as descriptions of observable staining, ICP-OES measurements, and DPC/UV-VIS measurements for each sample under the three environmental conditions: dry, normal, and humid water vapor concentration. Fig. 23 below shows photos of each fiber sample post-exposure for dry conditions. The alumina wool sample was photographed in a centrifuge tube. Following this figure, Table 3 contains descriptions of observable staining on each fiber sample as well as ICP-OES and DPC/UV-VIS results for dry conditions.

"Dry" (~0% H_2O) Air Conditions

Figure 23: Fibers post-exposure for dry conditions.

Table 3 – Comparison of appearance and Cr content for dry conditions.

	Quartz Wool	**Alumina Wool**	**Insulation #1**	**Insulation #2**
Color	Light green/ yellow and brown	Light yellow and brown.	Slightly off colored.	Light yellow, light brown.
Direct UV-VIS/DPC	<0.1 ppm	<0.1 ppm	<0.1 ppm	<0.1 ppm
ICP-OES	0.467 ppm	0.179 ppm	0.135 ppm	0.073 ppm

Next, Fig. 24 shows photos of each fiber sample post-exposure for normal water vapor concentration conditions. Following Fig. 24, Table 4 contains descriptions of observable staining on each fiber sample as well as ICP-OES and DPC/UV-VIS results.

"Normal" (~3% H_2O) Saturated Air Conditions

Figure 24: Fibers post-exposure for "normal" conditions.

Table 4 – Comparison of appearance and Cr content for "normal" conditions.

	Quartz	**Alumina**	**Insulation#1**	**Insulation#2**
Color	Yellow green, red brown.	Yellow, red brown	Yellow green.	Yellow green, brown.
UV-VIS/DPC	0.74 ppm	0.40 ppm	0.17 ppm	0.36 ppm
ICP-OES	1.339 ppm	1.976 ppm	0.651 ppm	0.727 ppm

Next, Fig. 25 shows photos of each fiber sample post-exposure for humid water vapor concentration conditions. The alumina wool sample was photographed in a centrifuge tube here as well. Following Fig. 25, Table 5 contains descriptions observable staining on each fiber sample as well as ICP-OES and DPC/UV-VIS results.

"Humid" (~10% H2O) Conditions

Figure 25: Fibers post-exposure for humid conditions, clockwise starting from top-left: quartz wool, alumina wool, insulation #1, and insulation #2.

Table 5 – Comparison of appearance and Cr content for humid conditions.

	Quartz	**Alumina**	**Insulation#1**	**Insulation#2**
Color	Yellow green, red brown.	Yellow, brown.	Yellow, brown.	Yellow, brown.
UV-VIS/DPC	1.78 ppm	2.52 ppm	0.27 ppm	0.60 ppm
ICP-OES	3.113 ppm	4.012 ppm	1.718 ppm	1.183 ppm

Finally, Fig. 26 below presents total Cr and Cr(VI) measurements obtained from ICP-OES and DPC/UV-VIS as a histogram plot with error bars (10% uncertainty) for each fiber sample with respect to water vapor concentration. To ensure repeatability, experiments for each sample have been at least duplicated (some triplicates). However, the methodology has evolved, and more refined characterization techniques were used in later iterations. The exact measurements have changed but the trends/differences in total Cr/Cr(VI) collection agree with respect to changes in

water vapor concentration. As a result, the 10% error bars in Fig. 26 may be an underestimate of the total error involved due to fiber packing and positioning in the quartz tube.

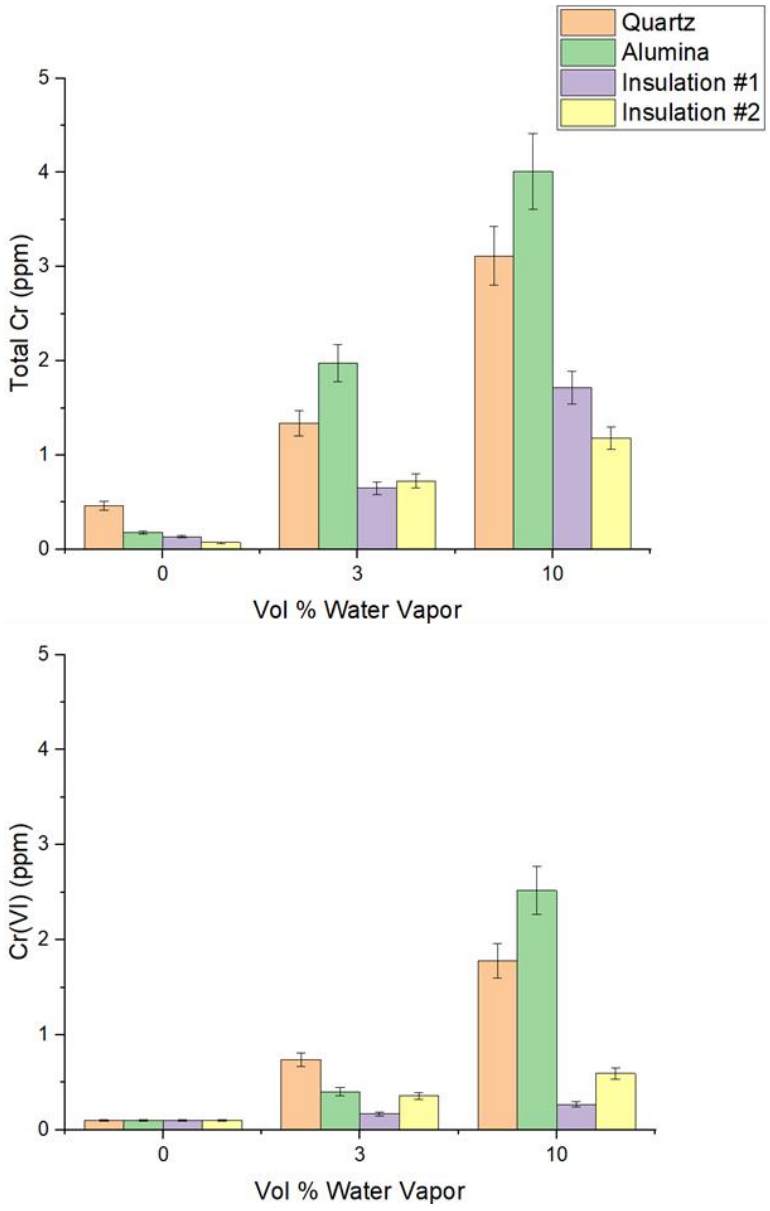

Figure 26: Histograms plots of total Cr (top) and Cr(VI) (bottom) for each fiber sample with respect to vol% water vapor with error bars (10% uncertainty).

Discussion

The post-exposure photos, ICP-OES measurements, and DPC/UV-VIS results show a general increase in loading of total Cr and Cr(VI) with increasing water concentration for all four sample types used in this study. Observing the staining on each sample from Fig. 23 to 24 to 25 shows a repeating pattern of color bands that becomes more evident on each sample as water concentration increases. Measurements from ICP-OES and from DPC/UV-VIS presented in Tables 3, 4, and 5 show an increase in total Cr and Cr(VI) with increasing water concentration. As seen in Fig. 26, quartz collects more total Cr for dry conditions and Cr(VI) for normal water vapor concentration conditions, but alumina collects the most Cr and Cr(VI) for humid water vapor concentration and the manufacturer insulations collected the least amount of Cr / Cr(VI). The differences in total Cr and Cr(VI) collection between samples could be due to differences in surface areas and chemical composition. Among the samples investigated, the quartz wool has the largest average and standard deviation fiber diameter in addition to a more random arrangement of fiber orientations. The alumina fibers are also more random in orientation than the manufacturer insulations which are more aligned and very similar in size due to their manufacturing process, however the average and standard deviation of the alumina fiber diameters is more akin to the manufacturer insulations than the quartz wool. Surface area (m^2/kg) can be estimated from the fiber diameter, but is also affected by the orientation, arrangement, and density of the fibers. The average and standard deviation measurements of fiber diameters can be used to approximate surface areas. Using this approximation, the surface areas for fibers in the alumina and manufacturer insulations are found to be comparable. The measurements of the quartz wool, however, reveal fibers with much smaller and larger surface areas than that of alumina or the

manufacturer insulations. Chemical composition is more similar amongst the quartz and manufacturer insulations, which is mostly silica. These observations are reinforced by the results from the studies of Tatar et al [78, 93, 94] that found alumina to collect more Cr than silica. Other studies focusing on the influences of other elements present in the substrate material, such as sulfur or alkaline metals like sodium, have found that these elements can influence the reactive condensation mechanics of Cr. For example, researchers observed that the formation of $SrCrO_4$ is promoted under combined Cr and S contaminating conditions [128]. It is possible that the small amounts of sulfur and sodium had some effect on the total Cr/Cr(VI) collected on the quartz wool sample.

The differences in observable stain colors in Fig. 23, 24, and 25 as well as the measured total Cr/Cr(VI) collected on the fibers as presented in Fig. 26 can be explained by a series of events proposed by Tatar et al [78, 93, 94]. The aluminosilicate fibers are exposed to volatile Cr species in an environment of air or air and water vapor at temperatures between 100–400°C. This temperature range encompasses the boiling point of chromic acid (~200°C), and the vapors may begin to become physiosorbed to the fiber surfaces at this point. Once physiosorbed, $CrO_2(OH)_2$ may dehydrate and form CrO_3. Further CrO_3 formation may occur from esterification reactions between chromate species and the aluminosilicate surfaces. Hydroxyl groups on the surfaces of the fibers function as anchoring points, allowing for stabilization and diffusion of Cr(VI) species. The color of the material loaded with these diffused chromate species at this point is yellow. As Cr loading increases, hydroxyl groups diminish and chromate species may form O-Cr-O bonds resulting in polychromate species, and eventually CrO_3. These polychromate species are minimally anchored to the surface and therefore minimally stabilized. At this stage, the color of the loaded

material is brown. De-hydroxylation, the process by which surface hydroxyl groups are effectively removed through bonding with hydrogen to form water, may also occur at elevated temperatures (>500℃)[162]. This could help explain the color gradient seen in the samples where the stained sections correspond to the area at which the temperature is close to the condensation point of Cr vapor, the inner unstained section is the area above the condensation point, and the outer unstained section is the point at which no more Cr vapor is left to condense. Fig. 27 below depicts a possible version of the process of chromate species formation and speciation on a hydroxylated metal oxide surface as Cr loading increases over time.

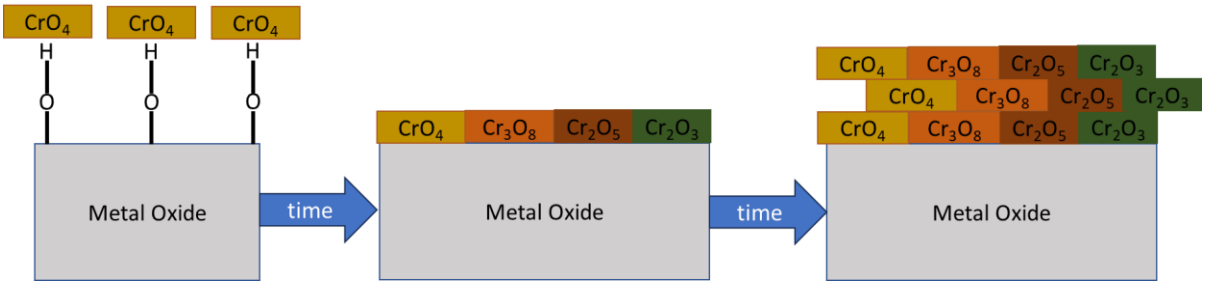

Figure 27: Cr species condensation and speciation on hydroxylated surface.

Dehydroxylation effects are more pronounced in the “dry” conditions than the “normal” or “humid” conditions. When water vapor is introduced into the atmosphere, rehydroxylation of dehydroxylated surfaces can occur and the rehydroxylation effect is increased with increased water vapor concentration. This effect can be compared to the effects of water vapor content on reactive evaporation rates. The partial pressure of Cr oxyhydroxide is higher by several orders of magnitude than Cr trioxide and becomes the dominant vapor species in the presence of water vapor, increasing reactive evaporation of Cr. Reactive condensation can be affected by increased water vapor content by preventing dehydroxylation of the surface in a high temperature environment through rehydroxylation, preserving or restoring hydroxyl groups on the surface of the substrate material.

This could explain the observation of condensed Cr/Cr(VI) on the surface of the fiber samples increasing with water vapor concentration. Differences in hydroxyl population densities of amorphous silica (2.35 OH nm^{-2}) and γ-Al_2O_3 (4-6 OH nm^{-2}) could explain the increased Cr/Cr(VI) collected on the alumina wool[80, 88]. This reinforces the observation that hydroxyl groups serve as anchoring points for volatile species and Cr deposition increases with increasing surface hydroxyl populations and basicity. Surface area also has an effect as more available surface area translates to more available hydroxyls. The surface area of the alumina wool is expected to be greater than that of quartz due to its smaller average fiber diameter. Fig. 28 below depicts the process of dehydroxylation on a hydroxylated metal oxide surface and the impact of this process on the surface chemistry.

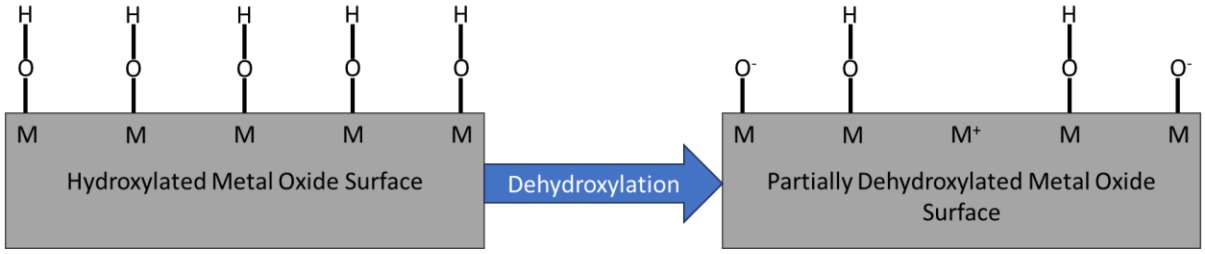

Figure 28: Dehydroxylation effect on hydroxylated metal oxide surface.

On the potential role of surface hydroxyl density, a partially dehydroxylated oxide surface has hydroxyl groups, coordinatively unsaturated metal cations, and oxygen anions. Coordinatively unsaturated cations at the surface can accept free electron pairs of adsorbed molecules and act as Lewis acid sites. The M+ sites behave like Lewis acids, and the O- ions are more basic than the bulk ions. Coordinative unsaturation becomes more extensive if dehydroxylation takes place[163]. The strength of these acid sites depends on the charge and size of the cations, both of which vary with the oxidation number of the cation. In hard soft acid base (HSAB) theory, cations of a higher

oxidation state are harder acids. The strength of these acid sites depends on the charge and size of the cations which vary with the oxidation state of the cation. Harder cations are smaller and less polarizable, and they will absorb or bind hard bases stronger than soft or polarizable bases.

A study on the role of hardness in the adsorption of Cr(VI) onto metal oxide nanoparticles indicated that the adsorption onto an oxide surface is influenced by their chemical hardness[164]. The hardness of the cation determines the basicity of surface OH groups which regulates adsorption as well as protonation and deprotonation. The hardness match between a sorbent and a sorbate may be interpreted as their chemical affinity and this was found to be the driving force for adsorption of Cr(VI) anions onto the oxides. Aluminum in alumina is a harder acid than silicon in silica, therefore the bonding between aluminum and oxygen is harder and more stable, leading to greater affinity for adsorption of Cr anions for the alumina wool compared to quartz wool, as was observed in this study.

Limitations of Study and Future Work Recommendations

Before presenting the conclusions, the limitations of this study need to be discussed. The placement and packing of the fibers within the furnace exit could influence Cr condensation. The fibers themselves are oriented differently and have varying surface areas from sample to sample, the specific placement of each sample could have an impact on internal pressure of the reaction tube, influencing the fluid mechanics of the gas flow across the fiber surfaces as well. Another aspect of fiber placement is the fluid flow past the fibers, it is not uniform and Cr vapors will not distribute equally across all fibers. This observation is reinforced by the detection of total Cr/Cr(VI) in the furnace effluent collected by the condenser. A second limitation is the acid digestion used for preparing samples to be analyzed via ICP-OES or DPC/UV-VIS

spectrophotometry. The efficacy of the digestion process used was quantified by measuring the difference in Cr(VI) detected after 1 hour at 90-95°C hot plate assisted nitric acid digestion and allowing the fibers to continue digesting for 12 hours unassisted. Measured Cr(VI) decreased by ~80%, meaning ~20% of the Cr remains on the fibers after hot plate assisted acid digestion. A third limitation is the differences in analytical techniques used. A single characterization technique that could be used for total Cr and Cr(VI) would provide more reliable data for comparison. Currently, the three different methods used limit the inter-sample comparisons or conclusions that can be drawn from the data. A fourth limitation is the experimental setup. Some Cr species interact and condense onto the surface of the quartz tubes used in the furnaces and this occurrence has been studied to optimize the experiment**[165]**. The authors of the study identified a method using a sodium carbonate coated thin alumina tube which effectively mitigates interference caused by chemical interactions between Cr vapor species and quartz and alumina furnace tube, allowing for improved assessment of Cr evaporation. Finally, the experiment could be improved to more accurately replicate service environments (e.g., thermal cycling, longer exposure times up to 1000 hours). However, this study was intended to create the extreme scenario of maximum Cr evaporation and condensation by using a pure chromia source and directly passing the vapors through the fiber samples.

Collection of both total Cr (in all forms) and Cr(VI) increases with increasing water concentration. As evident in Fig. 26, measurements from ICP-OES and from DPC/UV-VIS, also presented in Tables 3, 4, and 5, show an increase in total Cr and Cr(VI) with increasing water concentration across all samples. While the trends agree, the individual quantified data does not experience the same rate of change. This observation warrants further investigation such as in-situ

Cr / Cr(VI) measurements of the fibers using IR or Raman spectroscopy as a function of time, temperature, and Cr loading. High-temperature environments generate significant amounts of blackbody radiation and limit the methods of in-situ characterization of reaction mechanisms. However, advancements in IR and Raman spectroscopy in the past decade have successfully integrated these characterization techniques into SOFCs operating above 650℃ to correlate electrochemical performance with chemical processes occurring simultaneously within the system[166, 167].

Conclusions

In this study, silica- and alumina-based ceramic insulating fibers were exposed to Cr vapors produced by reacting chromia powder to high-temperature air with varying water concentrations. Similar ceramic insulating fibers from different manufacturers are tested under similar conditions for comparison. Chemical analyses are then carried out for each sample so that the results can be compared quantitatively. The effects of increasing water concentration have a significant impact on total Cr collection across all samples, most notably for humid conditions.

This study confirms the known relationship of increased water content on increased Cr vapor production, which results in a similar relationship for Cr condensation. The different amounts and speciation of Cr observed on the ceramic substrates also suggests different Cr condensation mechanisms for different ceramic surfaces and conditions, which invites further investigation. Implications for high-temperature systems such as SOFC/SOECs, chemical processing plants, steam power plants, or exhaust manifolds of large combustion engines include material selection and system design to consider the impacts of increased water concentration on corrosion of stainless-steel components within these systems and the resultant Cr vapor interaction

with downstream components such as ceramic insulating surfaces, sealing glasses, and cathode/anode materials.

CHAPTER FIVE - REACTIVE CONDENSATION OF CR VAOPRS ON ALUMINOSILICATE FIBERS CONTAINING ALKALINE OXIDES

Contribution of Authors and Co-Authors

Manuscript(s) in Chapter(s) 5

Author: Travis K. van Leeuwen

Contributions: Graduate research assistant, primary author

Co-Author: Amberly Guerrero

Contributions: Undergraduate research assistant, assisted in experimental setup and analysis

Co-Author: Ryan Dowdy

Contributions: Undergraduate research assistant, assisted in experimental setup and analysis

Co-Author: Bima Satritama

Contributions: Graduate student, thermodynamic equilibrium modelling

Co-Author: Akbar Rhamdhani

Contributions: Professor, thermodynamic equilibrium modelling

Co-Author: Geoffrey Will

Contributions: Professor, thermodynamic equilibrium modelling

Co-Author: Paul Gannon

Contributions: Primary investigator

Manuscript Information

T. K. van Leeuwen, A. Guerrero, R. Dowdy, B. Satritama, A. Rhamdhani, G. Will, and P.

Gannon

Journal of the Electrochemical Society

Status of Manuscript:
☐ Prepared for submission to a peer-reviewed journal
[x] Officially submitted to a peer-reviewed journal
☐ Accepted by a peer-reviewed journal
☐ Published in a peer-reviewed journal

IOP Publishing Limited
2024

Abstract

The objective of this research is to improve fundamental understanding of reactive condensation of Chromium (Cr) vapors, which are generated from Cr containing alloys used in many high-temperature (>500°C) process environments and can form potentially problematic condensed hexavalent (Cr(VI)) species downstream. This study focuses on the effects of alkaline oxide additives in aluminosilicate fibers on Cr condensation and speciation. Cr vapors were generated by flowing high-temperature (800°C) air containing 3% water vapor over chromia (Cr_2O_3) powder, with aluminosilicate fiber samples positioned downstream where the temperature decreases (<500°C). Total condensed Cr and ratios of oxidation states were measured using inductively coupled plasma optical emission spectroscopy (ICP-OES) and diphenyl carbazide (DPC) colorimetric/direct UV-VIS spectrophotometric analyses. Results indicate presence of hexavalent Cr (Cr(VI)) species condensed on all samples investigated. Total Cr and ratio of Cr(VI) to total Cr detected was significantly more on aluminosilicate fiber samples containing alkaline oxide (CaO and MgO) additions. Computational thermodynamic equilibrium modelling corroborated the experimental results showing stabilities of Ca and Mg chromate compounds. Comparative results and analyses are presented and discussed to help inform mechanistic understanding and future related research and engineering efforts.

Introduction

Chromium (Cr) vapors are generated in high-temperature (>500°C) systems that employ chromia (Cr_2O_3)-forming alloys such as stainless steels used in exhaust manifolds, steam turbines, boilers, or solid oxide fuel/electrolysis cell (SOFC/SOEC) systems. Reactive evaporation of Cr is

known to occur in oxygenated environments and increases in the presence of water vapor[2]. The generated Cr oxide and hydroxide vapors proceed downstream and interact with the surfaces of other components in the system. These component surfaces could be ceramic insulating fibers such as those found in insulation blankets used in power and chemical plants or the ceramic sealants or electrodes used in SOFCs. Understanding the interactions between volatilized Cr species and downstream components during operation is critical for improving system performance, environmental health, and safety as some condensed Cr forms carcinogenic hexavalent Cr(VI) species. Reactive evaporation of Cr from chromia-forming alloys, like stainless steels, commonly used in these systems is well-documented as the primary Cr vapor source implicated in Cr poisoning of SOFCs; however, the interactions between volatilized Cr species and surrounding interfaces during complex and dynamic system exposures is poorly understood. The objective of this study is to explore the effects of alkaline oxide additives in aluminosilicate fibers on Cr collection/condensation and speciation onto these ceramic fibers.

Reactive Evaporation

Reactive evaporation of chromia from the surface of stainless steels occurs in high temperature (>500°C) in oxygenated environments with or without water vapor. These environmental conditions degrade the otherwise protective chromia surface layers by encouraging reactive evaporation of surface compounds interacting with the gaseous environment. Common stainless steels containing Cr develop a Cr oxide scale when exposed to oxygen and this scale reaches a thickness which prevents further access of oxygen to the underlying metal. The scale thickness increases while the time required to reach it decreases with increasing temperature. Once this limiting thickness is reached, the rate of oxide scale growth equals the rate of Cr evaporation

at elevated temperatures [157]. Chromia in these layers may volatilize at a greater rate than it is reformed, eventually causing the oxide layer to become less protective, forming compounds such as $(Fe, Cr)_2O_3$ or iron oxides [37, 38]. Chromia in the oxide layer also transforms into a mobile vapor species upon reactive evaporation and interacts with the surrounding system. These interactions can form compounds that pose risks to human health, the environment, and degrade performance in electrochemical devices like SOFCs.

Reactive evaporation of Cr from chromia occurs in oxygenated environments to form $CrO_3(g)$. Example reactions for chromia evaporation include:

$$\tfrac{1}{2}Cr_2O_3(s) + \tfrac{3}{4}O_2(g) = CrO_3(g) \qquad \text{Eq. 1}$$

$$\tfrac{1}{2}Cr_2O_3(s) + H_2O(g) + \tfrac{3}{4}O_2(g) = CrO_2(OH)_2(g) \qquad \text{Eq. 2}$$

The evaporation rate increases in the presence of water vapor and leads to the formation of $CrO_2(OH)_2(g)$ [43-45]. Partial pressure of $CrO_2(OH)_2(g)$ is larger than that of $CrO_3(g)$ by several orders of magnitude in the presence of water vapor up to 1400 K [43-48] and thermodynamic data predicts an equilibrium partial pressure of Cr oxyhydroxide ($CrO_2(OH)_2(g)$) that is greater in the presence of water vapor by several orders of magnitude up to ~1500 K [49]. Thermodynamic data also predicts an equilibrium partial pressure of $\sim 8 \times 10^{-40}$ bar for $CrO_3(g)$ at ~298 K, which increases by several orders of magnitude to $\sim 1 \times 10^{-15}$ bar at ~800 K [49]. Although the partial pressures from experimental and thermodynamic data agree in general trends, they often differ in exact partial pressure values by an order of magnitude [45, 49].

Reactive Condensation

While reactive evaporation mechanisms of Cr are well-documented, there are relatively few publications focusing on the chemical and physical processes that occur during downstream reactive condensation[78, 93, 94]. Reactive condensation of Cr onto various surfaces under different conditions such as refractory ceramic materials like alumina and silica[168, 169], and on SOFC components, such as those made from manganese or strontium, is a well-known occurrence[136, 138]. Cr is also commonly used as a catalyst on ceramic supports, such as silicas, aluminas, and aluminosilicates[64, 67, 68, 70, 73, 75, 83, 85, 87, 90, 91, 104, 170]. However, unlike reactive condensation of Cr vapor, the impregnation of Cr onto catalyst supports is completed in an aqueous environment. Speciation of Cr deposited on catalyst supports depends on the support material, processing temperature, and Cr loading. Speciation of Cr condensed from its vapors can be initially identified by the color of stains appearing on the ceramic substrate materials (e.g., alumina). Green is indicative of trivalent chromium species whereas brown and yellow are indicative of hexavalent chromium species, or mixtures thereof. In one study, the following compounds were linked to specific staining colors: Condensed $Cr_2(OH)_2$ or CrO_3 (brown staining), CrO_4 (yellow staining), and Cr_2O_3 (green staining) [95].

Solid Oxide Fuel Cell Degradation

SOFCs operate using a series of individual cells, each consisting of two electrodes separated by an ion-conducting electrolyte [117]. Fuel (e.g., hydrogen) is oxidized at the anode/electrolyte interface during operation, and oxygen is then reduced at the cathode/electrolyte interface. Oxygen ions transported across the electrolyte prompt electrons to move through an external circuit to create a current. Individual cells, each with their own anode, cathode, and

electrolyte, typically produce less than 1 volt. To achieve useful voltage and power, cells are stacked and connected via interface materials called interconnects [118]. SOFCs that operate at lower temperatures (600-850°C) may use metallic interconnects, such as ferritic stainless steel (FSS) [119]. As discussed earlier in the introduction, chromia-forming stainless steels like FSS may release volatile chromium trioxide (CrO_3) and/or chromium oxyhydroxide ($CrO_2(OH)_2$)) when exposed to air and/or H_2O. These volatile species proceed downstream and deposit on the cathode through chemical and electrochemical deposition, an occurrence known as "chromium poisoning" [120-123]. In addition to Cr poisoning, chemical interactions between glass–ceramic sealants and FSS interconnects contribute to degradation of the system [127].

Cr poisoning also occurs at the cathode/electrolyte interface. This interface is referred to as the triple-phase boundary (TPB) and is the point at which the gas phase, electrolyte, and cathode meet. Cr deposition occurs at two-phase boundary points (cathode/gas, electrolyte/gas) as well. These Cr deposits degrade SOFC performance over time by forming secondary phases, which decrease the efficiency of ion exchange. Acceptable performance degradation is defined by the US Department of Energy as less than 0.2% per 1000 hours over 40,000 hours of operation [124]. Modern SOFC designs have achieved less than 0.1% performance degradation per 1,000 hours when operated for 17,000 and 19,000 hours [125, 126]. SOFC technology has great potential as an energy conversion technology, but improvements in performance and longer operation times are needed. Understanding Cr condensation reactions, such as Cr poisoning and SOFC degradation, is critical to achieving these goals.

Chromium Vapor Interactions with Sealing Glasses

Sealing materials in SOFC/SOEC stacks are used to protect against air and gas leaks between interconnects. Commonly used sealing materials are ceramic glasses belonging to the SiO_2–Al_2O_3 system and contain different compositions of oxides including CaO, Na_2O, MgO, K_2O, B_2O_3, Y_2O_3, and BaO [60, 61]. Another commonly used sealant material is compressed mica paper [62, 63]. Two types commonly used in SOFC applications are muscovite (potassium aluminum silicate hydroxide fluoride, $KAl_2(AlSi_3O_{10})(F,OH)_2$), and phlogopite (potassium magnesium aluminum silicate hydroxide, $KMg_3(AlSi_3O_{10})(OH)_2$).

Two sealing glass materials are classified as G18 and G#36. G18 is a barium alumino-silicate (BCAS)-based glass–ceramic [135] and G#36 is a mixture of $SrCO_3$, $CaCO_3$, boric acid, and various oxides [136]. Strontium chromate was observed to form from interactions between volatile Cr species and SOFC cathode materials such as lanthanum strontium cobalt ferrite (LSCF) and on sealing glasses containing SrO. Researchers placed G#36 pastes on 430 stainless steel substrate surfaces and held them at 800°C for one to two weeks [136]. Yellow staining on the glass was observed first forming around the edges before progressing inward over time. In another study, chromia and G18 powder were mixed and heated to 950°C in dry air for 24 hours. The resultant product was stained yellow and was analyzed via XRD which confirmed the formation of $SrCrO_4$ [137]. Researchers have reported similar findings from barium-calcium aluminosilicate-based glass-ceramic G18 and FSS. Reaction couples between G18 and FSS 446 coupons were heated to 850°C for one hour then lowered to 750°C for an additional four hours. Barium oxide was observed reacting with chromia and/or volatile Cr species to form a yellow $BaCrO_4$ resulting in the G18 detaching from the FSS 446 coupon. Separation of the two materials was due to differences in the respective coefficients of thermal expansion between $BaCrO_4$ and G18/FSS 446. While $BaCrO_4$

was not identified using a phase identification technique in this study, a separate study identified this phase using XRD [138].

Chromium "Getters"

To combat Cr poisoning of SOFC systems, materials that readily absorb and trap volatile Cr species have been developed. These materials, dubbed "chromium getters," are those that readily react with gaseous Cr to form thermodynamically stable surface species[50]. Cr getters are inserted within SOFC stacks to attract gaseous Cr and decrease the total amount in the system. A commonly used design involves coating fibers, wools, or honeycomb substrates with $Sr_xNi_yO_z$ [139-142].

Researchers have demonstrated novel methods to mitigate cathode degradation using Cr getters manufactured from low-cost materials [140, 142]. The getters use a cordierite honeycomb substrate coated with alkaline earth and transition metal oxides. The first getter design was tested for 500 h under SOFC cathode exposure conditions [142]. Chemical and structural analyses show gaseous Cr concentrated at the getter with only the end of the getter free of Cr. The second study measured the electrochemical performance of the SOFC system for 100 h at 850℃ with and without the Cr getter [140]. Stable electrochemical performance was maintained for the cell tests with getters, whereas the cell performance in the test without Cr getters rapidly decreased after 10 h. Results from tests with SOFCs and getters demonstrated the high efficiency of Cr capture technology for the preservation of cell performance.

Of these Cr getters, few if any consider disposal/recycling methods. For example, in some getters the thermodynamically stable Cr compounds formed are in a hexavalent oxidation state such as $SrCrO_4$(s) [139, 142]. The presence of Cr(VI) compounds on the getter renders it hazardous

waste and requires further chemical processing to become recyclable. The authors of one Cr getter study, however, did take this issue into account and developed a catalytic "Cr getter." Using a Ti/TiO_2 surface to capture Cr compounds, captured Cr(VI) compounds are then reduced to Cr(III) [171]. The reduction of Cr(VI) compounds to Cr(III) allows for the contaminated Cr getter to be recycled as a regular metal at the end of its service life.

The studies presented above show the potential for volatile Cr species generated from stainless steel in high-temperature systems to engage in reactive condensation onto ceramic surfaces to form trivalent Cr(III), and hexavalent Cr(VI) species. The influence of oxides on the surface is of interest as Cr(VI) species formation was observed to increase in the presence of Sr and Ba. Cr(VI) species also formed without these elements for example, Cr catalysts on ceramic supports that often lack alkaline earth metals, still support Cr(VI) formation[67, 72, 79, 80, 84]. Studying the interactions between these materials and Cr vapors has direct implications for the development of improved high-temperature processes and systems. A path towards this goal includes exploring the interactions between volatile Cr and ceramic surfaces such as aluminosilicates with or without alkaline oxide additives.

Experimental

Transpiration experiments involve flowing a reactant gas over a compound of interest in a temperature-controlled environment. In this investigation, the compound of interest is chromia and the reactant gas is 800°C air saturated with ~3 vol% water vapor, intended to simulate prototypical high-temperature system conditions. The gases then react with chromia to form volatile Cr species. As the vapor species move downstream toward the furnace exit, the temperature decreases, and gaseous compounds begin to condense. This is where the experimental sample fibers are

positioned, with temperatures ranging from ~100-500°C. Fig. 29 displays a schematic of experimental design, based on a design used by another research group [43]. Precision-controlled furnace systems are used to simulate common service environments. A water evaporator held at room temperature to achieve the desired water vapor content is attached to the inlet air line from a laboratory bench air supply to effectively filter incoming air and maintain water vapor saturation before reaching the furnace. Heat wrap controlled by a variable AC power supply is used to avoid water condensation before delivery to the tube furnace system. A flow meter is positioned near the exit of the furnace and a water-cooled condenser is used to further filter exhaust material. Temperatures are recorded throughout the system during flow conditions to promote uniformity in experiments.

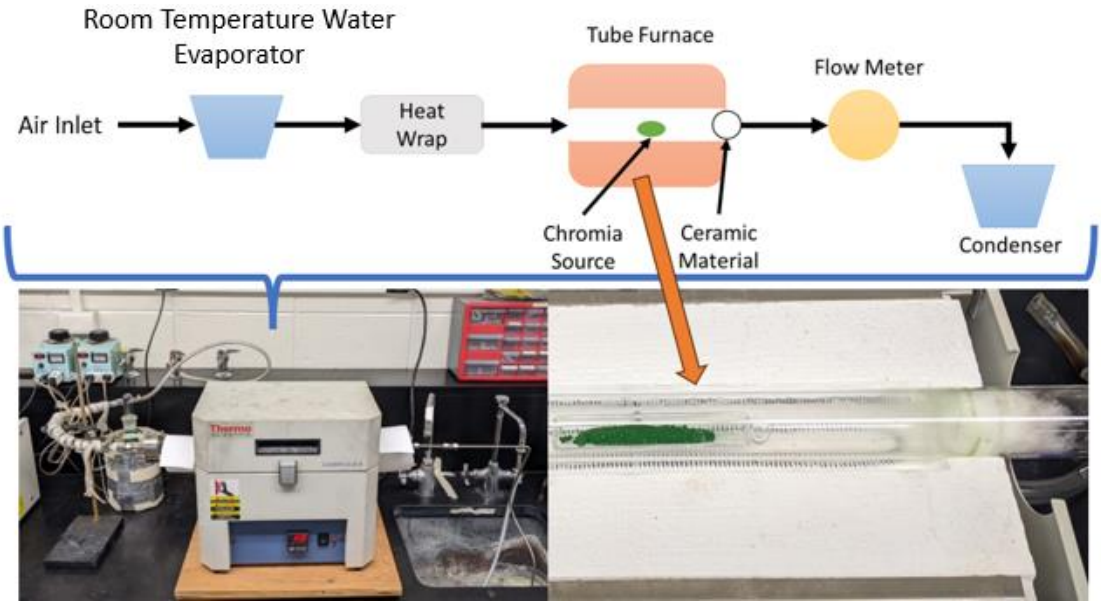

Figure 29: Experimental design diagram (top), experimental setup (bottom left), and chromia powder with ceramic insulation in furnace (bottom right).

A series of experiments were conducted to assess the effects of alkaline oxide additives on Cr reactive condensation. Prototypical ceramic fiber insulation materials used in this study included high-purity quartz and alumina fibers purchased from laboratory supply vendors Wale Apparatus and EA Consumables, respectively, while the two silica-based alkaline earth silicate (AES) fiber samples with varying alkaline oxide content were purchased from Lynn Manufacturing, an industrial thermal insulation vendor. Approximately 2 g of chromia powder and 2 g of ceramic insulating fiber material are used in each experiment. This is an arbitrary amount that is used for repeatability across samples. It could also be considered an extreme case of Cr vapor exposure to the HTIW samples as the Cr source would be mixed with other stainless-steel components if observed in the field. The tube furnace center where the chromia powder is placed was calibrated to 850℃ and temperature was recorded at the exit in three distinct locations where the ceramic material is placed using a thermocouple probe. These locations include inside the furnace at exit, at the threshold of the furnace exit, and outside the furnace exit are marked on the 2.54 cm (1 inch) quartz tube. The temperatures at each location are ~800℃, ~500℃, and ~160℃, respectively. Flow is calibrated to a face velocity of ~2 cm/s for each experiment and the experiment is run for 150 hrs. The resulting volumetric flow rate is ~10 cc/s or ~600 cc/min which places the Cr evaporation rate within the non-equilibrium linear evaporation rate regime according to other researchers [160],[161], however these Cr evaporation studies were conducted using alloys as the Cr source and not pure chromia. The location of the laboratory in which these experiments were conducted is at an elevation of 1,470 meters (4,820 feet) above sea level where the ambient pressure is approximately 84.9 kPa (637 mmHg).

Pre-exposure samples are characterized using a Zeiss SUPRA 55VP field emission scanning electron microscope (FE-SEM) with an energy-dispersive x-ray spectroscopy (EDX) detector. Total Cr and Cr(VI) is quantified using a SPECTROBLUE EOP TI inductively coupled plasma optical emission spectrometry (ICP-OES) and direct UV-VIS using a ThermoSci Genesys 20 spectrophotometer with a visual colorimetric diphenyl carbazide (DPC) water test kit from Chemetrics [172]. ICP-OES can detect metals and several non-metals in liquid samples at very low concentrations from 1-5 ppb and up to 100 ppm. DPC is a visual or spectroscopic colorimetry technique that utilizes a reaction between DPC and Cr(VI) in acidic conditions, creating a red-violet color in direct proportion to the Cr(VI) concentration. Measurements are made against a color comparator and expressed as ppm (mg/L) CrO_4. DPC is limited to lower concentrations (0-0.8 ppm) before relative standard deviation increases to 20-50% whereas direct UV-VIS can be used for concentrations above 0.8 ppm and up to 100 ppm with relative standard deviations of 0.5%[11]. Absorbance on the spectrophotometer is measured at λ=540 nm for DPC and λ=340 nm for direct UV-VIS. ICP-OES, DPC, and direct UV-VIS under these conditions produce uncertainties no greater than 10%. The uncertainty for ICP-OES measurements under 0.01 ppm, however, increases to 40%. Solid samples, such as the fibers in this study, need to be prepared via acid digestion before being analyzed. 0.7 M nitric acid is used to digest samples on a hot-plate at 90-95°C for one hour. Resulting solutions are diluted to 0.3 M before being analyzed via ICP-OES or DPC/direct UV-VIS. Fig. 30 and 31 below display the four fiber samples used in this study pre-exposure. Table 1 below presents the physical and chemical characteristics of each sample. Pre-exposure samples of AES #1 and AES #2 wools were also acid digested under the same conditions outlined above and then analyzed via ICP-OES to observe changes in leached Cr, Ca, Mg, Na, and

K. The results from ICP-OES and DPC/direct UV-VIS analyses are presented in the Results section as histogram plots in Fig. 33, 34, and 35.

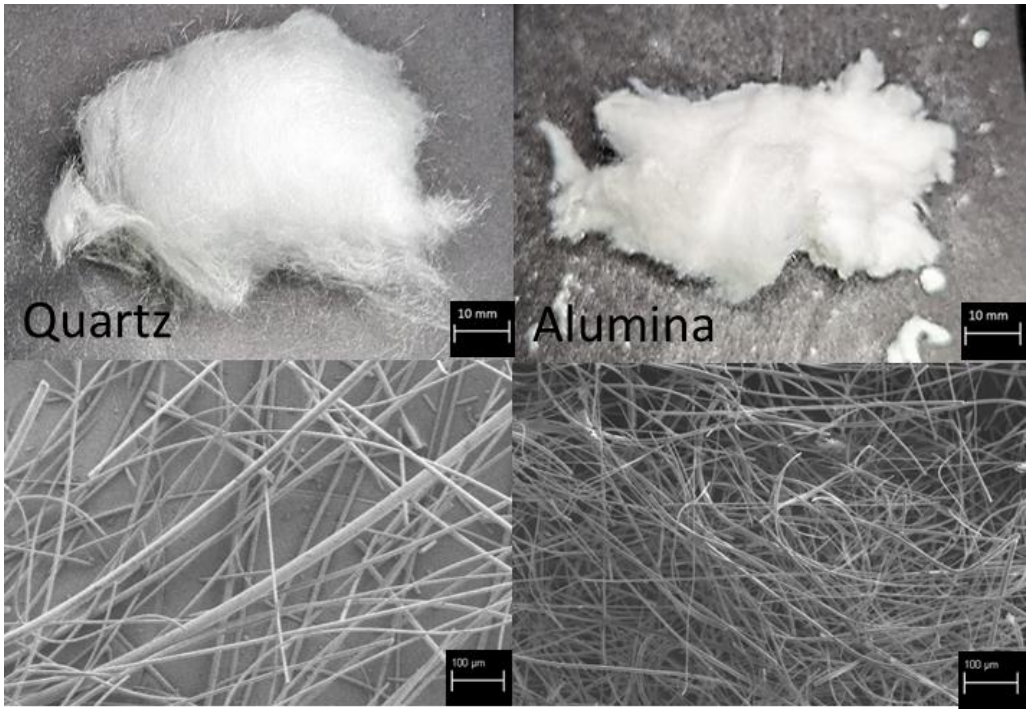

Figure 30: Fibers pre-exposure photographs (top) and SEM images (bottom) from left to right: quartz wool, alumina wool.

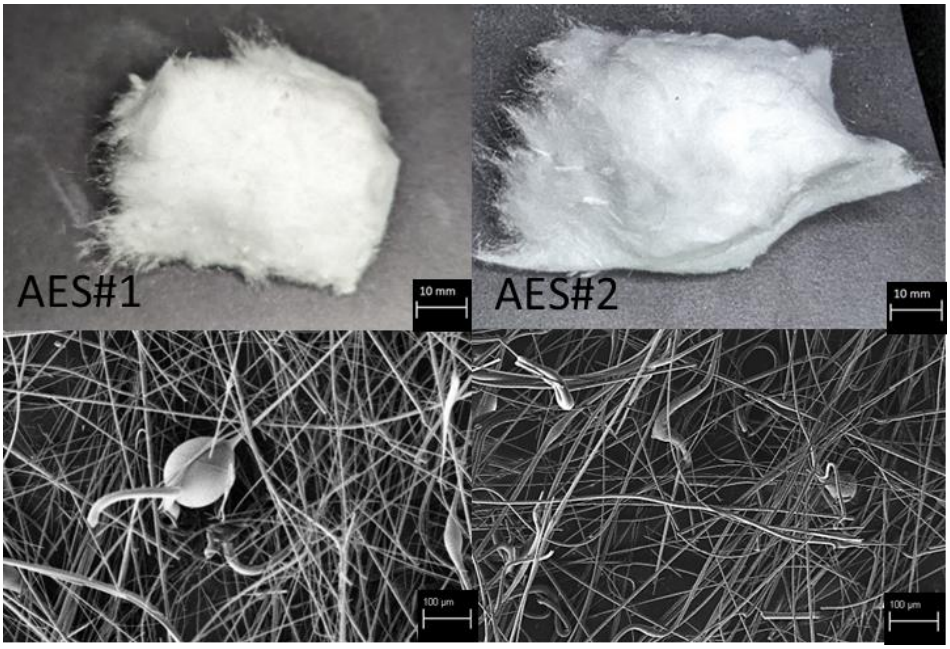

Figure 31: Fibers pre-exposure photographs (top) and SEM images (bottom) from left to right: manufacturer AES #1, and manufacturer AES #2.

Table 6 – Information on the ceramic fibers.

	Quartz Wool	**Alumina Wool**	**AES #1**	**AES #2**
Fiber Diameter, µm (Avg, Std Dev)	21.45, 14.30	9.67, 3.63	15.63, 7.03	15.05, 7.08
EDX Chemical Analysis (Oxygen Balance)	Si (46.3 wt%), S (0.5 wt%), and Na (0.3 wt%)	Al (54.2 wt%), Si (1.83 wt%)	Si (33.4 wt%), Ca (18.8 wt%), K (0.6 wt%), Al (0.5 wt%), Mg (0.4 wt%), and Na (0.3 wt%)	Si (28.5 wt%), Ca (21.3 wt%), Mg (3.0 wt%), S (0.5 wt%), and Na (0.3 wt%)

Computational thermodynamic equilibrium modelling of the system was completed using FactSage 8.2, with FactSage databases FactPS and FToxid. Ideal gases, pure solids, and all solutions were selected as products. The parameters used in the calculations include: 1 atm total pressure, 850℃ for evaporation, and 100-800℃ for condensation. It is worth noting here that the total pressure used in calculations does not match the ambient pressure where the experiments

were conducted at altitude, but the ratios of gases (O_2 and H_2O) used in the calculations are the same as those used in the experiment series. Calculations used in computational thermodynamic equilibrium modelling are presented below:

$$Cr_2O_3(s) + \langle A \rangle H_2O(g) + \langle B \rangle O_2(g) \qquad \text{Eq. 3}$$

$$\text{Gas stream of [3] + Quartz/Alumina/AES\#1/AES\#2} \qquad \text{Eq. 4}$$

Results

Results below are presented in photos of samples, observed staining colors on samples, as well as DPC/UV-VIS and ICP-OES measurements. Fig. 32 below shows the ceramic insulating fibers post-exposure. Following this figure, Table 7 presents the resulting observed staining colors and Cr(VI)/Total Cr measurements for each ceramic insulating fiber sample.

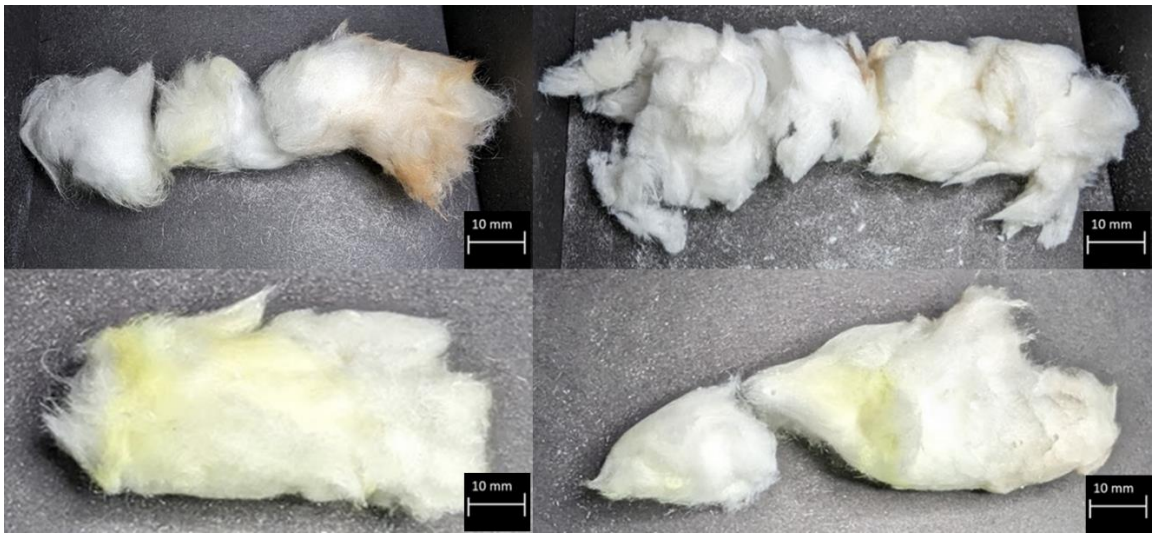

Figure 32: Ceramic insulating fibers post-exposure, counterclockwise from top left: quartz, AES #1, AES #2, and alumina wools.

Table 7 – Appearance and Cr content for quartz wool.

Metric	Quartz	Alumina	AES #1	AES #2
Color	Green, yellow, brown	Green, yellow, brown	Yellow	Yellow, brown
DPC/UV-VIS	0.739 ppm	0.403 ppm	0.873 ppm	1.747 ppm
ICP-OES	1.339 ppm	1.976 mg/L	2.170 ppm	3.040 ppm

Next, Fig. 33 below presents total Cr and Cr(VI) measurements obtained from ICP-OES and DPC/UV-VIS, respectively, as a histogram plot with error bars (10% uncertainty) for each fiber sample. To ensure repeatability, experiments for each sample have been at least duplicated (some triplicates). However, the methodology has evolved, and more refined characterization techniques were used in later iterations. For example, total Cr collected on samples was initially measured using inductively couples plasma mass spectroscopy (ICP-MS), but in later iterations was measured using ICP-OES, and initial measurements of Cr(VI) collected on samples was estimated using a visual color comparator provided with the DPC test kit, but in later iterations was measured directly using DPC/Direct UV-VIS with the aid of a spectrophotometer. The exact measurements have changed but the trends/differences in total Cr/Cr(VI) collection agree with respect to changes in water vapor concentration. As a result, the 10% error bars in Fig. 30 may be an underestimate of the total error involved due to fiber packing and positioning in the quartz tube.

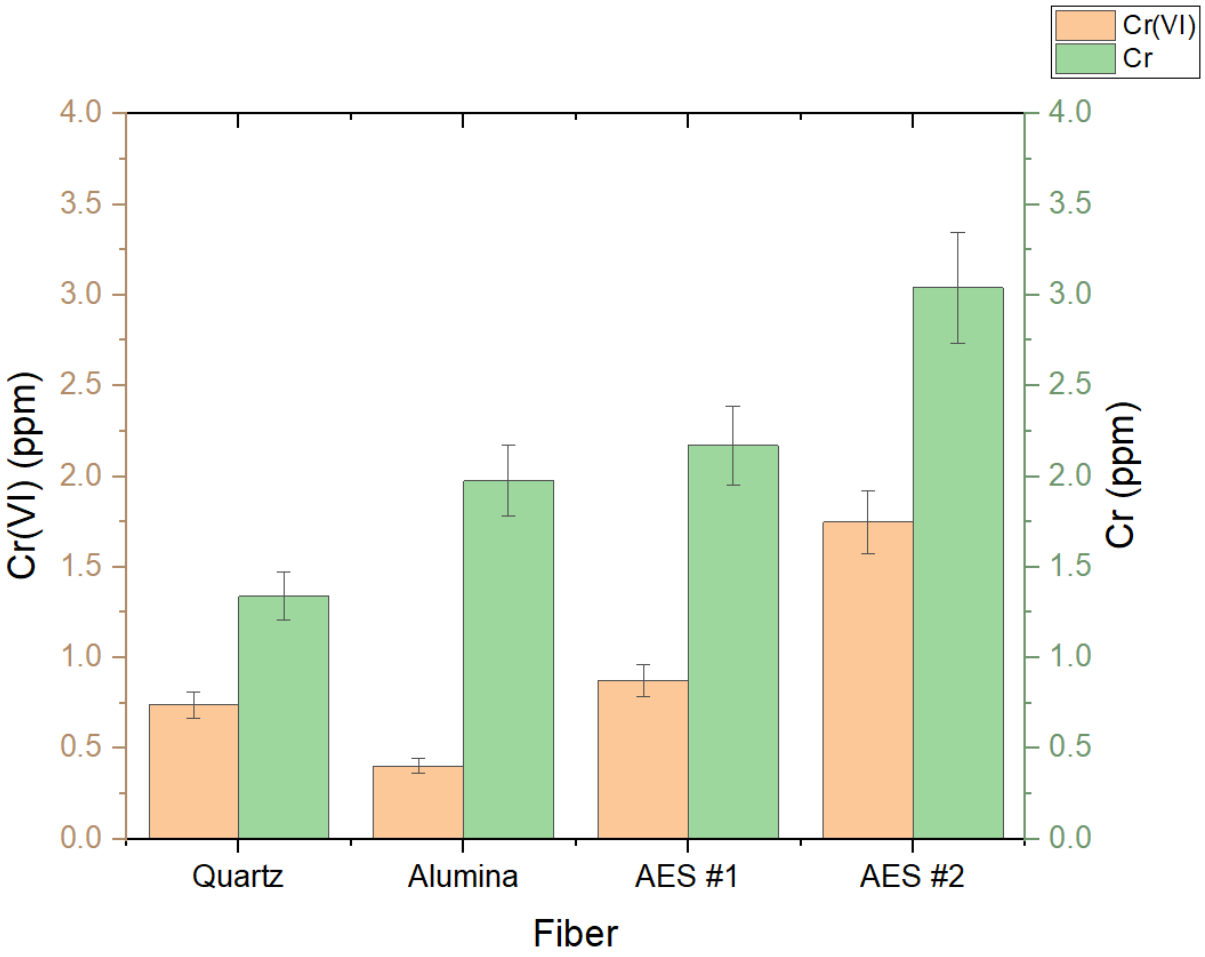

Figure 33: Collected Cr/Cr(VI) comparison amongst fiber types with error bars.

It can be inferred from Fig. 33 that alkaline content in the fiber samples increases Cr and Cr(VI) formation. A possible explanation for this observation is that alkaline-Cr compound formation reactions are more favorable compared to those formation reactions of the quartz or alumina fiber surface chemistries. Assuming that is the case, it is expected that leached alkaline elements between pre- and post-exposure samples will increase. To test this hypothesis, unexposed samples of each ceramic insulating fiber, also weighing 2g each, were acid digested under the same conditions as described in the experimental design section. The results of this experiment are presented below in histogram plots of ICP-OES elemental composition results for AES #1 and

AES #2 fibers. Each histogram plot contains results in ppm for Cr, Ca, Mg, Na, and K for post- and pre-exposure samples with error bars (10% uncertainty). Fig. 34 below displays the post- and pre-exposure ICP-OES results for AES #1 as well as the difference between post- and pre-exposure. The greatest difference in detected elemental concentrations between post- and pre-exposure are Cr and Ca at 2.17 ppm and 4.20 ppm, respectively. Na and K increased from pre- to post-exposure by 0.61 ppm and 0.35 ppm, respectively. Finally, Mg decreased from pre- to post-exposure by 0.21 ppm.

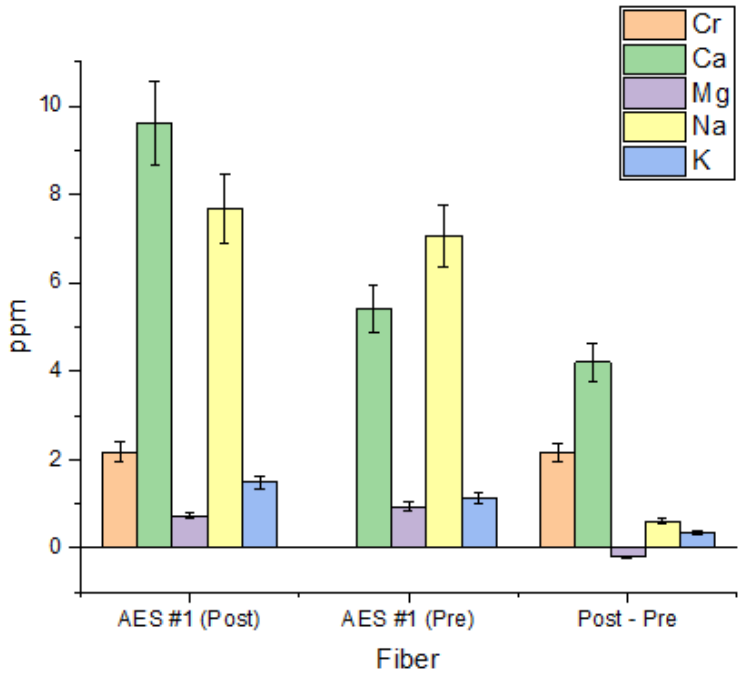

Figure 34: Histogram plot of ICP-OES analysis of AES#1 pre- and post-exposure reported in ppm.

Next, Figure 35 below displays the post- and pre-exposure ICP-OES results for AES #2 as well as the difference between post- and pre-exposure. The greatest difference in detected elemental concentrations between post- and pre-exposure are Cr and Ca at 3.03 ppm and 3.43 ppm,

respectively. Mg increased from pre- to post-exposure by 0.12 ppm. Finally, Na and K decreased from pre- to post-exposure by 0.23 ppm and 0.03 ppm, respectively.

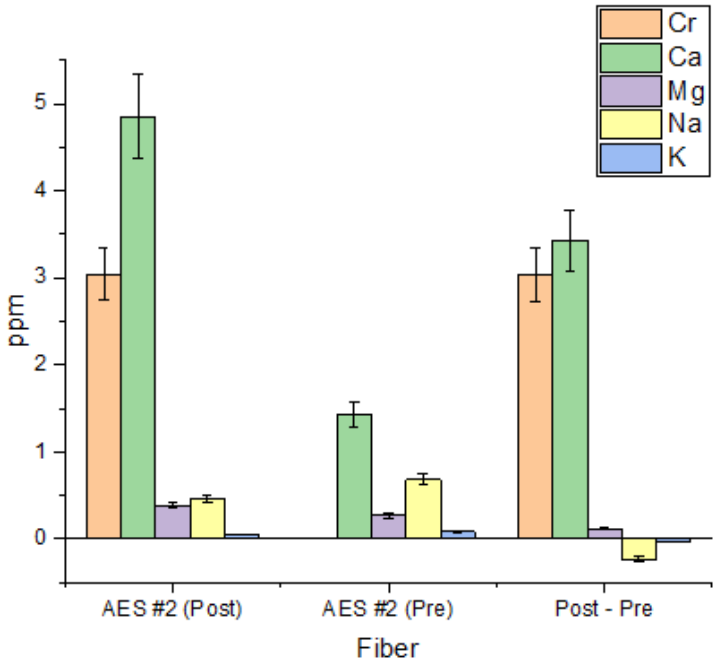

Figure 35: Histogram plot of ICP-OES analysis of AES#2 pre- and post-exposure reported in ppm.

FactSage-generated condensation reaction calculations of Cr vapor onto Quartz, Alumina, AES #1, and AES #2 fibers as functions of water vapor concentration were completed to interpet experimental results. Results are presented as calculated total condensed Cr species formed in grams on each ceramic insulating fiber from 100℃ to 800℃ for 3% H_2O water vapor content. Condensed Cr species formed for each fiber surface in the greatest quantity are interpreted as being the most stable.. For quartz wool, the calculated primary condensed Cr compounds formed are Cr_2O_3, $Cr_2(SO_4)_3$, and $Cr_2(CrO_4)_3$ (Cr(III) chromate), however $Cr_2(CrO_4)_3$ was calculated to only form at 100℃. For alumina wool, the calculated primary condensed Cr compounds formed are Cr_2O_3 (Cr(III)) and $Cr_2(CrO_4)_3$, however $Cr_2(CrO_4)_3$ was calculated only to form at 100℃ here as

well. For AES #1, the calculated primary condensed Cr compounds formed are $CaCrO_4$ (Cr(VI)) and $Ca_3Cr_2Si_3O_{12}$ (Cr(III) uvarovite), however $Ca_3Cr_2Si_3O_{12}$ was calculated to form only at 100°C. Finally, the calculated primary condensed Cr compounds formed for AES # 2 is $CaCrO_4$ (Cr(VI)).

Discussion

The photos, ICP-OES, and DPC/UV-VIS results tell a story of increasing loading of total Cr and Cr(VI) in the presence of alkaline oxide additions. Photos of post-exposure samples show that staining becomes more evident on each sample with greater total alkaline oxide content. Total Cr measurements from ICP-OES and Cr(VI) measurements from DPC/Direct UV-VIS also increase with increasing alkaline oxide content; however, they do not experience the same rate of change. The differences in total Cr and Cr(VI) collection between samples could be due to differences in surface areas. The alumina wool control has the finest fibers, the quartz wool has the largest standard deviation in fiber diameter, and the two manufactured AES insulation fibers are comparable in average and standard deviation diameter. The process, as it is understood according to these observations, by which reactive condensation of Cr vapors occurs on ceramic fiber surfaces is as follows: as CrO_3 or $Cr_2(OH)_2$ gases generated from high-temperature processes cool and fall onto surfaces they encounter eventually forming various stable Cr compounds depending on the surface chemistry on which they condense onto. These Cr compounds, according to the thermodynamic equilibrium calculations and experimental observations, include trivalent Cr compounds (Cr_2O_3, $Cr_2(SO_4)_3$, $Ca_3Cr_2Si_3O_{12}$), hexavalent Cr compounds ($CaCrO_4$), and combinations of hexavalent and trivalent Cr compounds ($Cr_2(CrO_4)_3$). Furthermore, according to experimental observations presented in Fig. 34 and 35, it is possible that Cr compounds formed on alkaline surfaces form chemically bonded alkaline chromates and pull the alkaline components out

of the fiber during acid digestion. The solubility of relevant Cr compounds could also be of importance to explaining these observations. Cr(III) compounds are generally insoluble to slightly soluble in water, whereas Cr(VI) compounds are very soluble. For example, Cr(III) oxide (Cr_2O_3) is completely insoluble in water at 20℃ while dehydrated chromic acid has a solubility of 1000 g/L and calcium chromate has a solubility of 22.3 g/L [24].

Seen across all samples is a similar pattern in staining. Observing the samples from left to right coordinates with the temperature zones of hot to cold, respectively, where the sample was placed in the furnace exit. Each sample starts with unstained sections on the left side where the temperature is >500℃. This observation agrees with expectations as the condensation point for Cr vapor, the boiling point of chromic acid, is ~250℃, and deposition at temperatures above the boiling point is not to be expected. Staining becomes more apparent in the middle and right side as the sample cools down below the boiling point of chromic acid. The computational thermodynamic equilibrium modelling also showed a variation in the species of stable condensed Cr and in the total amount of condensed Cr formed on each fiber. Stable Cr compounds from thermodynamic modelling are ascertained from the calculated total (in grams) of each calculated stable Cr species. The species with the largest calculated totals are determined to be the most stable. The calculated total Cr formed and was greater for AES #1 and AES #2 compared to quartz and alumina across all temperatures and the most stable species were calculated to be Cr(VI). These results are reinforced by observing the staining on each sample. Staining on AES #1 and AES #2 was more yellow and continuous than the stains observed on quartz or alumina. Cr(III) chromate only formed at 100℃ on quartz and alumina and therefore would fall towards the trailing edge of the ceramic insulating fiber plug in the tube furnace.

Hydroxyl populations on the surface are assumed to act as anchoring points for condensed Cr vapor species. De-hydroxylation, the process by which surface hydroxyl groups are effectively removed through bonding with hydrogen to form water, may also occur at elevated temperatures (>500°C)[162]. When water vapor is introduced into the atmosphere, rehydroxylation of dehydroxylated surfaces can occur and this rehydroxylation effect is increased with increased water vapor concentration. A partially dehydroxylated oxide surface has hydroxyl groups, coordinatively unsaturated metal cations, and oxygen anions. Coordinatively unsaturated cations at the surface can accept free electron pairs of adsorbed molecules and act as Lewis acid sites. The M+ sites behave like Lewis acids, and the O- ions are more basic than the bulk ions. Coordinative unsaturation becomes more extensive if dehydroxylation takes place[163]. The strength of these acid sites depends on the charge and size of the cations, both of which vary with the oxidation number of the cation. In hard soft acid base (HSAB) theory, cations of a higher oxidation state are harder acids. The strength of these acid sites depends on the charge and size of the cations which vary with the oxidation state of the cation. Harder cations are smaller and less polarizable, and they will absorb or bind hard bases stronger than soft or polarizable bases. A study on the role of hardness in the adsorption of Cr(VI) onto metal oxide nanoparticles indicated that the adsorption onto an oxide surface is influenced by their chemical hardness[164]. The hardness of the cation determines the basicity of surface OH groups which regulates adsorption as well as protonation and deprotonation. The hardness match between a sorbent and a sorbate may be interpreted as their chemical affinity and this was found to be the driving force for adsorption of Cr(VI) anions onto the oxides. Magnesium is a harder acid than calcium which is harder than aluminum which is harder than silicon, therefore the bonding between magnesium / oxygen or calcium / oxygen is

harder and more stable than that of aluminum / oxygen and silicon / oxygen, leading to a greater affinity for adsorption of Cr anions for the AES wools compared to alumina or quartz wool.

In a study of Cr(VI) formation in stainless steel refractory slags, the authors observed Cr(VI) formation increased in the presence of Ca **[168]**. The authors of the study also found that "slag basicity", the ratio between CaO/SiO_2, increases Cr(VI) formation. The replacement of Al_2O_3 by SiO_2 in Ca-aluminate slags decreases the amount of uncombined CaO that can react with chromite particles to form Cr(VI). This study also found that a decrease in chromite particle size increases the content of Cr(VI) because a larger surface area is available for the reaction to take place. Another study of stainless-steel slag also found the main Cr compound distributed in the soluble phase as hexavalent $CaCr_2O_4$ was formed below 1200℃ **[173]**. Increased boron oxide content was also found to increase Cr(VI) formation. The authors of both studies also observed that cooling rate affects the formation of Cr(VI), however the observations and conclusions drawn from each study do not agree. In the first study, an increase in cooling rate was observed to decrease the formation of Cr(VI) and this was assumed to be the result of limiting the kinetics of the formation. The second study's results demonstrated that a faster cooling rate prohibited Cr from entering the spinel phase and remained primarily in the silicate matrix. In this state, there was more tendency for Cr to oxidize to Cr(VI) in the subsequent cooling process.

The Gibb's free energy of formation for various condensed phase Cr species is presented below in Table 8. The reactions of alkaline chromate/chromite compounds are generally more favorable than those of oxide or hydroxide Cr compounds due to their lower Gibb's free energy.

Table 8 – Gibb's free energy for relevant Cr compound formation reactions[174].

Species	ΔG^{o}_{f298} (kcal/mol)
H_2CrO_4 (aq.)	-182.52
$HCrO_4^-$ (aq.)	-183.69
CrO_4^{2-} (aq.)	-174.81
$Cr_2O_7^{2-}$ (aq.)	-312.79
Cr_2O_3	-254.64
CrO_3	-122.50
$Cr_2(SO_4)_3$	-790.63
$Cr_2(CrO_4)_3$	-731.84
$CaCrO_4$	-310.2
K_2CrO_4	-309.82
$K_2Cr_2O_7$	-449.33
$MgCrO_4$	-276.17
$MgCr_2O_7$	-398.92
Na_2CrO_4	-295.54
$Na_2Cr_2O_7$	-431.61

The observation that alkaline oxides have a higher propensity for forming compounds with Cr vapors is reinforced by HSAB theory, studies of refractory slags, and the relative thermodynamic stability of alkaline chromates. Furthermore, when viewing the histogram plots in Fig. 34 and 35, it is evident that Cr and alkaline oxides, particularly Ca, are linked. A significant amount of Cr and Ca were detected in post-exposure samples when compared to pre-exposure samples. This could be evidence of calcium-chromium compounds forming chemical bonds and essentially removing Ca from the fibers during the acid digestion process. The results from thermodynamic modelling of the system also corroborate this assertation as the primary stable Cr compounds formed for the AES wools are Ca-based. Furthermore, the calculated thermodynamic equilibriums for condensed Cr compounds show increasing total condensed Cr across all temperatures and water vapor contents when comparing quartz to alumina to AES #1 and #2 fibers. The calculated primary condensed Cr species also show an increase in Cr(VI) compounds formed on AES #1 and AES #2 compared to quartz and alumina fibers. This is reinforced by the

experimental data in Fig. 33 that displays the same trend of increasing total condensed Cr compounds from quartz and alumina to AES #1 and #2 fibers.

Limitations of Study and Future Work Recommendations

Various experimental factors in this study limited this investigation and provided context for future work. For example, the placement and packing of the fibers within the furnace exit could influence Cr condensation. The fibers themselves are oriented differently and have varying surface areas from sample to sample, the specific placement of each sample could have an impact on internal pressure of the reaction tube, influencing the fluid mechanics of the gas flow across the fiber surfaces as well. Another aspect of fiber placement is the fluid flow past the fibers, it is not uniform and Cr vapors will not distribute equally across all fibers. This observation is reinforced by the detection of total Cr/Cr(VI) in the furnace effluent collected by the condenser. A second limitation is the acid digestion used for preparing samples to be analyzed via ICP-OES or DPC/UV-VIS spectrophotometry. The efficacy of the digestion process used was quantified by measuring the difference in Cr(VI) detected after 1 hour at 90-95°C hot plate assisted nitric acid digestion and allowing the fibers to continue digesting for 12 hours unassisted. Measured Cr(VI) decreased by ~80%, meaning ~20% of the Cr remains on the fibers after hot plate assisted acid digestion. A third limitation is the differences in analytical techniques used. A single characterization technique that could be used for total Cr and Cr(VI) would provide more reliable data for comparison. Currently, the three different methods used limit the inter-sample comparisons or conclusions that can be drawn from the data. A fourth limitation is the experimental setup. Some Cr species interact and condense onto the surface of the quartz tubes used in the furnaces and this occurrence has been studied to optimize the experiment **[165]**. The authors of the

study identified a method using a sodium carbonate coated thin alumina tube which effectively mitigates interference caused by chemical interactions between Cr vapor species and quartz and alumina furnace tube, allowing for improved assessment of Cr evaporation. Another limitation is the experimental setup, it could be improved to more accurately replicate service environments (e.g., thermal cycling, longer exposure times up to 1000 hours). However, this study was intended to create the extreme scenario of maximum Cr evaporation and condensation by using a relatively large amount of a pure chromia source and directly passing the vapors through the fiber samples. Finally, the thermodynamic equilibrium calculations and modelling could be improved. The calculations treat the modelled scenarios as ideal and that all reactants have equal potential to react when this is not the case in experimentation. Only the surface of the chromia source interacts with the reactant gases. The overall trends of observed condensed Cr species from experiment can be compared to the experimental results, but the exact amounts do not agree.

Total Cr (in all forms) and Cr(VI) collected on the ceramic insulating fiber samples increases in the presence of alkaline oxides in the fibers, specifically calcium content. As evident in Fig. 33, measurements from ICP-OES and from DPC/UV-VIS, also presented in Table 7, show an increase in total Cr and Cr(VI) with increased alkaline oxide content. While the trends agree, the individual quantified data does not experience the same rate of change. For example, alumina collected more total Cr than quartz wool, but quartz wool collected more Cr(VI). This could be due to the small amounts of S (~0.5 wt%) and Na (~0.3 wt%) present in the quartz wool sample. This observation is reinforced by the thermodynamic modelling of the quartz wool that calculated $Cr_2(SO_4)_3$ as a stable compound formed in the reaction. However, further investigation into these observations is required. In-situ Cr / Cr(VI) measurements of the fibers using IR or Raman

spectroscopy during testing as a function of time, temperature, and Cr loading could provide more insight into the mobility and evolution of Cr species on different surfaces. High-temperature environments, such as those generated in the experimental system, generate significant amounts of blackbody radiation, and limit the methods of in-situ characterization of reaction mechanisms. However, advancements in IR and Raman spectroscopy in the past decade have successfully integrated these characterization techniques into SOFCs operating above 650°C to correlate electrochemical performance with chemical processes occurring simultaneously within the system **[166, 167]**. These advanced spectroscopy systems could be applied to the experimental design employed in this study to obtain a more comprehensive picture of the dynamic reactions occurring during complex high-temperature processes.

Conclusions

In this study, silica-based aluminosilicate fibers were exposed to Cr vapors produced by reacting chromia powder to high-temperature (800°C) air with 3% water vapor content. Aluminosilicate fibers from different manufacturers were evaluated under similar conditions for comparison. Chemical analyses were then conducted for each sample for quantitative comparisons. Total Cr and Cr(VI), quantified using ICP-OES, were observed to collect on all samples including those without an appreciable amount of alkaline oxide content. The presence of alkaline oxides in the fiber, however, provides an opportunity to capture more Cr(VI). Total Cr collected increased in the presence of increasing alkaline oxide content as well. Computational thermodynamic equilibrium calculations carried out in FactSage were used to interpret these observations. The different amounts and speciation of Cr observed on the ceramic substrates also suggests different Cr condensation mechanisms for different ceramic surfaces and conditions, which invites further

investigation. Implications for SOFC/SOEC systems include material selection and system design to consider the impacts of increased alkaline oxide content on corrosion of stainless-steel components within these systems.

While this study confirms the preference for Cr vapors to condense on surfaces containing alkaline oxides, the results do not represent the likelihood or quantification of concentrations of Cr(VI) that would be found in actual industrial applications. Furthermore, as all fibers regardless of alkaline oxide content used in these applications capture Cr(VI), workplace regulatory rules governing the exposure to Cr(VI) should guide actions taken by users of stainless steel used at elevated temperatures.

CHAPTER SIX - CONCLUSION

Contents of Chapter Six

Chapter Six discusses the significance and implications results of the research detailed in Chapters Three, Four, and Five and thematically links the individual studies in context of improving understanding of Cr reactive condensation in SOFC/SOEC and related high-temperature materials and systems. Limitations of the completed research and the direction of future research are also discussed. The future work discussion includes content from a fourth first-authored research manuscript from the author of this dissertation titled “Effects of Upstream Presence of Alkaline Oxides on Reactive Evaporation and Condensation of Chromium Vapors onto Aluminosilicate Fibers”. This manuscript is currently in the process of being finished and will be submitted to the Journal of Electrochemical Society for publishing in May 2024. Co-authors for this manuscript in the Department of Chemical and Biological Engineering at Montana State University include Dr. Paul Gannon, undergraduate Ryan Dowdy, and undergraduate Amberly Guerrero. Co-authors that assisted with thermodynamic equilibrium modelling include Dr. Akbar Rhamdhani and graduate student Bima Satritama from the Department of Mechanical and Product Design Engineering at the Swinburne University of Technology include and Dr. Geoffrey Will from the School of Science, Technology and Engineering at Sunshine Coast University.

Discussion

This document attempts to organize and present a collection of work completed by the author with the assistance and support of their primary investigator, research group, industry partners, and academic colleagues to shine light on an area of scientific knowledge that was

previously unknown. The first manuscript, a literature review titled “Reactive Evaporation and Condensation of Chromium: A Review”[1], attempted to aggregate and organize the existing literature on topics related to reactive evaporation and condensation of Cr. This work served as a foundation of knowledge and reference list for the author to continue to build upon as the research progressed. The second manuscript, a research article titled “Influence of Water Concentration on High-Temperature Reactive Condensation of Chromium Vapors Generated in 800°C Air”[2], presented a study on the influence of water vapor concentration on total condensed Cr and Cr(VI) species. The results of this study confirmed the hypothesis that increased water vapor concentration increases total condensed Cr and Cr(VI) compounds on aluminosilicate surfaces. The third manuscript, an in-progress research article titled “Reactive Condensation of Cr Vapors on Aluminosilicate Fibers Containing Alkaline Oxides”, presented a study of the influence of alkaline oxides in aluminosilicate fibers on total condensed Cr and Cr(VI) compounds. The results of this study confirmed the hypothesis that increased alkaline oxide content increases total condensed Cr and Cr(VI) compounds. Thermodynamic equilibrium calculations were also completed to explain the results of these studies.

Limitations

Limitations are discussed in each chapter in the context of the study being presented. However, the overall limitations can be summarized as follows: unreliable placement and packing of the fibers in the quartz tube, non-uniform fluid flow past the fibers, incomplete acid digestion of samples, discrepancies in characterization techniques, an imperfect experimental model of representative systems, and imperfect thermodynamic equilibrium modelling calculations.

These limitations can be overcome or kept to a minimum by improving various aspects of the experimental and thermodynamic equilibrium models. Some possible improvements could include using fibers that are more similar in orientation and surface area can limit the influence of placement and packing of fibers in the furnace exit that influence fluid dynamics and the fibers' exposure to Cr vapors. The acid digestion protocol can be improved by increasing digestion times or temperatures. One way to do this is using pressurized vessels that allow for increased digestion temperatures and times without losing solution to evaporation. A single characterization technique that could be used for total Cr and Cr(VI) would provide more reliable data for comparison such as in-situ methods like IR or Raman spectroscopy. The experimental setup could also be improved to more accurately replicate service environments (e.g., thermal cycling, longer exposure times up to 1000 hours). Finally, thermodynamic equilibrium modelling could also be improved by setting more realistic constraints on the calculations. The calculations currently treat the modelled scenarios as ideal and that all reactants have equal potential to react when this is not the case in experimentation. Only the surface of the chromia source interacts with the reactant gases.

Future Work

Future work is also discussed in each chapter in the context of the study being presented. One area of future work is to continue improving the experimental and thermodynamic equilibrium models according to the points presented in the previous section on limitations.

Another area for future work is to continue probing environmental influences on reactive evaporation and condensation mechanisms of Cr vapors. A fourth research manuscript currently being prepared for publication by the author of this document focuses on the influence of alkaline oxides upstream from the aluminosilicate fibers. Preliminary results from experimentation reveal

a decrease in condensed Cr on quartz and alumina fibers exposed to vapors generated from mixed powders compared to those exposed to vapors generated from pure chromia. Preliminary thermodynamic modelling reveals a decrease in Cr vapors generated from chromia-CaO/MgO mixed powders compared to those generated from pure chromia. The thermodynamic calculations corroborate the experimental results and paint a picture of decreased Cr vapor generation in the presence of upstream alkaline oxides in the Cr source. Fig. 36 and 37 below show the mixed powders before and after exposure to heat and water vapor in the experimental setup. The change in color from Fig. 36 to 37 indicates a reaction between the chromia and alkaline oxides is occurring. Following these figures, Fig. 38 shows the thermodynamic calculations of generated Cr vapor species from each scenario. The raw thermodynamic modelling data is presented in Appendix A: Thermodynamic Equilibrium Modelling Data.

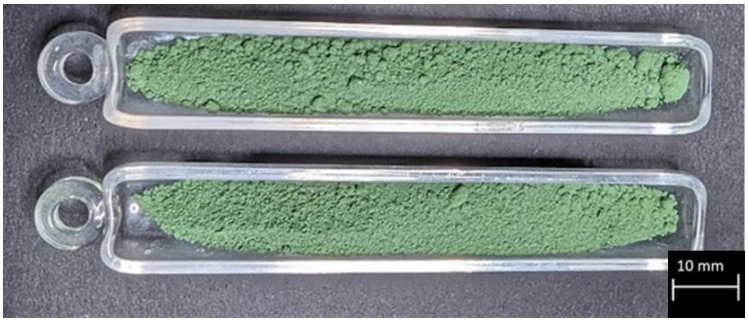

Figure 36: Mixed chromia-calcium oxide (top) and chromia-magnesium oxide powder (bottom).

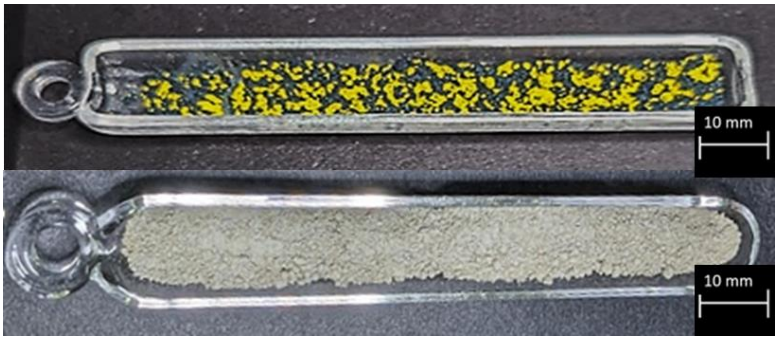

Figure 37: Mixed chromia-calcium oxide (top) and chromia-magnesium oxide (bottom) powders post-exposure to 800°C air for 100 h.

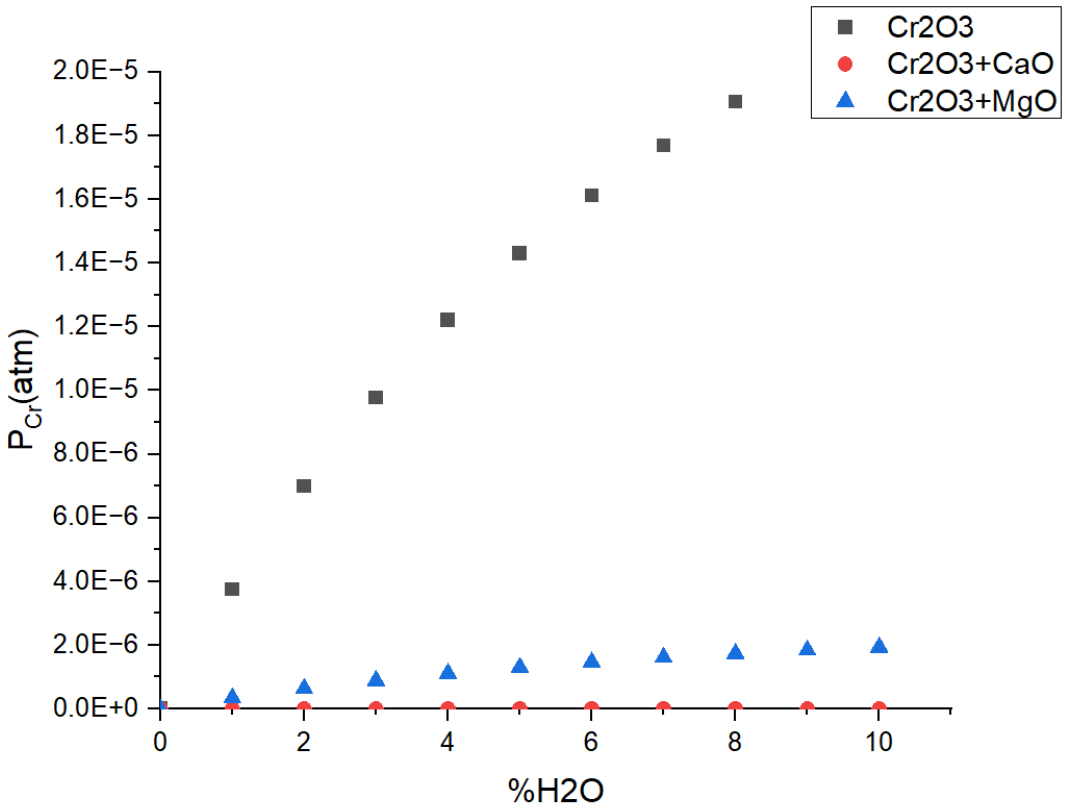

Figure 38: Thermodynamic equilibrium calculations of partial pressure of all total Cr vapor species generated from pure chromia, mixed chromia-CaO, and mixed chromia-MgO powders with respect to water vapor content.

In addition to the experimental and thermodynamic equilibrium modelling already completed, phase diagrams (such as the one presented below in Fig. 39 created by authors of a study into stainless steel smelting processes[173]) are to be generated to further explain the

experimental results. In this study, researchers combined Cr_2O_3 powders with $CaCO_3$ powders in a compact held at temperature for 2 h with subsequent XRD analyses for phase identification. Reaction forming Cr(VI) species ($CaCrO_4$) appears to occur within a temperature window of ~700-1000C, below and above which Cr(III) species are favored. Future experiments and modelling are intended to verify and add context to these results.

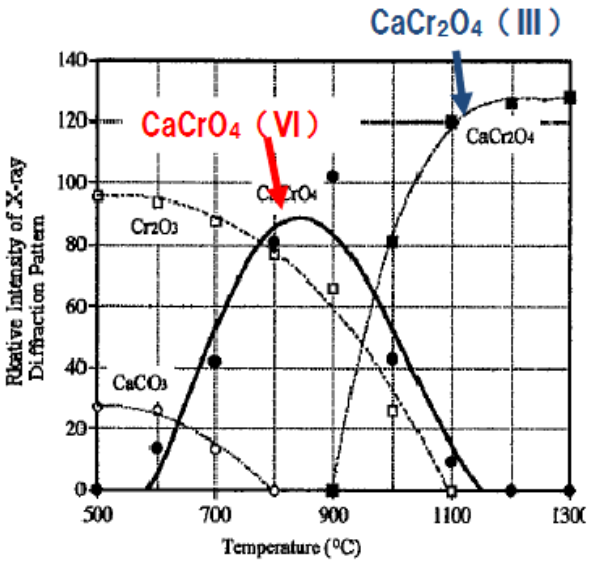

Figure 39: Phase diagram of calcium-chromate species stabilities with respect to temperature[173].

Conclusions

While the research objective of improving understanding of reactive condensation of Cr vapors was met, the results of the presented studies do not fully address the problem as there are limitations to each study presented and new questions that have yet to be answered. The results from these studies can be used to better mitigate issues associated with reactive evaporation and condensation of Cr in high-temperature systems, they also have great potential to be improved upon and produce more accurate models of representative systems.

The overall results from the studies included in this document reveal that Cr vapors condense and form stable Cr/Cr(VI) compounds on all aluminosilicate surfaces tested, regardless of water vapor concentration in the surrounding atmosphere or the presence of alkaline oxides in the substrate material or alkaline oxides present in the Cr source, upstream from the substrate material. Although it is worth noting that increasing water vapor concentration and increasing alkaline oxide presence in the fibers leads to an increase in Cr/Cr(VI) condensed species collected on HTIW fibers, which agrees with the author's original hypotheses. On the other hand, alkaline oxide presence in the Cr source, upstream from the HTIW samples, negatively impacts and decreases the generated Cr species' vapor pressures. This limits the amount of free Cr vapor species that can condense on the HTIW samples, which proved the third hypothesis offered by the author to be incorrect. These findings will facilitate further investigations to detail mechanistic understanding and inform future high-temperature materials science and engineering.

REFERENCES CITED

[1] T. K. van Leeuwen, R. Dowdy, A. Guerrero, and P. Gannon, "Reactive evaporation and condensation of chromium: A review," *Journal of Power Sources*, vol. 572, p. 233065, 2023/07/15/ 2023, doi: https://doi.org/10.1016/j.jpowsour.2023.233065.

[2] T. K. van Leeuwen, R. Dowdy, A. Guerrero, and P. Gannon, "Influence of Water Concentration on High-Temperature Reactive Condensation of Chromium Vapors Generated in 800 °C Air," *Journal of The Electrochemical Society*, vol. 171, no. 1, p. 011503, 2024/01/17 2024, doi: 10.1149/1945-7111/ad1acd.

[3] N. G. Gonzalez, R. Baar, J. Drueckhammer, and C. Kaeppner, "The Thermodynamics of Exhaust Gas Condensation," *SAE International Journal of Engines*, vol. 10, no. 4, pp. 1411-1421, 2017. [Online]. Available: https://www.jstor.org/stable/26422533.

[4] N. Mu, K. Y. Jung, N. M. Yanar, G. H. Meier, F. S. Pettit, and G. R. Holcomb, "Water Vapor Effects on the Oxidation Behavior of Fe–Cr and Ni–Cr Alloys in Atmospheres Relevant to Oxy-fuel Combustion," *Oxidation of metals*, vol. 78, no. 3-4, pp. 221-237, 2012, doi: 10.1007/s11085-012-9302-x.

[5] U. o. Cambridge. "Solid oxide fuell cells (SOFCs)." https://www.doitpoms.ac.uk/tlplib/fuel-cells/figures/flat_plate_sofc_sml.png (accessed 2024).

[6] U. M. Insights. "Solid Oxide Fuell Cell Market." https://univdatos.com/wp-content/uploads/2022/05/Solid-Oxide-Fuel-Cell.png (accessed 2024).

[7] G. A. Center. "Pressurised SOFC system in Stuttgart." https://www.dlr.de/en/images/institutes-1/institute-of-engineering-thermodynamics/tt-pressurised-sofc-system-main-image/@@images/image-1600-c98857ceda7ca56b65e10b140bb097d0.jpeg (accessed 2024).

[8] I. DMC. "Oil and Gas Engineering." https://www.dmcinfo.com/portals/0/2015_Web_Images/Manufacturing_Automation_and_Intelligence/Oil_and_Gas/oil-and-gas-refinery-and-process-thumbnail.png (accessed 2024).

[9] T. Jackets. "Valve Insulation Jackets." https://www.thermaxxjackets.com/wp-content/uploads/2012/06/AngleStopCheckValve-001-Covered.jpg#keepProtocol (accessed 2024).

[10] A. Materials. "Enhancing Automotive Performance with Improved Insulation." https://d12oja0ew7x0i8.cloudfront.net/image-handler/ts/20180618104422/ri/750/src/images/Article_Images/ImageForArticle_16173(3).jpg (accessed 2024).

[11] A. Sanchez-Hachair and A. Hofmann, "Hexavalent chromium quantification in solution: Comparing direct UV–visible spectrometry with 1,5-diphenylcarbazide colorimetry," *Comptes Rendus Chimie,* vol. 21, no. 9, pp. 890-896, 2018/09/01/ 2018, doi: https://doi.org/10.1016/j.crci.2018.05.002.

[12] (1996). *METHOD 3050B: ACID DIGESTION OF SEDIMENTS, SLUDGES, AND SOILS*. [Online] Available: https://www.epa.gov/sites/default/files/2015-12/documents/3050b.pdf

[13] EnergyUK, "Hexavalent Chromium Safety Bulletin Summary," 2019. [Online]. Available: https://www.energy-uk.org.uk/files/docs/EnergyUKHexavalentChromiumSummary.pdf

[14] Eneria. "Hexavalent Chromium or Chromium 6 (Cr-6) on Engines." https://www.eneria.fr/en/hexavalent-chromium-or-chromium-6-cr-6-on-engines/ (accessed 2021).

[15] K. R. Baldwin, M. J. Robinson, and C. J. E. Smith, "The corrosion resistance of electrodeposited zinc-nickel alloy coatings," *Corrosion Science,* vol. 35, no. 5, pp. 1267-1272, 1993/01/01/ 1993, doi: https://doi.org/10.1016/0010-938X(93)90347-J.

[16] M. Heydarzadeh Sohi and M. Jalali, "Study of the corrosion properties of zinc–nickel alloy electrodeposits before and after chromating," *Journal of Materials Processing Technology,* vol. 138, no. 1, pp. 63-66, 2003/07/20/ 2003, doi: https://doi.org/10.1016/S0924-0136(03)00050-5.

[17] H. S. Klapper, N. S. Zadorozne, and R. B. Rebak, "Localized Corrosion Characteristics of Nickel Alloys: A Review," *Acta Metallurgica Sinica (English Letters),* vol. 30, no. 4, pp. 296-305, 2017/04/01 2017, doi: 10.1007/s40195-017-0553-z.

[18] B. M. Weckhuysen, A. A. Verberckmoes, A. L. Buttiens, and R. A. Schoonheydt, "Diffuse Reflectance Spectroscopy Study of the Thermal Genesis and Molecular Structure of Chromium-Supported Catalysts," *American Chemical Society,* 1994.

[19] F. D. Hardcastle and I. E. Wachs, "Raman spectroscopy of chromium oxide supported on Al2O3, TiO2 and SiO2: a comparative study," *Journal of Molecular Catalysis,* vol. 46, pp. 173-186, 1988.

[20] W. K. Jozwiak and D. L. I. G., "Interactions between the chromium oxide phase and support surface; redispersion of [small alpha]-chromia on silica, alumina and magnesia," *Journal of the Chemical Society, Faraday Transactions,* vol. 93(15), pp. 2583-2589, 1997.

[21] B. M. Weckhuysen, I. E. Wachs, and R. A. Schoonheydt, "Surface Chemistry and Spectroscopy of Chromium in Inorganic Oxides," *Chemical Reviews*, vol. 96(8), 1996.

[22] B. M. Weckhuysen, L. M. De Ridder, P. J. Grobet, and R. A. Schoonheydt, "Redox Behavior and Dispersion of Supported Chromium Catalysts," *Journal of Physical Chemistry*, 1995.

[23] M. I. Zaki, S. A. A. Mansour, F. Taha, and G. A. H. Mekhemer, "Chromia on Silica and Alumina Catalysts," *Zeitschrift für Physikalische Chemie*, 1991.

[24] S. Wilbur *et al.*, "Toxicological Profle for Chromium" *Agency for Toxic Substances and Disease Registry*, 2012.

[25] S. A. Katz and H. Salem, "The toxicology of chromium with respect to its chemical speciation: A review," *Journal of Applied Toxicology* vol. 13(3): 217-224, 1993.

[26] R. Saha, R. Nandi, and B. Saha, "Sources and toxicity of hexavalent chromium," *Journal of Coordination Chemistry*, vol. 64, no. 10, pp. 1782-1806, 2011, doi: 10.1080/00958972.2011.583646.

[27] "Chromium: Fact Sheet for Health Professionals." National Institutes of Health. https://ods.od.nih.gov/factsheets/Chromium-HealthProfessional/ (accessed 2022).

[28] C. European *et al.*, *SCOEL/REC/386 Chromium VI compounds : recommendation from the Scientific Committee on Occupational Exposure Limits*. Publications Office, 2017.

[29] (2008). *Release of Hexavalent Chromium by Ash and Soils in Wildfire-Impacted Areas*. [Online] Available: https://pubs.usgs.gov/of/2008/1345/pdf/OF08-1345_508.pdf

[30] K. E. Ukhurebor *et al.*, "Effect of hexavalent chromium on the environment and removal techniques: A review," *Journal of environmental management*, vol. 280, p. 111809, 2021, doi: 10.1016/j.jenvman.2020.111809.

[31] H. I. McHenry, "The Properties of Austenitic Stainless Steel at Cryogenic Temperatures," in *Austenitic Steels at Low Temperatures*, R. P. Reed and T. Horiuchi Eds. Boston, MA: Springer US, 1983, pp. 1-27.

[32] D. J. Young, *High Temperature Oxidation and Corrosion of Metals*. Jordan Hill, UNITED KINGDOM: Elsevier Science & Technology, 2008.

[33] MatWeb. "310 Stainless Steel, annealed bar." https://www.matweb.com/search/datasheet.aspx?matguid=db1542ad8b2844d8a70d5421b459cb60 (accessed 2023).

[34] MatWeb. "330 Stainless Steel." https://www.matweb.com/search/datasheet.aspx?matguid=d0318cac53444aac93d9e89c89e52e55 (accessed 2023).

[35] (2009). *Development of Alumina-Forming Austenitic (AFA) Stainless Steels*. [Online] Available: https://netl.doe.gov/sites/default/files/event-proceedings/2009/fem/YamamotoY.pdf

[36] K. A. Cashell and N. R. Baddoo, "Ferritic stainless steels in structural applications," *Thin-Walled Structures*, vol. 83, pp. 169-181, 2014/10/01/ 2014, doi: https://doi.org/10.1016/j.tws.2014.03.014.

[37] H. Asteman, Svensson, J. E., and Johansson, L. G., "Evidence for Chromium Evaporation Influencing the Oxidation of 304L: The Effect of Temperature and Flow Rate," *Oxidation of Metals*, vol. 57(3): 193-216, 2002.

[38] K. Segerdahl, Svensson, J.-E. and Johansson, L.-G. , "The high temperature oxidation of 11% chromium steel: Part I – Influence of pH2O," *Materials and Corrosion* vol. 53(4): 247-255., 2002.

[39] C. Collins *et al.*, "Chromium volatility of coated and uncoated steel interconnects for SOFCs," *Surface and Coatings Technology*, vol. 201, no. 7, pp. 4467-4470, 2006.

[40] G. R. Holcomb and D. E. Alman, "Effect of manganese addition on reactive evaporation of chromium in Ni-Cr alloys," *Journal of Materials Engineering and Performance*, vol. 15, no. 4, pp. 394-398, 2006/08/01 2006, doi: 10.1361/105994906X117170.

[41] K. Hilpert, D. Das, M. Miller, D. H. Peck, and R. Weiss, "Chromium vapor species over solid oxide fuel cell interconnect materials and their potential for degradation processes," *Journal of the Electrochemical Society*, vol. 143, no. 11, pp. 3642-3647, 1996, doi: 10.1149/1.1837264.

[42] D.-H. Peck, M. Miller, and K. Hilpert, "Vaporization and thermodynamics of La1-xSrxCrO3-δ investigated by Knudsen effusion mass spectrometry," *Solid State Ionics*, vol. 143, no. 3-4, pp. 401-412, 2001.

[43] E. J. Opila *et al.*, "Theoretical and Experimental Investigation of the Thermochemistry of CrO2(OH)2(g)," *Journal of Physical Chemistry*, vol. 111, 1971-1980, 2007.

[44] N. Jacobson, D. Myers, E. Opila, and E. Copland, "Interactions of water vapor with oxides at elevated temperatures," *Journal of Physics and Chemistry of Solids*, vol. 66, no. 2, pp. 471-478, 2005, doi: 10.1016/j.jpcs.2004.06.044.

[45] C. Gindorf, L. Singheiser, and K. Hilpert, "Vaporisation of chromia in humid air," *Journal of Physics and Chemistry of Solids*, vol. 66, no. 2, pp. 384-387, 2005, doi: 10.1016/j.jpcs.2004.06.092.

[46] H. Kurokawa, C. P. Jacobson, L. C. Dejonghe, and S. J. Visco, "Chromium vaporization of bare and of coated iron-chromium alloys at 1073K," *Solid State Ionics*, vol. 178, no. 3-4, pp. 287-296, 2007, doi: 10.1016/j.ssi.2006.12.010.

[47] M. Stanislowski *et al.*, "Reduction of chromium vaporization from SOFC interconnectors by highly effective coatings," *Journal of power sources*, vol. 164, no. 2, pp. 578-589, 2007, doi: 10.1016/j.jpowsour.2006.08.013.

[48] G. R. Holcomb, "Calculation of Reactive-evaporation Rates of Chromia," *Oxidation of Metals*, vol. 69, no. 3-4, pp. 163-180, 2008, doi: 10.1007/s11085-008-9091-4.

[49] B. B. Ebbinghaus, "Thermodynamics of gas phase chromium species: The chromium oxides, the chromium oxyhydroxides, and volatility calculations in waste incineration processes," *Combustion and Flame*, vol. 93, no. 1, pp. 119-137, 1993, doi: 10.1016/0010-2180(93)90087-J.

[50] L. Zhou, J. H. Mason, W. Li, and X. Liu, "Comprehensive review of chromium deposition and poisoning of solid oxide fuel cells (SOFCs) cathode materials," *Renewable & sustainable energy reviews*, vol. 134, no. C, p. 110320, 2020, doi: 10.1016/j.rser.2020.110320.

[51] C. Key, J. Eziashi, J. Froitzheim, R. Amendola, R. Smith, and P. Gannon, "Methods to quantify reactive chromium vaporization from solid oxide fuel cell interconnects," *Journal of The Electrochemical Society*, vol. 161, no. 9, p. C373, 2014.

[52] J. J. Eziashi, C. Key, R. Smith, R. Amendola, P. E. Gannon, and J. Froitzheim, "Measuring Cr Volatility from Ferritic Stainless Steels: Novel and Conventional Methods Compared," in *ECS Transactions*, 2013, vol. 50: The Electrochemical Society, Inc, 44 ed., pp. 43-49, doi: 10.1149/05044.0043ecst.

[53] L. Zhou *et al.*, "Chromium evaporation and oxidation characteristics of alumina-forming austenitic stainless steels for balance of plant applications in solid oxide fuel cells," *International Journal of Hydrogen Energy*, vol. 46, no. 41, pp. 21619-21633, 2021/06/15/ 2021, doi: https://doi.org/10.1016/j.ijhydene.2021.04.002.

[54] E. J. Opila, "Volatility of Common Protective Oxides in High-Temperature Water Vapor: Current Understanding and Unanswered Questions," *Materials Science Forum*, 2004.

[55] P. S. Koukkari, "Introduction to constrained Gibbs energy methods in process and materials research," 2014.

[56] I. Wichterle, J. Linek, Z. Wagner, J.-C. Fontaine, K. Sosnkowska-Kehiaian, and H. V. Kehiaian, "Vapor-Liquid Equilibrium of the Mixture CF4+ CHF3(LB3808, EVLM 1131): Datasheet from Landolt-Börnstein - Group IV," *Journal of Physical Chemistry*, vol. 13A2:, doi: 10.1007/978-3-540-70745-5_1182.

[57] T. Y. H. Hiyama, "Organofluorine Compounds : Chemistry and Applications," (in English), 2000. [Online]. Available: https://public.ebookcentral.proquest.com/choice/publicfullrecord.aspx?p=3097611.

[58] J. R. T. Johnson and I. Panas, "Hydrolysis on Transition Metal Oxide Clusters and the Stabilities of M−O−M Bridges," *Inorganic Chemistry*, vol. 39, no. 15, pp. 3192-3204, 2000, doi: 10.1021/ic991144l.

[59] J. R. T. Johnson and I. Panas, "Water Adsorption and Hydrolysis on Molecular Transition Metal Oxides and Oxyhydroxides," *Inorganic Chemistry*, vol. 39, no. 15, pp. 3181-3191, 2000, doi: 10.1021/ic991150h.

[60] N. S. Saetova *et al.*, "Alumina–silica glass–ceramic sealants for tubular solid oxide fuel cells," *Journal of Materials Science*, vol. 54, no. 6, pp. 4532-4545, 2019/03/01 2019, doi: 10.1007/s10853-018-3181-8.

[61] Y.-S. Chou, J. P. Choi, and J. W. Stevenson, "Compliant alkali silicate sealing glass for solid oxide fuel cell applications: The effect of protective alumina coating on electrical stability in dual environment," *International Journal of Hydrogen Energy*, vol. 37, no. 23, pp. 18372-18380, 2012/12/01/ 2012, doi: https://doi.org/10.1016/j.ijhydene.2012.08.084.

[62] S. P. Simner and J. W. Stevenson, "Compressive mica seals for SOFC applications," *Journal of Power Sources*, vol. 102, no. 1, pp. 310-316, 2001/12/01/ 2001, doi: https://doi.org/10.1016/S0378-7753(01)00811-4.

[63] X.-V. Nguyen *et al.*, "Study of sealants for SOFC," *International Journal of Hydrogen Energy*, vol. 41, no. 46, pp. 21812-21819, 2016/12/14/ 2016, doi: https://doi.org/10.1016/j.ijhydene.2016.07.156.

[64] B. M. Weckhuysen and R. A. Schoonheydt, "Olefin polymerization over supported chromium oxide catalysts," *Catalysis Today*, vol. 51, no. 2, pp. 215-221, 1999, doi: 10.1016/S0920-5861(99)00046-2.

[65] L. Spiccia and W. Marty, "The fate of "active" chromium hydroxide, Cr(OH)3.3H2O, in aqueous suspension. Study of the chemical changes involved in its aging," *Inorganic Chemistry*, vol. 25, no. 3, pp. 266-271, 1986, doi: 10.1021/ic00223a007.

[66] M. A. Vuurman, F. D. Hardcastle, and I. E. Wachs, "Characterization of CrO3/Al2O3 catalysts under ambient conditions: Influence of coverage and calcination temperature," *Journal of Molecular Catalysis,* 1993.

[67] S. A. Best, R. G. Squires, and R. A. Walton, "The X-ray photoelectron spectra of heterogeneous catalysts: II. The chromia-silica catalyst system," *Journal of Catalysis,* vol. 47, no. 3, pp. 292-299, 1977, doi: 10.1016/0021-9517(77)90178-6.

[68] F. Cavani *et al.*, "Chemical and Physical Characterization of Alumina-Supported Chromia-Based Catalysts and Their Activity in Dehydrogenation of Isobutane," *Journal of Catalysis,* vol. 158, no. 1, pp. 236-250, 1996, doi: 10.1006/jcat.1996.0023.

[69] T. J. Dines and S. Inglis, "Raman spectroscopic study of supported chromium(vi) oxide catalysts," *Physical Chemistry and Chemical Physics,* vol. 5, no. 6, pp. 1320-1328, 2003, doi: 10.1039/b211857b.

[70] P. P. M. M. Wittgen, C. Groeneveld, J. H. G. J. Janssens, M. L. J. A. Wetzels, and G. C. A. Schuit, "Hydrogenation of olefins and polymerization of ethene over chromium oxide/silica catalysts," *Journal of Catalysis,* vol. 59, no. 2, pp. 168-175, 1979, doi: 10.1016/S0021-9517(79)80022-6.

[71] W. Hill and G. Öhlmann, "Thermal decomposition of chromium(VI)-oxide supported on silica," *Reaction Kinetics and Catalysis Letters,* vol. 38, no. 2, pp. 289-294, 1989/09/01 1989, doi: 10.1007/BF02062120.

[72] M. P. McDaniel, K. S. Collins, E. A. Benham, and T. H. Cymbaluk, "The activation of Phillips Cr/silica catalysts V. Stability of Cr(VI)," *Applied catalysis. A, General,* vol. 335, no. 2, pp. 252-261, 2008, doi: 10.1016/j.apcata.2007.11.031.

[73] P. C. ThüNe, R. Linke, W. J. H. Van Gennip, A. M. De Jong, and J. W. Niemantsverdriet, "Bonding of Supported Chromium during Thermal Activation of the CrOx/SiO2 (Phillips) Ethylene Polymerization Catalyst," *The journal of physical chemistry. B,* vol. 105, no. 15, pp. 3073-3078, 2001, doi: 10.1021/jp0039417.

[74] M. A. Vuurman, I. E. Wachs, D. J. Stufkens, and A. Oskam, "Characterization of chromium oxide supported on Al2O3, ZrO2, TiO2, and SiO2 under dehydrated conditions," *Journal of Molecular Catalysis,* vol. 80, 209-227, 1993.

[75] B. M. Weckhuysen and I. E. Wachs, "In Situ Raman Spectroscopy of Supported Chromium Oxide Catalysts: 18O2−16O2 Isotopic Labeling Studies," *Journal of Physical Chemistry,* vol. 101, no. 15, pp. 2793-2796, 1997, doi: 10.1021/jp963101l.

[76] I. E. Wachs, "Raman and IR studies of surface metal oxide species on oxide supports: Supported metal oxide catalysts," *Catalysis Today,* vol. 27, 437-455, 1996.

[77] A. Zecchina, E. Garrone, G. Ghiotti, C. Morterra, and E. Borello, "On the chemistry of silica supported chromium ions. I. Characterization of the samples," *Journal of Physical Chemistry*, vol. 79, 10, 1975.

[78] G. S. Tatar, "Reactive Evaporation of Chromium from Stainless Steel and the Reactive Condensation of Chromium Vapor Species on Ceramic Surfaces," Chemical Engineering, Montana State University, ProQuest Dissertations, 2018. [Online]. Available: https://www.proquest.com/docview/2169988635?pq-origsite=gscholar&fromopenview=true

[79] M. P. McDaniel, "The state of Cr(VI) on the Cr/Silica polymerization catalyst," *Journal of Catalysis*, vol. 67. 71-76 1981.

[80] M. P. McDaniel, "The state of Cr(VI) on the Phillips polymerization catalyst: II. The reaction between silica and CrO2Cl2," *Journal of Catalysis*, vol. 76, 17-28, 1982.

[81] M. I. Zaki, N. E. Fouad, J. Leyrer, and H. Knözinger, "Physicochemical investigation of calcined chromia-coated silica and alumina catalysts: Characterization of chromium-oxygen species," 1986.

[82] B. Fubini, G. Ghiotti, L. Stradella, E. Garrone, and C. Morterra, "The chemistry of silica-supported Cr ions: A characterization of the reduced and oxidized forms of chromia/silica catalyst by calorimetry and ultraviolet-visible spectroscopy," *Journal of Catalysis*, vol. 66, 200-213, 1980.

[83] B. Liu, Y. Fang, and M. Terano, "High resolution X-ray photoelectron spectroscopic analysis of transformation of surface chromium species on Phillips CrOx/SiO2 catalysts isothermally calcined at various temperatures," *Journal of Molecular Catalysis A: Chemical* vol. 219, 165–173, 2004.

[84] M. P. McDaniel, "The state of Cr(VI) on the Phillips polymerization catalyst: IV. Saturation coverage," *Journal of Catalysis*, vol. 76, 37-47, 1982.

[85] M. A. Vuurman, D. J. Stufkens, A. Oskam, J. A. Moulijn, and F. Kapteijn, "Raman spectra of chromium oxide species in CrO3/Al2O3 catalysts," *Journal of Molecular Catalysis*, 1990.

[86] B. M. Weckhuysen, L. M. De Ridder, and R. A. Schoonheydt, "A quantitative diffuse reflectance spectroscopy study of supported chromium catalysts," *Journal of Physical Chemistry*, 1993.

[87] A. Kytökivi, J.-P. Jacobs, A. Hakuli, J. Meriläinen, and H. H. Brongersma, "Surface Characteristics and Activity of Chromia/Alumina Catalysts Prepared by Atomic Layer

Epitaxy," *Journal of Catalysis,* vol. 162, no. 2, pp. 190-197, 1996, doi: 10.1006/jcat.1996.0276.

[88] H. Knözinger and P. Ratnasamy, "Catalytic Aluminas: Surface Models and Characterization of Surface Sites," *Catalysis reviews. Science and engineering,* vol. 17, no. 1, pp. 31-70, 1978, doi: 10.1080/03602457808080878.

[89] T. K. Phung, A. Lagazzo, M. Á. Rivero Crespo, V. Sánchez Escribano, and G. Busca, "A study of commercial transition aluminas and of their catalytic activity in the dehydration of ethanol," *Journal of Catalysis,* vol. 311, pp. 102-113, 2014, doi: 10.1016/j.jcat.2013.11.010.

[90] A. Ebrahim, M. Zahra, R. Sajjad, A. Mohammad Hasan, H. Mohammad Hossein, and R. Mahmood, "Phillips catalysts synthesized over various silica supports: Characterization and their catalytic evaluation in ethylene polymerization," *Polyolefins Journal,* vol. 3, no. 1, pp. 23-36, 2016, doi: 10.22063/poj.2016.1268.

[91] M. McDaniel, "Manipulating polymerization chemistry of Cr/silica catalysts through calcination," *Applied catalysis. A, General,* vol. 542, pp. 392-410, 2017, doi: 10.1016/j.apcata.2016.12.001.

[92] N. E. Fouad, H. Knözinger, and M. I. Zaki, "Chromia on Silica and Alumina Catalysts: Temperature-Programmed Reduction and Structure of Surface Chromates," *Zeitschrift für Physikalische Chemie,* vol. 186, no. 2, pp. 231-244, 1994, doi: doi:10.1524/zpch.1994.186.Part_2.231.

[93] G. Tatar, P. Gannon, N. Swain, R. Mason, E. Remington, and S. Dansereau, "Investigation of surface interactions between volatile chromium species and ceramics," *Surface and Interface Analysis,* vol. 51, no. 5, pp. 506-515, 2019.

[94] G. Tatar, P. Gannon, N. Swain, R. Mason, E. Remington, and S. Dansereau, "XPS Characterization of Aluminosilicate Fibers Post Interaction with Chromium Oxyhydroxide at 100–230 C," *Journal of The Electrochemical Society,* vol. 165, no. 10, p. C624, 2018.

[95] A. Lennartson, "The colours of chromium," *Nature Chemistry,* vol. 6, no. 10, p. 942, Oct 2014, doi: 10.1038/nchem.2068.

[96] C. M. Pradier *et al.,* "Supported chromia catalysts for oxidation of organic compounds: The state of chromia phase and catalytic performance," *Applied Catalysis,* 2000.

[97] M. C. Biesinger, B. P. Payne, A. P. Grosvenor, L. W. M. Lau, A. R. Gerson, and R. S. C. Smart, "Resolving surface chemical states in XPS analysis of first row transition metals, oxides and hydroxides: Cr, Mn, Fe, Co and Ni," *Applied Surface Sciences,* 2011.

[98] M. C. Biesinger, C. Brown, J. R. Mycroft, R. D. Davidson, and N. S. McIntryre, "X-ray photoelectron spectroscopy studies of chromium compounds," *Surface and Interface Analysis,* 2004.

[99] R. Merryfield, M. McDaniel, and G. Parks, "An XPS study of the Phillips Cr/silica polymerization catalyst," *Journal of Catalysis,* 1982.

[100] G. P. Halada and C. R. Clayton, "Photoreduction of Hexavalent Chromium during X-Ray Photoelectron Spectroscopy Analysis of Electrochemical and Thermal Films," *Journal of The Electrochemical Society,* 1991.

[101] A. Rahman, M. H. Mohamed, M. Ahmed, and A. M. Aitani, "Characterization of chromia/alumina catalysts by X-ray photoelectron spectroscopy, proton induced X-ray emission and thermogravimetric analysis," *Applied Catalysis,* 1995.

[102] S. V. Kagwade, C. R. Clayton, and G. P. Halada, "Causes and prevention of photochemical reduction of hexavalent chromium during x-ray photoelectron spectroscopy," *Surface and Interface Analysis,* 2001.

[103] I. Ikemoto, K. Ishii, S. Kinoshita, H. Kuroda, M. A. Alario Franco, and J. M. Thomas, "X-ray photoelectron spectroscopic studies of CrO 2 and some related chromium compounds," *Journal of Solid State Chemistry,* 1976.

[104] M. I. Zaki, N. E. Fouad, J. Leyrer, and H. Kno″zinger, "Physicochemical investigation of calcined chromia-coated silica and alumina catalysts: Characterization of chromium-oxygen species," *Applied catalysis,* vol. 21, no. 2, pp. 359-377, 1986, doi: 10.1016/S0166-9834(00)81368-8.

[105] A. M. Turek, I. E. Wachs, and E. DeCanio, "Acidic properties of alumina-supported metal oxide catalysts: an infrared spectroscopy study," *Journal of Physical Chemistry,* vol. 96, 5000-5007, 1992.

[106] B. Liu and M. Terano, "Investigation of the physico-chemical state and aggregation mechanism of surface Cr species on a Phillips CrOx/SiO2 catalyst by XPS and EPMA," *Journal of Molecular Catalysis,* 2001.

[107] C. P. Poole, W. L. Kehl, and D. S. Maclver, "Physical properties of coprecipitated chromia-alumina catalysts," *Journal of Catalysis,* 1962.

[108] G. L. Gaines and W. Vedder, "Dehydroxylation of muscovite," *Nature (London),* vol. 201, no. 4918, pp. 495-495, 1964, doi: 10.1038/201495a0.

[109] E. McCafferty and W. J. P., "Determination of the concentration of surface hydroxyl groups on metal oxide films by a quantitative XPS method," *Surface and Interface Analysis,* 1998.

[110] E. J. Opila, N. S. Jacobson, D. L. Myers, and E. H. Copland, "Predicting oxide stability in high-temperature water vapor," *JOM,* vol. 58, 22-28, 2006.

[111] J. A. Young, "Chromium(VI) Oxide, CrO3," *Journal of Chemical Education,* 2003.

[112] E. N. Bunting, "Phase equilibria in the system Cr2O3-Al2O3," *Bureau of Standards Journal of Research,* 1931

[113] G. Busca, "The surface of transitional aluminas: A critical review," *Catalysis Today,* 2014.

[114] C. Contescu, Jagiello, J., and Schwarz, J. A., "Heterogeneity of proton binding sites at the oxide/solution interface," *Langmuir,* 1993.

[115] P. Innocenzi, "Infrared spectroscopy of sol–gel derived silica-based films: a spectra-microstructure overview," *Journal of Non-Crystalline Solids,* 2003.

[116] K. Leung, I. M. B. Nielsen, and L. J. Criscenti, "Elucidating the Bimodal Acid−Base Behavior of the Water−Silica Interface from First Principles," *Journal of the American Chemical Society,* 2009.

[117] A. B. a. E. T. Stambouli, "Solid oxide fuel cells (SOFCs): a review of an environmentally clean and efficient source of energy," *Renewable and Sustainable Energy Reviews* vol. 6(5): 433-455, 2002.

[118] S. P. S. Badwal and K. Foger, "Solid oxide electrolyte fuel cell review," *Ceramics International,* vol. 22, no. 3, pp. 257-265, 1996, doi: 10.1016/0272-8842(95)00101-8.

[119] S. Fontana, Amendola, R., Chevalier, S., Piccardo, P., Caboche, G., Viviani, M., and R. Molins, and Sennour, M. , "Metallic interconnects for SOFC: Characterisation of corrosion resistance and conductivity evaluation at operating temperature of differently coated alloys.," *Journal of Power Sources,* vol. 171(2): 652-662, 2007.

[120] J. W. Fergus, "Effect of cathode and electrolyte transport properties on chromium poisoning in solid oxide fuel cells," *International journal of hydrogen energy,* vol. 32, no. 16, pp. 3664-3671, 2007, doi: 10.1016/j.ijhydene.2006.08.005.

[121] S. P. Jiang and X. Chen, "Chromium deposition and poisoning of cathodes of solid oxide fuel cells — A review," *International journal of hydrogen energy,* vol. 39, no. 1, pp. 505-531, 2014, doi: 10.1016/j.ijhydene.2013.10.042.

[122] C. Liang, B. Hu, A. Aphale, M. Venkataraman, M. K. Mahapatra, and P. Singh, "Mitigation of Chromium Assisted Degradation of LSM Cathode in SOFC," *ECS Transactions,* vol. 75, no. 28, pp. 57-64, 2017, doi: 10.1149/07528.0057ecst.

[123] T. Komatsu, R. Chiba, H. Arai, and K. Sato, "Chemical compatibility and electrochemical property of intermediate-temperature SOFC cathodes under Cr poisoning condition," *Journal of power sources,* vol. 176, no. 1, pp. 132-137, 2008, doi: 10.1016/j.jpowsour.2007.10.068.

[124] S. Vora, "Department of Energy Office of Fossil Energy's Solid Oxide Fuel Cell (SOFC) Program," in *17th Annual SOFC Workshop* Pittsburgh, PA, 2016.

[125] N. H. Menzler, P. Batfalsky, S. Groß, V. Shemet, and F. Tietz, "Post-Test Characterization of an SOFC Short-Stack after 17,000 Hours of Steady Operation," 2011 2011, vol. 35, 1 ed., pp. 195-206, doi: 10.1149/1.3569994.

[126] J. Malzbender, P. Batfalsky, R. Vaßen, V. Shemet, and F. Tietz, "Component interactions after long-term operation of an SOFC stack with LSM cathode," *Journal of power sources,* vol. 201, pp. 196-203, 2012, doi: 10.1016/j.jpowsour.2011.10.117.

[127] H. Yokokawa, H. Tu, B. Iwanschitz, and A. Mai, "Fundamental mechanisms limiting solid oxide fuel cell durability," *Journal of Power Sources,* vol. 182, no. 2, pp. 400-412, 2008/08/01/ 2008, doi: https://doi.org/10.1016/j.jpowsour.2008.02.016.

[128] J. A. Schuler *et al.*, "Combined Cr and S poisoning in solid oxide fuel cell cathodes," *Journal of Power Sources,* vol. 201, pp. 112-120, 2012/03/01/ 2012, doi: https://doi.org/10.1016/j.jpowsour.2011.10.123.

[129] S. C. Paulson and V. I. Birss, "Chromium poisoning of LSM-YSZ SOFC cathodes. I. Detailed study of the distribution of chromium species at a porous, single-phase cathode," *Journal of the Electrochemical Society,* vol. 151, no. 11, pp. A1961-A1968, 2004, doi: 10.1149/1.1806392.

[130] G. Y. Lau, M. C. Tucker, C. P. Jacobson, S. J. Visco, S. H. Gleixner, and L. C. DeJonghe, "Chromium transport by solid state diffusion on solid oxide fuel cell cathode," *Journal of power sources,* vol. 195, no. 22, pp. 7540-7547, 2010, doi: 10.1016/j.jpowsour.2010.06.017.

[131] S. P. S. Badwal, R. Deller, K. Foger, Y. Ramprakash, and J. P. Zhang, "Interaction between chromia forming alloy interconnects and air electrode of solid oxide fuel cells," *Solid State Ionics,* vol. 99, no. 3, pp. 297-310, 1997, doi: 10.1016/S0167-2738(97)00247-6.

[132] Y. Matsuzaki and I. Yasuda, "Electrochemical properties of a SOFC cathode in contact with a chromium-containing alloy separator," *Solid State Ionics*, vol. 132, no. 3, pp. 271-278, 2000, doi: 10.1016/S0167-2738(00)00654-8.

[133] S. P. Jiang, S. Zhang, and Y. D. Zhen, "Early interaction between Fe–Cr alloy metallic interconnect and Sr-doped LaMnO3 cathodes of solid oxide fuel cells," *Journal of materials research*, vol. 20, no. 3, pp. 747-758, 2005, doi: 10.1557/JMR.2005.0101.

[134] M. C. Tucker, H. Kurokawa, C. P. Jacobson, L. C. De Jonghe, and S. J. Visco, "A fundamental study of chromium deposition on solid oxide fuel cell cathode materials," *Journal of power sources*, vol. 160, no. 1, pp. 130-138, 2006, doi: 10.1016/j.jpowsour.2006.02.017.

[135] J. Milhans, M. Khaleel, X. Sun, M. Tehrani, M. Al-Haik, and H. Garmestani, "Creep properties of solid oxide fuel cell glass–ceramic seal G18," *Journal of Power Sources*, vol. 195, no. 11, pp. 3631-3635, 2010/06/01/ 2010, doi: https://doi.org/10.1016/j.jpowsour.2009.12.038.

[136] T. Zhang, R. K. Brow, W. G. Fahrenholtz, and S. T. Reis, "Chromate formation at the interface between a solid oxide fuel cell sealing glass and interconnect alloy," *Journal of power sources*, vol. 205, pp. 301-306, 2012, doi: 10.1016/j.jpowsour.2012.01.043.

[137] Z. Yang, G. Xia, K. D. Meinhardt, S. K. Weil, and J. W. Stevenson, "Chemical Stability of Glass Seal Interfaces in Intermediate Temperature Solid Oxide Fuel Cells," *Journal of materials engineering and performance*, vol. 13, no. 3, pp. 327-334, 2004, doi: 10.1361/10599490419298.

[138] Y. Zhenguo, K. D. Meinhardt, and J. W. Stevenson, "Chemical compatibility of barium-calcium-aluminosilicate-based sealing glasses with the ferritic stainless steel interconnect in SOFCs," *Journal of the Electrochemical Society*, vol. 150, no. 8, pp. 1095-1101, 2003, doi: 10.1149/1.1590325.

[139] S. J. Heo, J. Hong, A. Aphale, B. Hu, and P. Singh, "Chromium Poisoning of La1-xSrxMnO3±δ Cathodes and Electrochemical Validation of Chromium Getters in Intermediate Temperature-Solid Oxide Fuel Cells," *Journal of the Electrochemical Society*, vol. 166, no. 13, pp. F990-F995, 2019, doi: 10.1149/2.0931913jes.

[140] A. Au - Aphale, J. Au - Hong, B. Au - Hu, and P. Au - Singh, "Development and Validation of Chromium Getters for Solid Oxide Fuel Cell Power Systems," *JoVE*, no. 147, p. e59623, 2019/05/26/ 2019, doi: doi:10.3791/59623.

[141] M. A. Uddin, A. N. Aphale, B. Hu, U. Pasaogullari, and P. Singh, "In-Cell Chromium Getters to Mitigate Cathode Poisoning in SOFC Stack," *ECS Transactions*, vol. 78, no. 1, pp. 1039-1046, 2017/05/30 2017, doi: 10.1149/07801.1039ecst.

[142] A. Aphale, B. Hu, and P. Singh, "Low-Cost Getters for Gaseous Chromium Removal in High-Temperature Electrochemical Systems," *JOM (1989)*, vol. 71, no. 1, pp. 124-130, 2018, doi: 10.1007/s11837-018-3196-2.

[143] H. G. Seo, A. Staerz, G. Dimitrakopoulos, D. Kim, B. Yildiz, and H. L. Tuller, "Degradation and recovery of solid oxide fuel cell performance by control of cathode surface acidity: Case study – Impact of Cr followed by Ca infiltration," *Journal of Power Sources*, vol. 558, p. 232589, 2023/02/28/ 2023, doi: https://doi.org/10.1016/j.jpowsour.2022.232589.

[144] Z. Zhu, M. Sugimoto, U. Pal, S. Gopalan, and S. Basu, "Electrochemical cleaning: An in-Situ method to reverse chromium poisoning in solid oxide fuel cell cathodes," *Journal of Power Sources*, vol. 471, p. 228474, 2020/09/30/ 2020, doi: https://doi.org/10.1016/j.jpowsour.2020.228474.

[145] G. Spini, A. Profumo, C. Riolo, G. M. Beone, and E. Zecca, "Determination of hexavalent, trivalent and metallic chromium in welding fumes," *Toxicological and environmental chemistry*, vol. 41, no. 3-4, pp. 209-219, 1994, doi: 10.1080/02772249409357976.

[146] A. Wiryawan, R. Retnowati, P. Burhan, and S. Syekhfani, "METHOD OF ANALYSIS FOR DETERMINATION OF THE CHROMIUM (Cr) SPECIES IN WATER SAMPLES BY SPECTROPHOTOMETRY WITH DIPHENYLCARBAZIDE," *Journal of Environmental Engineering and Sustainable Technology; Vol 5, No 1 (2018)*, 12/07/ 2018. [Online]. Available: https://jeest.ub.ac.id/index.php/jeest/article/view/120.

[147] J. Wang, T. Hoang, E. L. Floyd, and J. L. Regens, "Characterization of Particulate Fume and Oxides Emission from Stainless Steel Plasma Cutting," *Annals of work exposures and health*, vol. 61, no. 3, pp. 311-320, 2017, doi: 10.1093/annweh/wxw031.

[148] K. L. Kamerud, K. A. Hobbie, and K. A. Anderson, "Stainless Steel Leaches Nickel and Chromium into Foods during Cooking," *Journal of Agricultural and Food Chemistry*, vol. 61, no. 39, pp. 9495-9501, 2013/10/02 2013, doi: 10.1021/jf402400v.

[149] Aletek. *Hexavalent Chromium: Thermal Blankets Hazard*. (2020). [Online]. Available: https://www.aletek.com.au/blog/white-paper-hexavalent-chromium-thermal-blankets-hazard

[150] Kavarmat. "Calcium-Free Insulation Jackets." https://en.kavarmat.com/ (accessed 2021).

[151] J. M. McHale, A. Navrotsky, and A. J. Perrotta, "Effects of Increased Surface Area and Chemisorbed H2O on the Relative Stability of Nanocrystalline γ-Al2O3 and α-Al2O3," *The journal of physical chemistry. B*, vol. 101, no. 4, pp. 603-613, 1997, doi: 10.1021/jp9627584.

[152] D. S. Maciver, H. H. Tobin, and R. T. Barth, "Catalytic aluminas I. Surface chemistry of eta and gamma alumina," *Journal of catalysis,* vol. 2, no. 6, pp. 485-497, 1963, doi: 10.1016/0021-9517(63)90004-6.

[153] S. Carre, N. S. Gnep, R. Revel, and P. Magnoux, "Characterization of the acid–base properties of transition aluminas by model reaction," *Applied catalysis. A, General,* vol. 348, no. 1, pp. 71-78, 2008, doi: 10.1016/j.apcata.2008.06.024.

[154] R. G. Pearson, "Hard and soft acids and bases, HSAB, part 1: Fundamental principles," *Journal of chemical education,* vol. 45, no. 9, p. 581, 1968, doi: 10.1021/ed045p581.

[155] B. M. Weckhuysen *et al.*, "Combined DRS-RS-EXAFS-XANES-TPR study of supported chromium catalysts," *Journal of the Chemical Society. Faraday transactions,* vol. 91, no. 18, pp. 3245-3253, 1995, doi: 10.1039/FT9959103245.

[156] D. J. Gardiner, C. J. Littleton, K. M. Thomas, and K. N. Strafford, "Distribution and characterization of high temperature air corrosion products on iron-chromium alloys by Raman microscopy," *Oxidation of metals,* vol. 27, no. 1-2, pp. 57-72, 1987, doi: 10.1007/BF00656729.

[157] C. S. Tedmon, "The Effect of Oxide Volatilization on the Oxidation Kinetics of Cr and Fe-Cr Alloys," *Journal of The Electrochemical Society,* vol. 113, no. 8, p. 766, 1966/08/01 1966, doi: 10.1149/1.2424115.

[158] U. Merten and W. E. Bell, "A High-Temperature Transpiration Apparatus For the Study of Atmosphere Above Viscous, Incongruently Vaporizing Melts," in *Characterization of High Temperature Vapors and Gases*, J. W. Hastie Ed. NY: John Wiley & Sons, Inc, 1979, pp. 91-114.

[159] C. Gindorf, K. Hilpert, and L. Singheiser, "Determination of Chromium Vaporization Rates of Different Interconnect Alloys by Transpiration Experiments," *ECS Proceedings Volumes,* vol. 2001-16, no. 1, p. 793, 2001/01/01 2001, doi: 10.1149/200116.0793PV.

[160] M. Stanislowski, E. Wessel, K. Hilpert, T. Markus, and L. Singheiser, "Chromium Vaporization from High-Temperature Alloys: I. Chromia-Forming Steels and the Influence of Outer Oxide Layers," *Journal of The Electrochemical Society,* vol. 154, no. 4, p. A295, 2007/02/13 2007, doi: 10.1149/1.2434690.

[161] J. Froitzheim, H. Ravash, E. Larsson, L. G. Johansson, and J. E. Svensson, "Investigation of Chromium Volatilization from FeCr Interconnects by a Denuder Technique," *Journal of The Electrochemical Society,* vol. 157, no. 9, p. B1295, 2010/07/19 2010, doi: 10.1149/1.3462987.

[162] L. T. Zhuravlev, "The surface chemistry of amorphous silica. Zhuravlev model," *Colloids and Surfaces A: Physicochemical and Engineering Aspects,* vol. 173, no. 1, pp. 1-38, 2000/11/10/ 2000, doi: https://doi.org/10.1016/S0927-7757(00)00556-2.

[163] H. H. Kung, *Transition Metal Oxides: Surface Chemistry and Catalysis*. Elsevier, 1989.

[164] Y. J. Suh, J. W. Chae, H. D. Jang, and K. Cho, "Role of chemical hardness in the adsorption of hexavalent chromium species onto metal oxide nanoparticles," *Chemical Engineering Journal,* vol. 273, pp. 401-405, 2015/08/01/ 2015, doi: https://doi.org/10.1016/j.cej.2015.03.095.

[165] L. Zhou *et al.*, "Improved Assessment of Chromium Evaporation Rates in Solid Oxide Cell Balance of Plant Component Alloys," *High Temperature Corrosion of Materials,* 2023/10/31 2023, doi: 10.1007/s11085-023-10207-w.

[166] B. C. Eigenbrodt and R. A. Walker, "In Situ Raman Measurements of Direct Methanol Solid Oxide Fuel Cell Devices," (in English), *Spectroscopy,* vol. 29, no. 12, pp. 24-30, Dec 2014, 2023-09-20 2014.

[167] M. B. Pomfret, J. C. Owrutsky, and R. A. Walker, "In Situ Optical Studies of Solid-Oxide Fuel Cells," *Annual Review of Analytical Chemistry,* vol. 3, no. 1, pp. 151-174, 2010/06/01 2010, doi: 10.1146/annurev.anchem.111808.073641.

[168] Y. Lee and C. L. Nassaralla, "Formation of hexavalent chromium by reaction between slag and magnesite-chrome refractory," *Metallurgical and Materials Transactions B,* vol. 29, no. 2, pp. 405-410, 1998/04/01 1998, doi: 10.1007/s11663-998-0117-8.

[169] Y. Wu, S. Song, A. M. Garbers-Craig, and Z. Xue, "Formation and leachability of hexavalent chromium in the Al2O3-CaO-MgO-Cr2O3 system," *Journal of the European Ceramic Society,* vol. 38, no. 6, pp. 2649-2661, 2018/06/01/ 2018, doi: https://doi.org/10.1016/j.jeurceramsoc.2018.01.012.

[170] P. G. Harrison, P. G. Lloyd, W. Daniell, C. Bailey, and W. Azelee, "Evolution of Microstructure during the Thermal Activation of Chromium-Promoted Tin(IV) Oxide Catalysts: An FT-IR, FT-Raman, XRD, TEM, and XANES/EXAFS Study," *Chemistry of Materials,* 1999.

[171] Y. De Vos, "Removal of Gaseous Hexavalent Chromium Species in a SOFC System By a Chromium Getter," *ECS Meeting Abstracts,* vol. MA2017-03, no. 1, p. 66, 2017/07/01 2017, doi: 10.1149/MA2017-03/1/66.

[172] L. CHEMetrics. "Hexavalent Chromium Testing | Chromate in Water Test Kits." https://www.chemetrics.com/product-category/test-kits/chromate-hexavalent/ (accessed 2023).

[173] W. Li and X. Xue, "Emission reduction research and formation of hexavalent chromium in stainless steel smelting: Cooling rate and boron oxide addition effects," *Process Safety and Environmental Protection,* vol. 122, pp. 131-143, 2019/02/01/ 2019, doi: https://doi.org/10.1016/j.psep.2018.11.025.

[174] R. Schmidt, "Thermodynamic properties and environmental chemistry of chromium," Pacific Northwest National Lab.(PNNL), Richland, WA (United States), 1984.

APPENDIX - THERMODYNAMIC EQUILIBRIUM MODELLING DATA

Condensation of Cr Vapors on Quartz Fibers (3% Water Vapor Content)

Table A.1 – Calculated condensed compounds in grams with respect to temperature generated from FactSage 8.2. The table is broken up to fit the page but is continuous from the top 8-rows starting from the first column of temperatures at the top and moving to the right, then repeating.

(Cr_2O_3+O_2+3H_2O) gas + Quartz fibers

T(C)	Cr2O3(s)	Cr2(CrO4)3(s)	Cr2(SO4)3(s)	Total Cr	SiO2(s)	SiO2(s2)
100	0	0.040711648	0.019719288	0.028646953	1.97	0
200	0.034217867	0	0.019719176	0.028641101	1.97	0
300	0.034126063	0	0.019695802	0.02857209	1.97	0
400	0.035486946	0	0.014775948	0.028198575	1.97	0
500	0.039383969	0	0	0.026946678	1.97	0
600	0.034890707	0	0	0.023872369	0	1.97
700	0.025958756	0	0	0.017761091	0	1.97
800	0.010655186	0	0	0.007290323	0	1.97

Na2SO4(s)	Na2SO4(s2)	Na2SO4(s3)	a O2(g)	a H2O(g)	a Cr(g)	a CrO(g)	a CrO2(g)	a CrO3(g)	a CrOH(g)
0	0	0.022917808	0.87163018	0.12836982	1.7601E-123	1.02559E-92	2.8138E-57	4.61024E-31	1.08834E-96
0.022917808	0	0	0.87163064	0.12836936	5.93522E-94	3.16489E-70	3.94119E-43	1.53761E-23	1.1196E-73
0	0.022917808	0	0.87163064	0.12836934	4.54594E-75	6.29082E-56	2.88258E-34	5.60627E-19	4.93168E-59
0	0.022917808	0	0.8716301	0.12836907	8.13068E-62	6.69637E-46	4.64554E-28	8.70178E-16	9.26251E-49
0	0.022917808	0	0.87162828	0.12836846	5.22894E-52	1.74475E-38	1.78519E-23	1.96918E-13	3.69917E-41
0	0.022917799	0	0.87162816	0.12836752	1.85122E-44	8.81809E-33	5.93316E-20	1.26337E-11	2.61054E-35
0	0.022916989	0	0.87162794	0.12836554	1.79834E-38	2.92316E-28	3.63798E-17	3.39579E-10	1.13223E-30
0	0.022882253	0	0.87162733	0.12836193	1.31229E-33	1.36308E-24	6.61383E-15	4.88221E-09	6.59308E-27

a CrOOH(g)	a Cr(OH)2(g)	a CrO2OH(g)	a CrO(OH)2(g)	a Cr(OH)3(g)	a CrO2(OH)2(g)	a CrO(OH)3(g)	a Cr(OH)4(g)
5.30326E-54	5.77566E-62	3.05342E-32	1.64247E-35	4.52867E-44	1.39801E-11	3.80505E-21	4.00715E-35
1.35391E-40	2.28805E-47	1.68683E-24	3.20795E-27	3.3661E-34	2.03281E-09	4.8708E-17	1.00876E-28
3.44481E-32	3.40515E-38	8.88868E-20	3.97335E-22	4.53903E-28	2.5591E-08	1.18455E-14	7.87539E-25
2.72591E-26	9.21481E-32	1.83671E-16	1.52477E-18	9.42201E-24	1.53075E-07	5.85507E-13	4.53705E-22
6.30283E-22	5.25929E-27	5.23743E-14	6.95674E-16	1.51159E-20	5.80356E-07	1.08475E-11	5.24647E-20
1.43406E-18	2.3883E-23	4.07069E-12	7.82494E-14	4.50066E-18	1.62971E-06	1.05038E-10	2.09935E-18
6.56509E-16	1.88576E-20	1.28693E-10	3.33555E-12	4.17053E-16	3.71491E-06	6.47023E-10	4.01275E-17
9.47175E-14	4.22667E-18	2.12697E-09	7.0591E-11	1.6645E-14	7.28048E-06	2.86967E-09	4.48978E-16

a CrO(OH)4(g)	a Cr(OH)5(g)	a Cr(OH)6(g)	a CrS(g)	a Na2SO4(s)	a Na2SO4(s2)	a Na2SO4(s3)
4.1631E-28	1.12343E-46	5.64414E-64	2.5652E-181	0.98487342	0.41395842	1
7.03531E-24	1.34081E-38	1.34974E-53	2.5879E-136	1	0.80657622	0.99773762
2.09794E-21	1.33474E-33	4.35794E-47	3.4985E-107	0.76327361	1	0.75291595
1.2163E-19	4.72736E-30	1.81456E-42	9.15966E-87	0.53254412	1	0.52112568
2.56767E-18	2.14608E-27	5.1904E-39	4.34271E-73	0.4078673	1	0.39675869
2.77715E-17	2.50677E-25	2.53323E-36	4.35695E-63	0.33518274	1	0.32456427
1.88376E-16	1.13764E-23	3.61288E-34	3.05127E-55	0.29081759	1	0.28058205
9.10325E-16	2.60077E-22	2.11312E-32	5.4185E-49	0.26331716	1	0.25329871

a Cr2(CrO4)3(s)	a Cr2(SO4)3(s)	a SiO2(s)	a SiO2(s2)	a Cr2O3(s)	GAS	O2(g)	H2O(g)	Cr(g)	CrO(g)
1	1	1	0.71330133	0.11027121	1701.6285	1571.3394	130.28908	0	0
0.014334204	1	1	0.8213943	1	1701.635	1571.3459	130.28908	0	1.21239E-66
2.90909E-05	1	1	0.89909506	1	1701.6351	1571.3459	130.28905	1.33168E-71	2.40987E-52
4.27031E-07	1	1	0.95376813	1	1701.6387	1571.3457	130.28885	2.38179E-58	2.56522E-42
2.10144E-08	5.8633E-05	1	0.98787757	1	1701.6495	1571.3452	130.28845	1.53176E-48	6.68376E-35
2.28295E-09	1.01145E-09	0.9945392	1	1	1701.654	1571.3439	130.28741	5.42294E-41	3.37801E-29
4.28155E-10	1.0544E-13	0.9201283	1	1	1701.663	1571.3415	130.28524	5.26804E-35	1.11979E-24
1.18847E-10	2.9464E-17	0.79760426	1	1	1701.6783	1571.337	130.2813	3.84419E-30	5.22163E-21

CrO2(g)	CrO3(g)	CrOH(g)	CrOOH(g)	Cr(OH)2(g)	CrO2OH(g)	CrO(OH)2(g)	Cr(OH)3(g)
1.33153E-53	2.59719E-27	0	2.53969E-50	2.79871E-58	1.73749E-28	9.43941E-32	2.62838E-40
1.86503E-39	8.66215E-20	4.3525E-70	6.48377E-37	1.10872E-43	9.5986E-21	1.84364E-23	1.95365E-30
1.36408E-30	3.15831E-15	1.91722E-55	1.6497E-28	1.65004E-34	5.05794E-16	2.28353E-18	2.63441E-24
2.19834E-24	4.90218E-12	3.60085E-45	1.30542E-22	4.46524E-28	1.04515E-12	8.76299E-15	5.46844E-20
8.44779E-20	1.10935E-09	1.43808E-37	3.01839E-18	2.54851E-23	2.98027E-10	3.99812E-12	8.77313E-17
2.80766E-16	7.11723E-08	1.01486E-31	6.86763E-15	1.15731E-19	2.31635E-08	4.49708E-10	2.61214E-14
1.72155E-13	1.91303E-06	4.40162E-27	3.14398E-12	9.13789E-17	7.32306E-07	1.91697E-08	2.42053E-12
3.12976E-11	2.75041E-05	2.56309E-23	4.53595E-10	2.04812E-14	1.21031E-05	4.05693E-07	9.66054E-11

Condensation of Cr Vapors on Alumina Fibers (3% Water Vapor Content)

Table A.2 – Calculated condensed compounds in grams with respect to temperature generated from FactSage 8.2. The table is broken up to fit the page but is continuous from the top 8-rows starting from the first column of temperatures at the top and moving to the right, then repeating.

(Cr_2O_3+O_2+3H_2O) gas + Alumina fibers						
T(C)	Cr2O3(CORU)	Cr2(CrO4)3(s)	Cr2O3(s)	Total Cr	Al2O3(H2O)(s)	Al2Si4O10(OH)2(s)
100	0	0.049801956	0	0.028646686	2.2342465	0.11039874
200	0.020384611	0	0.021475475	0.028640848	0	0
300	0.041777261	0	0	0.028584178	0	0
400	0.041559632	0	0	0.028435276	0	0
500	0.041044352	0	0	0.028082719	0	0
600	0.040218948	0	0	0.027517974	0	0
700	0.03902999	0	0	0.026704484	0	0
800	0.037501246	0	0	0.025658511	0	0

SiO2(s)	a O2(g)	a H2O(g)	a Cr(g)	a CrO(g)	a CrO2(g)	a CrO3(g)	a CrOH(g)	a CrOOH(g)
0	0.87192338	0.12807662	1.7594E-123	1.02535E-92	2.81361E-57	4.61071E-31	1.08675E-96	5.2964E-54
0.073638387	0.87163099	0.128369	5.93522E-94	3.16489E-70	3.94119E-43	1.53761E-23	1.1196E-73	1.3539E-40
0.073638387	0.87163099	0.12836899	3.79753E-75	5.25515E-56	2.40801E-34	4.6833E-19	4.11976E-59	2.87768E-32
0.073638387	0.87163099	0.12836894	3.83539E-62	3.1588E-46	2.19139E-28	4.1048E-16	4.3693E-49	1.28586E-26
0	0.87163098	0.12836883	1.73489E-52	5.78888E-39	5.92303E-24	6.53352E-14	1.22734E-41	2.0912E-22
0	0.87163095	0.12836865	4.37681E-45	2.08485E-33	1.40277E-20	2.98697E-12	6.17208E-36	3.39055E-19
0	0.87163087	0.12836834	3.20866E-39	5.21559E-29	6.49102E-18	6.0589E-11	2.02019E-31	1.17138E-16
0	0.87163054	0.12836768	1.83611E-34	1.90718E-25	9.25389E-16	6.83107E-10	9.22504E-28	1.32529E-14

a Cr(OH)2(g)	a CrO2OH(g)	a CrO(OH)2(g)	a Cr(OH)3(g)	a CrO2(OH)2(g)	a CrO(OH)3(g)	a Cr(OH)4(g)
5.76111E-62	3.04998E-32	1.63861E-35	4.51248E-44	1.39495E-11	3.79209E-21	3.98859E-35
2.28804E-47	1.68683E-24	3.20794E-27	3.36609E-34	2.0328E-09	4.87078E-17	1.00875E-28
2.84454E-38	7.42531E-20	3.3192E-22	3.79175E-28	2.13778E-08	9.89528E-15	6.57881E-25
4.34679E-32	8.6641E-17	7.1926E-19	4.44453E-24	7.22082E-08	2.76194E-13	2.14021E-22
1.74497E-27	1.73772E-14	2.30817E-16	5.01529E-21	1.92556E-07	3.5991E-12	1.74073E-20
5.64669E-24	9.62434E-13	1.85006E-14	1.0641E-18	3.85316E-07	2.48343E-11	4.96356E-19
3.36472E-21	2.29622E-11	5.95154E-13	7.44144E-17	6.62844E-07	1.15448E-10	7.16001E-18
5.9141E-19	2.97607E-10	9.87734E-12	2.32907E-15	1.01871E-06	4.01544E-10	6.28254E-17

a CrO(OH)4(g)	a Cr(OH)5(g)	a Cr(OH)6(g)	a Cr2O3(CORU)	a Al2O3(H2O)(s)	a Al2Si4O10(OH)2(s)	a Cr2(CrO4)3(s)
4.14452E-28	1.11705E-46	5.60612E-64	0.11023836	1	1	1
7.03527E-24	1.3408E-38	1.34973E-53	1.0000037	0.16570513	0.2282013	0.014334217
1.75254E-21	1.11499E-33	3.64045E-47	0.69784145	0.003600074	0.006896772	1.18344E-05
5.73749E-20	2.22998E-30	8.5596E-43	0.22251925	0.000223536	0.00061925	9.97417E-09
8.51927E-19	7.1205E-28	1.72213E-39	0.11008333	2.61437E-05	7.15998E-05	8.4493E-11
6.56612E-18	5.92687E-26	5.98945E-37	0.055898805	4.6547E-06	9.50137E-06	1.68657E-12
3.36123E-17	2.02993E-24	6.44666E-35	0.031835022	1.10849E-06	1.91173E-06	7.74221E-14
1.27382E-16	3.63934E-23	2.95702E-33	0.019576842	3.26146E-07	5.16626E-07	6.37302E-15

a SiO2(s)	a Cr2O3(s)	GAS	Mull#1	CORU	a Mull#1	a Mull#2	a CORU
0.98105112	0.11023783	1701.291	0	0	0.004637371	0.004637371	0.332656
1	1	1701.64	0	1.9503846	0.50301083	0.50301083	1
1	0.6978393	1701.6401	0	1.9717773	0.70884569	0.70884569	1
1	0.22251866	1701.6403	0	1.9715596	0.90791606	0.90791606	1
0.90874068	0.11008308	1701.6408	0.23959097	1.8050918	1	1	1
0.77123215	0.055898691	1701.6416	0.24399808	1.7998593	1	1	1
0.6299851	0.031834964	1701.6428	0.24847449	1.7941939	1	1	1
0.48946186	0.019576809	1701.6443	0.25303553	1.7881041	1	1	1

O2(g)	H2O(g)	Cr(g)	CrO(g)	CrO2(g)	CrO3(g)	CrOH(g)	CrOOH(g)
1571.343	129.94807	0	0	1.33099E-53	2.59658E-27	0	2.53556E-50
1571.3509	130.28908	0	1.2124E-66	1.86504E-39	8.66218E-20	4.35251E-70	6.48378E-37
1571.3509	130.28906	1.11244E-71	2.01313E-52	1.13951E-30	2.63836E-15	1.60158E-55	1.37811E-28
1571.3508	130.28901	1.12354E-58	1.21007E-42	1.037E-24	2.31246E-12	1.69859E-45	6.15792E-23
1571.3506	130.28888	5.08218E-49	2.21759E-35	2.80287E-20	3.68069E-10	4.77136E-38	1.00147E-18
1571.3504	130.28868	1.28214E-41	7.9866E-30	6.63814E-17	1.68272E-08	2.39944E-32	1.62372E-15
1571.3499	130.28834	9.39941E-36	1.99798E-25	3.07165E-14	3.41331E-07	7.85362E-28	5.60968E-13
1571.3491	130.28766	5.37869E-31	7.30598E-22	4.37909E-12	3.84832E-06	3.58629E-24	6.34674E-11

Condensation of Cr Vapors on AES#1 Fibers (3% Water Vapor Content)

Table A.3 – Calculated condensed compounds in grams with respect to temperature generated from FactSage 8.2. The table is broken up to fit the page but is continuous from the top 8-rows starting from the first column of temperatures at the top and moving to the right, then repeating.

(Cr_2O_3+O_2+3H_2O) gas + AES #1

T(C)	g-Ca3Cr2Si3O12(GARN)	g-CaCrO4(s)	Total Cr	g-O2(g)	g-H2O(g)	g-Cr(g)
100	3.88978E-15	0.08598613	0.028646727	1571.3377	130.28792	0
200	0	0.08598613	0.028646727	1571.3377	130.28908	0
300	0	0.08598613	0.028646727	1571.3377	130.28908	0
400	0	0.085986101	0.028646718	1571.3377	130.28908	5.19061E-63
500	0	0.085983648	0.0286459	1571.3377	130.28908	7.44964E-52
600	0	0.085910458	0.028621517	1571.3377	130.28906	2.86345E-43
700	0	0.084841172	0.028265278	1571.3376	130.28889	1.84592E-36
800	0	0.075417573	0.025125757	1571.3373	130.28747	6.33747E-31

g-CrO(g)	g-CrO2(g)	g-CrO3(g)	g-CrOH(g)	g-CrOOH(g)	g-Cr(OH)2(g)	g-CrO2OH(g)
0	3.3018E-66	6.44027E-40	0	6.29767E-63	6.93994E-71	4.30845E-41
0	1.53973E-48	7.15131E-29	0	5.35289E-46	9.15345E-53	7.92443E-30
7.89638E-59	4.46965E-37	1.03488E-21	6.28214E-62	5.40556E-35	5.40669E-41	1.65733E-22
5.59036E-47	4.79082E-29	1.06833E-16	7.84732E-50	2.8449E-27	9.73112E-33	2.27768E-17
3.25062E-38	4.10854E-23	5.39527E-13	6.99406E-41	1.46799E-21	1.23947E-26	1.44945E-13
1.78367E-31	1.48252E-18	3.75808E-10	5.35877E-34	3.62631E-17	6.11099E-22	1.22311E-10
3.92376E-26	6.03232E-15	6.70329E-08	1.54236E-28	1.10167E-13	3.20203E-18	2.56605E-08
8.60829E-22	5.15967E-12	4.53429E-06	4.22557E-24	7.47809E-11	3.37667E-15	1.99536E-06

g-CrO(OH)2(g)	g-Cr(OH)3(g)	g-CrO2(OH)2(g)	g-CrO(OH)3(g)	g-Cr(OH)4(g)	g-CrO(OH)4(g)	g-Cr(OH)5(g)	g-Cr(OH)6(g)
2.34068E-44	6.51755E-53	2.30477E-20	6.32663E-30	6.71904E-44	7.91104E-37	2.15064E-55	0
1.52208E-32	1.61291E-39	1.11579E-14	2.69637E-22	5.63157E-34	4.45113E-29	8.546E-44	9.67062E-59
7.48244E-25	8.63218E-31	5.57502E-11	2.60259E-17	1.74498E-27	5.26812E-24	3.3765E-36	1.23926E-49
1.90972E-19	1.19174E-24	2.21791E-08	8.55594E-14	6.6861E-23	2.03135E-20	7.95373E-31	3.4319E-43
1.94449E-15	4.26684E-20	1.87659E-06	3.53754E-11	1.72545E-19	9.57015E-18	8.05815E-27	2.1908E-38
2.37462E-12	1.37931E-16	5.72135E-05	3.71902E-09	7.49611E-17	1.12382E-15	1.02193E-23	1.1609E-34
6.71732E-10	8.48197E-14	0.00086547	1.52028E-07	9.50857E-15	5.05877E-14	3.07778E-21	1.09876E-31
6.68853E-08	1.59274E-11	0.007980236	3.17243E-06	5.00562E-13	1.1502E-12	3.31053E-19	3.0237E-29

g-Ca2Mg5Si8O22(OH)2(s)	g-SiO2(s)	g-SiO2(s2)	g-NaAlSi3O8(s)	g-Na2Ca3Si6O16(s)	a-O2(g)	a-H2O(g)
0.052405016	0.79355254	0	0	0.076228395	0.87163105	0.12836895
0	0.79065116	0	0.019531809	0.053975225	0.87163005	0.12836995
0	0.79068607	0	0.018820682	0.053983164	0.87163005	0.12836995
0	0.79075595	0	0.017088851	0.053996075	0.87163005	0.12836995
0	0.79086054	0	0	0.05401839	0.87163005	0.12836995
0	0	0.79093902	0	0.054021114	0.87163005	0.12836993
0	0	0.79063363	0	0.054024651	0.87163	0.12836975
0	0	0.78707417	0	0.053979854	0.87162969	0.12836834

a-Cr(g)	a-CrO(g)	a-CrO2(g)	a-CrO3(g)	a-CrOH(g)	a-CrOOH(g)	a-Cr(OH)2(g)	a-CrO2OH(g)
4.3646E-136	2.5432E-105	6.97741E-70	1.14321E-43	2.6988E-109	1.31505E-66	1.43219E-74	7.57158E-45
4.9E-103	2.61288E-79	3.25379E-52	1.26942E-32	9.24326E-83	1.11777E-49	1.88898E-56	1.39262E-33
1.48957E-81	2.06131E-62	9.44533E-41	1.83701E-25	1.61597E-65	1.12876E-38	1.11577E-44	2.91256E-26
1.77192E-66	1.45934E-50	1.0124E-32	1.89638E-20	2.01859E-53	5.94059E-31	2.0082E-36	4.00275E-21
2.54308E-55	8.48559E-42	8.68223E-27	9.5771E-17	1.7991E-44	3.06539E-25	2.55788E-30	2.54723E-17
9.77495E-47	4.6562E-35	3.13288E-22	6.67094E-14	1.37845E-37	7.57231E-21	1.26112E-25	2.14946E-14
6.30143E-40	1.02428E-29	1.27476E-18	1.1899E-11	3.96744E-32	2.30047E-17	6.60798E-22	4.50953E-12
2.16342E-34	2.24715E-25	1.09035E-15	8.04878E-10	1.08695E-27	1.56154E-14	6.96838E-19	3.5066E-10

a-CrO(OH)2(g)	a-Cr(OH)3(g)	a-CrO2(OH)2(g)	a-CrO(OH)3(g)	a-Cr(OH)4(g)	a-CrO(OH)4(g)	a-Cr(OH)5(g)	a-Cr(OH)6(g)
4.07282E-48	1.12297E-56	3.46663E-24	9.43535E-34	9.93644E-48	1.03232E-40	2.78574E-59	0
2.64844E-36	2.77902E-43	1.67826E-18	4.02128E-26	8.32822E-38	5.80829E-33	1.10697E-47	1.11434E-62
1.30195E-28	1.48732E-34	8.38543E-15	3.88143E-21	2.58055E-31	6.87438E-28	4.3736E-40	1.42799E-53
3.32294E-23	2.05336E-28	3.33598E-12	1.27601E-17	9.88771E-27	2.65071E-24	1.03025E-34	3.95455E-47
3.38344E-19	7.35173E-24	2.82259E-10	5.27579E-15	2.55167E-23	1.24881E-21	1.04378E-30	2.52444E-42
4.13187E-16	2.37655E-20	8.60553E-09	5.54644E-13	1.10856E-20	1.46647E-19	1.32371E-27	1.33769E-38
1.16882E-13	1.46144E-17	1.30176E-07	2.2673E-11	1.40617E-18	6.6012E-18	3.98666E-25	1.26609E-35
1.16381E-11	2.74428E-15	1.20031E-06	4.73127E-10	7.40254E-17	1.5009E-16	4.28814E-23	3.48419E-33

Condensation of Cr Vapors on AES#2 Fibers (3% Water Vapor Content)

Table A.4 – Calculated condensed compounds in grams with respect to temperature generated from FactSage 8.2. The table is broken up to fit the page but is continuous from the top 8-rows starting from the first column of temperatures at the top and moving to the right, then repeating.

(Cr_2O_3+O_2+3H_2O) gas + AES #2

T(C)	g-CaCrO4(s)	Total Cr	g-O2(g)	g-H2O(g)	g-Cr(g)	g-CrO(g)
100	0.08598613	0.028646727	1571.3324	130.27996	0	0
200	0.08598613	0.028646727	1571.3324	130.28908	0	0
300	0.08598613	0.028646727	1571.3324	130.28908	0	7.89636E-59
400	0.085986101	0.028646718	1571.3324	130.28908	5.1906E-63	5.59035E-47
500	0.085983648	0.0286459	1571.3324	130.28908	7.44967E-52	3.25063E-38
600	0.085910455	0.028621516	1571.3324	130.28906	2.86354E-43	1.78373E-31
700	0.084841029	0.028265231	1571.3324	130.28889	1.84615E-36	3.92425E-26
800	0.07541387	0.025124524	1571.3342	130.28747	6.33974E-31	8.61137E-22

g-CrO2(g)	g-CrO3(g)	g-CrOH(g)	g-CrOOH(g)	g-Cr(OH)2(g)	g-CrO2OH(g)	g-CrO(OH)2(g)
3.30175E-66	6.4402E-40	0	6.29741E-63	6.93947E-71	4.30828E-41	2.34053E-44
1.53973E-48	7.15128E-29	0	5.35288E-46	9.15345E-53	7.92442E-30	1.52208E-32
4.46964E-37	1.03488E-21	6.28213E-62	5.40555E-35	5.40669E-41	1.65733E-22	7.48244E-25
4.79081E-29	1.06832E-16	7.84732E-50	2.84489E-27	9.73113E-33	2.27768E-17	1.90972E-19
4.10856E-23	5.39529E-13	6.99409E-41	1.468E-21	1.23948E-26	1.44946E-13	1.9445E-15
1.48256E-18	3.7582E-10	5.35895E-34	3.62643E-17	6.1112E-22	1.22315E-10	2.3747E-12
6.03306E-15	6.70411E-08	1.54255E-28	1.10181E-13	3.20243E-18	2.56637E-08	6.71816E-10
5.1615E-12	4.53589E-06	4.22708E-24	7.48074E-11	3.37787E-15	1.99606E-06	6.69089E-08

g-Cr(OH)3(g)	g-CrO2(OH)2(g)	g-CrO(OH)3(g)	g-Cr(OH)4(g)	g-CrO(OH)4(g)	g-Cr(OH)5(g)	g-Cr(OH)6(g)	g-CrS(g)
6.51695E-53	2.30463E-20	6.32607E-30	6.71827E-44	7.91016E-37	2.15035E-55	0	0
1.61291E-39	1.11579E-14	2.69637E-22	5.63159E-34	4.45114E-29	8.54603E-44	9.67068E-59	0
8.6322E-31	5.57502E-11	2.6026E-17	1.74498E-27	5.26813E-24	3.37652E-36	1.23926E-49	0
1.19174E-24	2.21791E-08	8.55596E-14	6.68613E-23	2.03135E-20	7.95377E-31	3.43192E-43	0
4.26688E-20	1.8766E-06	3.53757E-11	1.72547E-19	9.57024E-18	8.05823E-27	2.19082E-38	0
1.37936E-16	5.72154E-05	3.71916E-09	7.49638E-17	1.12386E-15	1.02197E-23	1.16094E-34	3.58106E-65
8.48305E-14	0.000865578	1.52047E-07	9.50979E-15	5.05941E-14	3.07818E-21	1.0989E-31	1.56462E-54
1.5933E-11	0.007983032	3.17355E-06	5.00738E-13	1.1506E-12	3.31168E-19	3.02475E-29	6.68206E-46

g-Ca2Mg5Si8O22(OH)2(s)	g-CaSO4(s)	g-SiO2(s)	g-SiO2(s2)	g-Na2Ca3Si6O16(s)	a-O2(g)	a-H2O(g)	a-Cr(g)
0.41117784	0.044626647	0.4441905	0	0.076247442	0.87163751	0.12836249	4.3646E-136
0	0.044626647	0.47460206	0	0.076247442	0.87162968	0.12837032	4.9E-103
0	0.044626647	0.47460206	0	0.076247442	0.87162968	0.12837032	1.48957E-81
0	0.044626647	0.47460205	0	0.076247442	0.87162968	0.12837032	1.77192E-66
0	0.044626621	0.47460109	0	0.076247442	0.87162968	0.12837032	2.5431E-55
0	0.044619897	0	0.47456995	0.076247431	0.87162967	0.1283703	9.77529E-47
0	0.043991995	0	0.47388151	0.076246183	0.87162955	0.12837011	6.30222E-40
0	0.012174541	0	0.45623796	0.07615433	0.87162579	0.12836802	2.16419E-34

a-CrO(g)	a-CrO2(g)	a-CrO3(g)	a-CrOH(g)	a-CrOOH(g)	a-Cr(OH)2(g)	a-CrO2OH(g)	a-CrO(OH)2(g)	a-Cr(OH)3(g)
2.5431E-105	6.97739E-70	1.14321E-43	2.6987E-109	1.31501E-66	1.43211E-74	7.57138E-45	4.0726E-48	1.12288E-56
2.61288E-79	3.25379E-52	1.26942E-32	9.24328E-83	1.11777E-49	1.88899E-56	1.39263E-33	2.64845E-36	2.77903E-43
2.06132E-62	9.44534E-41	1.83701E-25	1.61597E-65	1.12877E-38	1.11577E-44	2.91257E-26	1.30196E-28	1.48732E-34
1.45934E-50	1.0124E-32	1.89638E-20	2.01859E-53	5.9406E-31	2.0082E-36	4.00276E-21	3.32296E-23	2.05337E-28
8.48564E-42	8.68229E-27	9.57717E-17	1.79911E-44	3.06542E-25	2.5579E-30	2.54725E-17	3.38347E-19	7.35181E-24
4.65636E-35	3.13298E-22	6.67117E-14	1.3785E-37	7.57258E-21	1.26116E-25	2.14954E-14	4.13202E-16	2.37664E-20
1.02441E-29	1.27492E-18	1.19004E-11	3.96795E-32	2.30076E-17	6.60883E-22	4.5101E-12	1.16897E-13	1.46163E-17
2.24795E-25	1.09073E-15	8.0516E-10	1.08734E-27	1.56209E-14	6.97084E-19	3.50782E-10	1.16422E-11	2.74524E-15

a-CrO2(OH)2(g)	a-CrO(OH)3(g)	a-Cr(OH)4(g)	a-CrO(OH)4(g)	a-Cr(OH)5(g)	a-Cr(OH)6(g)	a-CrS(g)	a-Ca2Mg5Si8O22(OH)2(s)
3.46646E-24	9.43462E-34	9.93541E-48	1.03221E-40	2.78539E-59	0	4.5567E-209	1
1.67827E-18	4.0213E-26	8.32827E-38	5.80832E-33	1.10697E-47	1.11435E-62	3.5584E-157	0.028582565
8.38545E-15	3.88145E-21	2.58057E-31	6.87442E-28	4.37363E-40	1.428E-53	1.9147E-123	0.001641458
3.33599E-12	1.27601E-17	9.88778E-27	2.65073E-24	1.03026E-34	3.95459E-47	8.7666E-100	0.000231802
2.82262E-10	5.27584E-15	2.55171E-23	1.24883E-21	1.04379E-30	2.52448E-42	2.73859E-82	5.66651E-05
8.60584E-09	5.54666E-13	1.1086E-20	1.46653E-19	1.32376E-27	1.33775E-38	7.5616E-69	1.97372E-05
1.30193E-07	2.26759E-11	1.40636E-18	6.60206E-18	3.98719E-25	1.26626E-35	3.30379E-58	8.82317E-06
1.20073E-06	4.73292E-10	7.40512E-17	1.50142E-16	4.28962E-23	3.48538E-33	1.41095E-49	4.76859E-06

Evaporation of Cr Vapors from Chromia and Mixed Chromia-CaO/MgO Powders

Table A.5 – Calculated vapor species in grams generated from FactSage 8.2. The species are calculated with respect to water vapor and total amounts are presented in the last column.

Evaporation $Cr_2O_3+O_2$																	
%H2O	a Cr(g)	a CrO(g)	a CrO2(g)	a CrO3(g)	a CrOH(g)	a CrOOH(g)	a Cr(OH)2(g)	a CrO2OH(g)	a CrO(OH)2(g)	a Cr(OH)3(g)	a CrO2(OH)2(g)	a CrO(OH)3(g)	a Cr(OH)4(g)	a CrO(OH)4(g)	a Cr(OH)5(g)	a Cr(OH)6(g)	Total
0	1.50E-31	5.08E-23	6.48E-14	1.71E-08													1.71E-08
1	1.56E-31	5.14E-23	6.40E-14	1.65E-08	1.60E-25	4.86E-13	1.53E-17	4.48E-09	9.68E-11	1.76E-14	3.73E-06	1.23E-09	1.68E-16	2.48E-16	8.13E-23	6.09E-33	3.75E-06
2	1.61E-31	5.20E-23	6.33E-14	1.60E-08	2.28E-25	6.75E-13	2.99E-17	6.08E-09	1.85E-10	4.71E-14	6.96E-06	3.22E-09	6.18E-16	8.92E-16	4.11E-22	4.23E-32	6.98E-06
3	1.67E-31	5.25E-23	6.26E-14	1.54E-08	2.80E-25	8.13E-13	4.38E-17	7.16E-09	2.65E-10	8.22E-14	9.75E-06	5.49E-09	1.28E-15	1.81E-15	1.02E-21	1.24E-31	9.78E-06
4	1.72E-31	5.31E-23	6.19E-14	1.49E-08	3.25E-25	9.23E-13	5.72E-17	7.95E-09	3.38E-10	1.20E-13	1.22E-05	7.87E-09	2.11E-15	2.92E-15	1.88E-21	2.58E-31	1.22E-05
5	1.78E-31	5.37E-23	6.13E-14	1.45E-08	3.66E-25	1.02E-12	6.99E-17	8.56E-09	4.04E-10	1.60E-13	1.43E-05	1.03E-08	3.06E-15	4.14E-15	2.97E-21	4.44E-31	1.43E-05
6	1.84E-31	5.42E-23	6.06E-14	1.40E-08	4.03E-25	1.10E-12	8.22E-17	9.05E-09	4.66E-10	2.01E-13	1.61E-05	1.26E-08	4.10E-15	5.43E-15	4.24E-21	6.77E-31	1.61E-05
7	1.89E-31	5.48E-23	6.00E-14	1.36E-08	4.37E-25	1.17E-12	9.40E-17	9.43E-09	5.22E-10	2.42E-13	1.77E-05	1.49E-08	5.20E-15	6.74E-15	5.66E-21	9.52E-31	1.77E-05
8	1.95E-31	5.54E-23	5.94E-14	1.32E-08	4.70E-25	1.23E-12	1.05E-16	9.74E-09	5.73E-10	2.83E-13	1.90E-05	1.70E-08	6.34E-15	8.06E-15	7.20E-21	1.26E-30	1.91E-05
9	2.01E-31	5.59E-23	5.88E-14	1.28E-08	5.01E-25	1.28E-12	1.16E-16	9.98E-09	6.20E-10	3.24E-13	2.02E-05	1.91E-08	7.50E-15	9.35E-15	8.82E-21	1.60E-30	2.02E-05
10	2.07E-31	5.65E-23	5.83E-14	1.24E-08	5.31E-25	1.33E-12	1.27E-16	1.02E-08	6.64E-10	3.64E-13	2.12E-05	2.10E-08	8.68E-15	1.06E-14	1.05E-20	1.97E-30	2.12E-05
Evaporation $Cr_2O_3+CaO+O_2$																	
%H2O	a Cr(g)	a CrO(g)	a CrO2(g)	a CrO3(g)	a CrOH(g)	a CrOOH(g)	a Cr(OH)2(g)	a CrO2OH(g)	a CrO(OH)2(g)	a Cr(OH)3(g)	a CrO2(OH)2(g)	a CrO(OH)3(g)	a Cr(OH)4(g)	a CrO(OH)4(g)	a Cr(OH)5(g)	a Cr(OH)6(g)	Total
0	3.41E-36	1.15E-27	1.47E-18	3.88E-13													3.88E-13
1	3.66E-36	1.21E-27	1.50E-18	3.88E-13	3.76E-30	1.14E-17	3.60E-22	1.05E-13	2.27E-15	4.13E-19	8.77E-11	2.88E-14	3.94E-21	5.82E-21	1.91E-27	1.43E-37	8.82E-11
2	3.92E-36	1.26E-27	1.54E-18	3.88E-13	5.54E-30	1.64E-17	7.28E-22	1.48E-13	4.49E-15	1.15E-18	1.69E-10	7.82E-14	1.50E-20	2.17E-20	1.00E-26	1.03E-36	1.70E-10
3	4.19E-36	1.32E-27	1.57E-18	3.88E-13	7.05E-30	2.04E-17	1.10E-21	1.80E-13	6.66E-15	2.07E-18	2.45E-10	1.38E-13	3.23E-20	4.56E-20	2.56E-26	3.13E-36	2.46E-10
4	4.48E-36	1.38E-27	1.61E-18	3.88E-13	8.45E-30	2.40E-17	1.49E-21	2.07E-13	8.77E-15	3.13E-18	3.16E-10	2.04E-13	5.49E-20	7.58E-20	4.89E-26	6.72E-36	3.17E-10
5	4.77E-36	1.44E-27	1.64E-18	3.88E-13	9.81E-30	2.72E-17	1.88E-21	2.30E-13	1.08E-14	4.30E-18	3.83E-10	2.75E-13	8.22E-20	1.11E-19	7.96E-26	1.19E-35	3.84E-10
6	5.08E-36	1.50E-27	1.68E-18	3.88E-13	1.11E-29	3.03E-17	2.28E-21	2.50E-13	1.29E-14	5.57E-18	4.45E-10	3.49E-13	1.14E-19	1.50E-19	1.17E-25	1.87E-35	4.46E-10
7	5.40E-36	1.56E-27	1.71E-18	3.88E-13	1.25E-29	3.33E-17	2.68E-21	2.69E-13	1.49E-14	6.92E-18	5.04E-10	4.24E-13	1.48E-19	1.92E-19	1.62E-25	2.72E-35	5.05E-10
8	5.74E-36	1.63E-27	1.75E-18	3.88E-13	1.38E-29	3.61E-17	3.10E-21	2.86E-13	1.69E-14	8.33E-18	5.59E-10	5.01E-13	1.87E-19	2.37E-19	2.12E-25	3.72E-35	5.61E-10
9	6.09E-36	1.69E-27	1.78E-18	3.88E-13	1.52E-29	3.89E-17	3.53E-21	3.02E-13	1.88E-14	9.82E-18	6.12E-10	5.79E-13	2.27E-19	2.83E-19	2.67E-25	4.86E-35	6.13E-10
10	6.45E-36	1.76E-27	1.82E-18	3.88E-13	1.66E-29	4.16E-17	3.96E-21	3.17E-13	2.07E-14	1.14E-17	6.61E-10	6.56E-13	2.71E-19	3.31E-19	3.28E-25	6.13E-35	6.62E-10
Evaporation $Cr_2O_3+MgO+O_2$																	
%H2O	a Cr(g)	a CrO(g)	a CrO2(g)	a CrO3(g)	a CrOH(g)	a CrOOH(g)	a Cr(OH)2(g)	a CrO2OH(g)	a CrO(OH)2(g)	a Cr(OH)3(g)	a CrO2(OH)2(g)	a CrO(OH)3(g)	a Cr(OH)4(g)	a CrO(OH)4(g)	a Cr(OH)5(g)	a Cr(OH)6(g)	Total
0	1.37E-32	4.64E-24	5.92E-15	1.56E-09													1.56E-09
1	1.42E-32	4.69E-24	5.85E-15	1.51E-09	1.46E-26	4.44E-14	1.40E-18	4.09E-10	8.84E-12	1.61E-15	3.41E-07	1.12E-10	1.53E-17	2.26E-17	7.43E-24	5.56E-34	3.43E-07
2	1.47E-32	4.75E-24	5.78E-15	1.46E-09	2.08E-26	6.17E-14	2.73E-18	5.55E-10	1.69E-11	4.31E-15	6.36E-07	2.94E-10	5.65E-17	8.15E-17	3.76E-23	3.86E-33	6.38E-07
3	1.52E-32	4.80E-24	5.72E-15	1.41E-09	2.56E-26	7.42E-14	4.01E-18	6.54E-10	2.42E-11	7.51E-15	8.91E-07	5.01E-10	1.17E-16	1.65E-16	9.29E-23	1.14E-32	8.93E-07
4	1.57E-32	4.85E-24	5.66E-15	1.36E-09	2.97E-26	8.43E-14	5.22E-18	7.26E-10	3.09E-11	1.10E-14	1.11E-06	7.19E-10	1.93E-16	2.66E-16	1.72E-22	2.36E-32	1.11E-06
5	1.63E-32	4.90E-24	5.60E-15	1.32E-09	3.34E-26	9.28E-14	6.39E-18	7.82E-10	3.69E-11	1.47E-14	1.30E-06	9.37E-10	2.80E-16	3.78E-16	2.71E-22	4.06E-32	1.31E-06
6	1.68E-32	4.96E-24	5.54E-15	1.28E-09	3.68E-26	1.00E-13	7.51E-18	8.26E-10	4.25E-11	1.84E-14	1.47E-06	1.15E-09	3.75E-16	4.96E-16	3.87E-22	6.19E-32	1.47E-06
7	1.73E-32	5.01E-24	5.48E-15	1.24E-09	3.99E-26	1.06E-13	8.59E-18	8.61E-10	4.77E-11	2.21E-14	1.61E-06	1.36E-09	4.75E-16	6.16E-16	5.17E-22	8.70E-32	1.62E-06
8	1.78E-32	5.06E-24	5.43E-15	1.20E-09	4.29E-26	1.12E-13	9.63E-18	8.89E-10	5.24E-11	2.59E-14	1.74E-06	1.56E-09	5.79E-16	7.36E-16	6.58E-22	1.15E-31	1.74E-06
9	1.84E-32	5.11E-24	5.37E-15	1.17E-09	4.58E-26	1.17E-13	1.06E-17	9.12E-10	5.67E-11	2.96E-14	1.84E-06	1.74E-09	6.86E-16	8.54E-16	8.06E-22	1.46E-31	1.85E-06
10	1.89E-32	5.16E-24	5.32E-15	1.14E-09	4.85E-26	1.22E-13	1.16E-17	9.30E-10	6.07E-11	3.32E-14	1.94E-06	1.92E-09	7.93E-16	9.69E-16	9.60E-22	1.80E-31	1.94E-06